NASA Contractor Report 3847

Investigation on Experimental Techniques To Detect, Locate, and Quantify Gear Noise in Helicopter Transmissions

Patrick M. Flanagan and William J. Atherton

NASA

ERRATA

NASA Contractor Report 3847

INVESTIGATION ON EXPERIMENTAL TECHNIQUES TO DETECT, LOCATE, AND QUANTIFY
GEAR NOISE IN HELICOPTER TRANSMISSIONS

Patrick M. Flanagan and William J. Atherton
January 1985

Page 43:   Table 8-1 should read

	Input	Output
Speed (RPM)	6060	347.5
Load (in-lbs)	3086	53116
Power (HP)	296.7	292.9

NASA Contractor Report 3847

Investigation on Experimental
Techniques To Detect, Locate,
and Quantify Gear Noise in
Helicopter Transmissions

Patrick M. Flanagan and William J. Atherton
Cleveland State University
Cleveland, Ohio

N/\S/\
National Aeronautics
and Space Administration

**Scientific and Technical
Information Branch**

1985

CONTENTS

1.0 INTRODUCTION

A robotic system to automate the detection, location, and quantification of gear noise using acoustic intensity measurement techniques has been successfully developed. Major system components fabricated under this grant include an instrumentation robot arm, a robot digital control unit and system software. A commercial desktop computer, spectrum analvzer and two microphone probe complete the equipment required for the Robotic Acoustic Intensity Measurement System (RAIMS). A multielement acoustic intensity probe was also addressed in this study.

Large-scale acoustic studies of gear noise in helicopter transmissions cannot be performed accurately and reliably using presently available instrumentation and techniques. Operator safety is a major concern in certain gear noise studies due to the operating environment. The man-hours needed to document a noise field in situ is another short coming of present techniques. RAIMS was designed to reduce the labor and hazard in collecting data and to improve the accuracy and repeatability of characterizing the acoustic field by automating the measurement process. Using RAIMS a system operator can remotely control the instrumentation robot to scan surface areas and volumes generating acoustic intensity information using the "two microphone" technique. Acoustic intensity studies requiring hours of scan time can be performed automatically without operator assistance. During a scan sequence, the acoustic intensity probe is positioned by the robot and acoustic intensity data is collected, processed, and

1

stored.

The following is a final report of the work performed under NASA/Lewis Grant No. NAG3-315 during the period from 1 September 1981 to 1 January 1984.

2.0 SUMMARY

The objective of this study was to develop experimental techniques to detect, locate and quantify gear noise in helicopter transmissions. Operating conditions for evaluating helicopter transmission noise required the fabrication of a remotely controlled acoustic intensity measurement test system. A Robotic Acoustic Intensity Measurement System (RAIMS) was designed and contructed under this grant to accomplish this task. Specifications for this system are summarized in Table 2-1.

TABLE 2-1

REQUIREMENTS FOR GEAR NOISE STUDIES AT NASA/LEWIS

* Technique to analyze noise sources in situ

* Remotely controlled data collection system

* System flexibility for in-depth noise analysis

The design philosophy used in the development of RAIMS was to interface commercially available measurement equipment to the necessary robotic instrumentation for automating acoustic intensity studies. Under this grant, an instrumentation robot, digital control unit, and system software were built for RAIMS. A multi-element acoustic intensity probe was also investigated and several designs are being evaluated.

Preliminary test results using RAIMS to characterize the acoustic intensity field generated by a speaker system demonstrates the accuracy and repeatibility of detecting, locating and quantifing a noise source. The accuracy and repeatibility of noise source location is due primarily to the spatial data provided by the instrumentation robot.
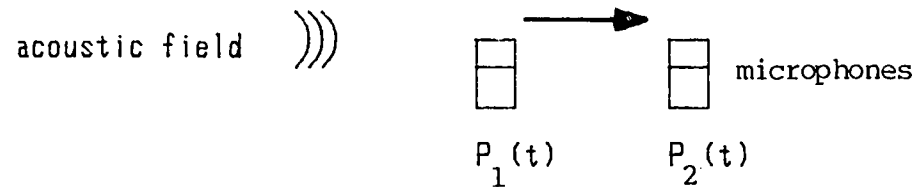
2.1   ACOUSTIC INTENSITY MEASUREMENTS

The "two microphone" technique for measuring acoustic intensity has been tested in several investigations (Ref. 1-7). These studies have documented its potential use in identifying and analyzing noise sources in complex reverberant environments. The mathematics involved in computing acoustic intensity using the two-microphone technique is reviewed in Figure 2-1. Both the direct and indirect method has been used with success in calculating local acoustic intensity .

A major goal in this research was automating the acoustic intensity measurement process. Automation required the development of a robotic acoustic intensity measurement system (RAIMS).

This system would position and/or sweep the acoustic intensity probe over a predetermined surface in an acoustic field,

ACOUSTIC INTENSITY MEASUREMENT
USING THE TWO MICROPHONE TECHNIQUE

$I = \overline{P(t) * U(t)}$ — vector quantity

acoustic field $)))$ ⬚ ⟶ ⬚ microphones

$P_1(t)$ $P_2(t)$

where   I = acoustic intensity
$P(t)$, $P_1(t)$, $P_2(t)$ = instantaneous pressure
.U(t) = instantaneous particle velocity

Direct Method: $I = -(1/(2p\triangle r))[P_1(t) + P_2(t)]\int (P_2(t) - P_1(t))dt$

Indirect Method: $I = -\int (Im(G_{12}(f)/(2\pi fp\triangle r))df$

Figure 2-1. Direct and indirect method for measuring acoustic
intensity using the two microphone technique.

calculate the local acoustic intensity, display the results, and reposition and/or adjust the sweep for the next measurement site. After initializing RAIMS, the measurement process is completely automated.

2.2   RAIMS

The Robotic Acoustic Intensity Measurement System developed under this grant consists of five major hardware components and the operating system software. A schematic of RAIMS is shown in Figure 2-2. All hardware components in RAIMS are interconnected via an IEEE-488 bus. The acoustic intensity probe is indirectly connected through the spectrum analyzer.

The major hardware components are either commercial electronic boxes or prototype robotic instrumentation. Two electronic boxes, the desktop calculator and the two channel spectrum analyzer are commercially available. The Hewlett-Packard (HP) 3582 and HP 200 series desktop computer were selected for this system because of their portability, measurement and computational capabilities, and cost. A multielement acoustic intensity probe was investigated under this grant. Results from this study showed that an intensity probe consisting of three pairs of phase matched microphones are necessary for calculating acoustic intensity in the 50 to 10,000 Hz bandwidth. The design of a multi-element probe using commercially available microphones is in progress.

The instrumentation robot's design specifications, shown in Table 2-2, required the development of a new manipulator. This

Noise Field

**Acoustic Intensity
Probe**

**Instrumentation
Robot**

**Digital
Control Unit**

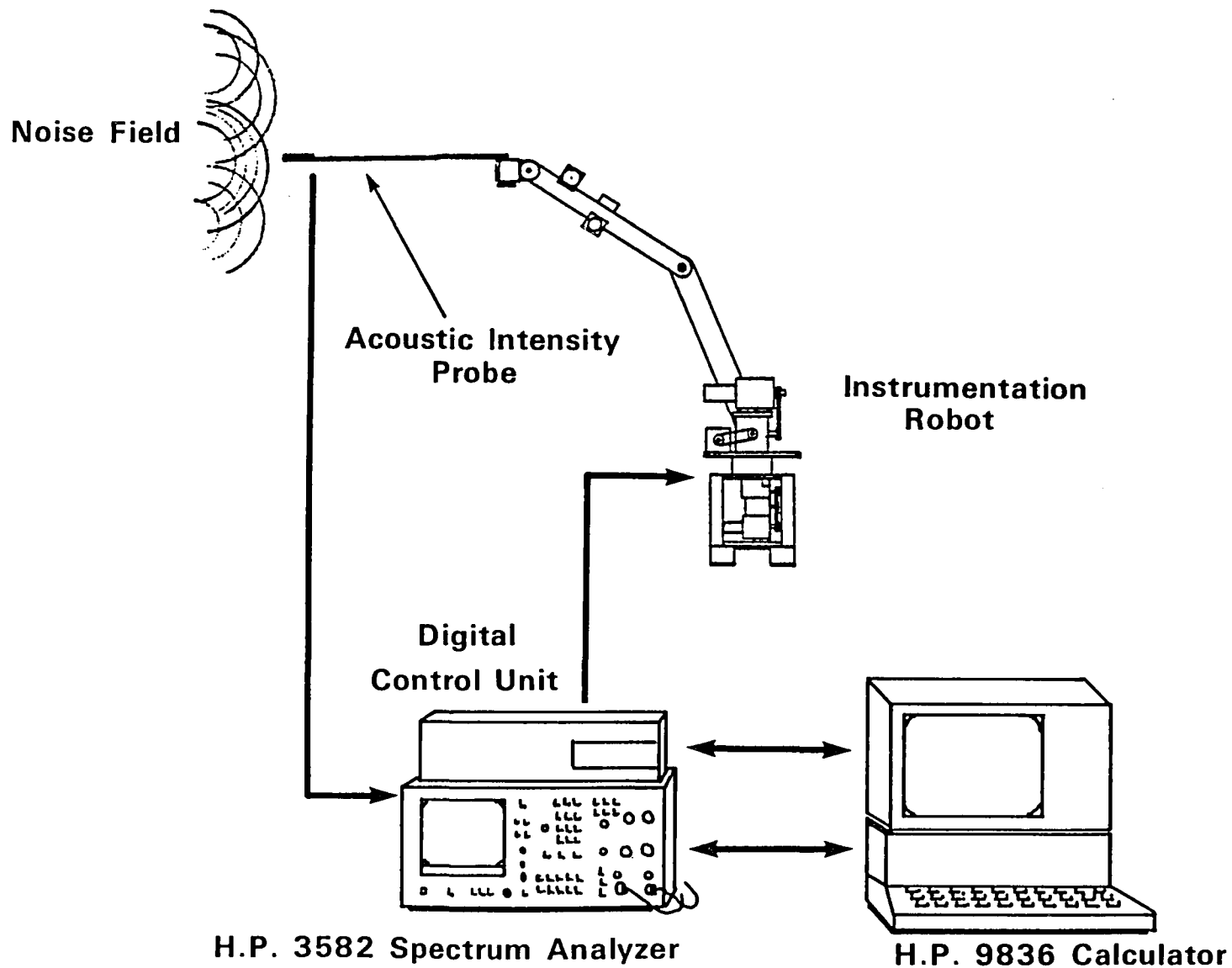**H.P. 3582 Spectrum Analyzer**

H.P. 9836 Calculator

Figure 2-2. Schematic of the Robotic Acoustic Intensity Measurement System.

robot arm has a five degree of freedom motion, all powered by D.C. servo-motors. Each degree of freedom has both position and velocity feedback. The manipulator weighs less than 35 kilograms and has a reach of over one meter. Worst case spatial resolution of .75 centimeter is due to the bit size of the absolute optic encoder position feedback system.

TABLE 2-2

REQUIREMENTS FOR INSTRUMENTATION ROBOT

* A one meter radius working volume with five degrees of freedom motion

* Lightweight and portable with an operating noise level of less than 70 dBA

* Interfaced with system controller with programmable velocity and position control

* A .75 cm. worst case spatial accuracy and 0.1 cm/sec velocity resolution

* 1.0 kilogram load carrying capacity

The instrumentation robot arm is interfaced to the RAIMS controller (200 series computer) by the digital control unit (DCU). The DCU receives "scan data and parameters" via a IEEE-488 bus from the RAIMS contoller and drives the robot arm accordingly. The entire unit consists of a MPU board, an IEEE-488 bus, a feedback control board, a robot interface circuit, and a power drive circuit board. An external D.C. power supply is required to power

the motors.

Each component of RAIMS is portable for conducting gear noise tests at a number of test sites. The programmable and programmed scan selections, and the user friendly control softkeys should provide the novice operator with sufficient controls to conduct meaningful acoustic intensity studies.

2.3   CONCLUSIONS

From preliminary test results using a speaker system, the following operating characteristics of the system can be summarized.

1)   Once a scan algorithm is programmed into memory, collecting acoustic intensity data is labor free.

2)   Acoustic intensity data obtained during multiple scans over the same area of a noise source shows good repeatability.

3)   Spatial data provided by RAIMS improves the system's capability for locating noise sources.

3.0 INSTRUMENTATION ROBOT

The concept of an instrumentation robot is a novel yet natural extension of the recent surge of robotic applications. The manipulator for RAIMS was specially designed and constructed for the acoustic intensity application. This special design permitted the robot to be tailored to meet the application needs much better than available commercial units. More importantly, the robot's digital control unit could be designed to interface

over a common laboratory instrumentation bus, the IEEE-488, resulting in a totally integrated measurement system controlled from a central desktop computer.

3.1 DESIGN GUIDELINES

The functions performed by an instrumentation robot are greatly different from those of current industrial robots. Currently available robots perform a variety of tasks in the industrial setting: materials handling, machine loading and unloading, parts inspection, welding, and painting. These jobs however, are significantly different from the role of the instrumentation robot. The purpose of the instrumentation robot is to carry a small and delicate transducer through various positions and orientations. The following goals were established to develop design guidelines for the instrumentation robot.

1) The robot should be lightweight so it will be portable. This dictates not only a lightweight design but also a robot structure that will fold compactly so it is easy to transport.

2) The robot should have a relatively long reach and have good dexterity. The long reach will enable the manipulator to scan over a large area, thus covering a large portion of a given noise source and reducing the need to move the robot base to a new scanning position. Good dexterity will permit the mechanical arm to reach into tight areas for detailed measurements.

3) The robot should have slow and smooth motion. Speed is not a major concern since slow movement will be used during data scanning. Smooth motion is desirable also because irregular scanning speed may bias the acoustic intensity data.

4) The robot's drive system should operate quietly so as not to interfere with the acoustic intensity measurements.

5) The robot should have a limited payload capacity of no more than one kg. Since its purpose is to carry the transducer, a large payload is not important and the additional structural strength would work against the lightweight goal.

6) The robot should only have five degrees of freedom instead of six. The sixth axis is wrist rotation and is not needed for acoustic intensity measurements since it makes no difference if the transducer is right side up or up side down. This reduces the complexity of the arm and also the overall weight.

These guidelines were used to select the best manipulator design. The result was an articulated arm design, driven by DC servo-motors with a maximum reach of over one meter. The articulated arm design was selected over other robot geometries (rectangular, post type, spherical) because it gives the maximum working volume with a minimum operating volume. Thus it is best suited to reach into tight places. It also permits a very long reach without a large heavy base allowing the robot to be lightweight. The DC servo-motors were chosen because of their quiet operation and good speed/torque characteristics. The instrumentation robot finally constructed meets these guidelines.

3.2 ROBOT COMPONENTS

The robot is constructed of 2024T aluminum for strength as well as lightweight. Each of the five axes is driven individually

by servo-motors which are mounted at the base of the robot arm as can be seen in Figure 3-1. The base rotation motor is mounted in the base section while the remaining four motors are mounted on the base platter and transmit torques to the respective axes through gearboxes and a series of chains and sprockets. The wrist joint has both pitch and yaw capability which is obtained from a simple differential consisting of two bevel gears.

The drive system for each axis was designed for the required spacial velocity and static torque load. Analysis showed the inertia torques were insignificant compared to the static and friction loads unless the desired velocities were greatly increased. The motors are DC servo-motors, selected for their good speed/torque characteristics. The base rotation is driven by a timing belt from the 180:1 gearhead reduction box on the motor. The shoulder joint is driven directly by a rigid coupling attachment to a 250:1 gearbox. The motor drives this gearbox through an additional 1.5:1 ratio by a timing belt. The elbow joint has a similar arrangement except the torque is transmitted to the appropriate joint through a chain that runs from the shoulder axis to the elbow.

The position of each axis is measured by absolute optic encoders with ten bit resolution. The robot is only required to operate in its front hemisphere where its five axes need to rotate only 180°. The full rotation of the optic encoders is utilized by driving them from the robot's axes through a 2:1 ratio. A study was performed early in the research project which determined that ten bit encoders would give satisfactory position discrimination.
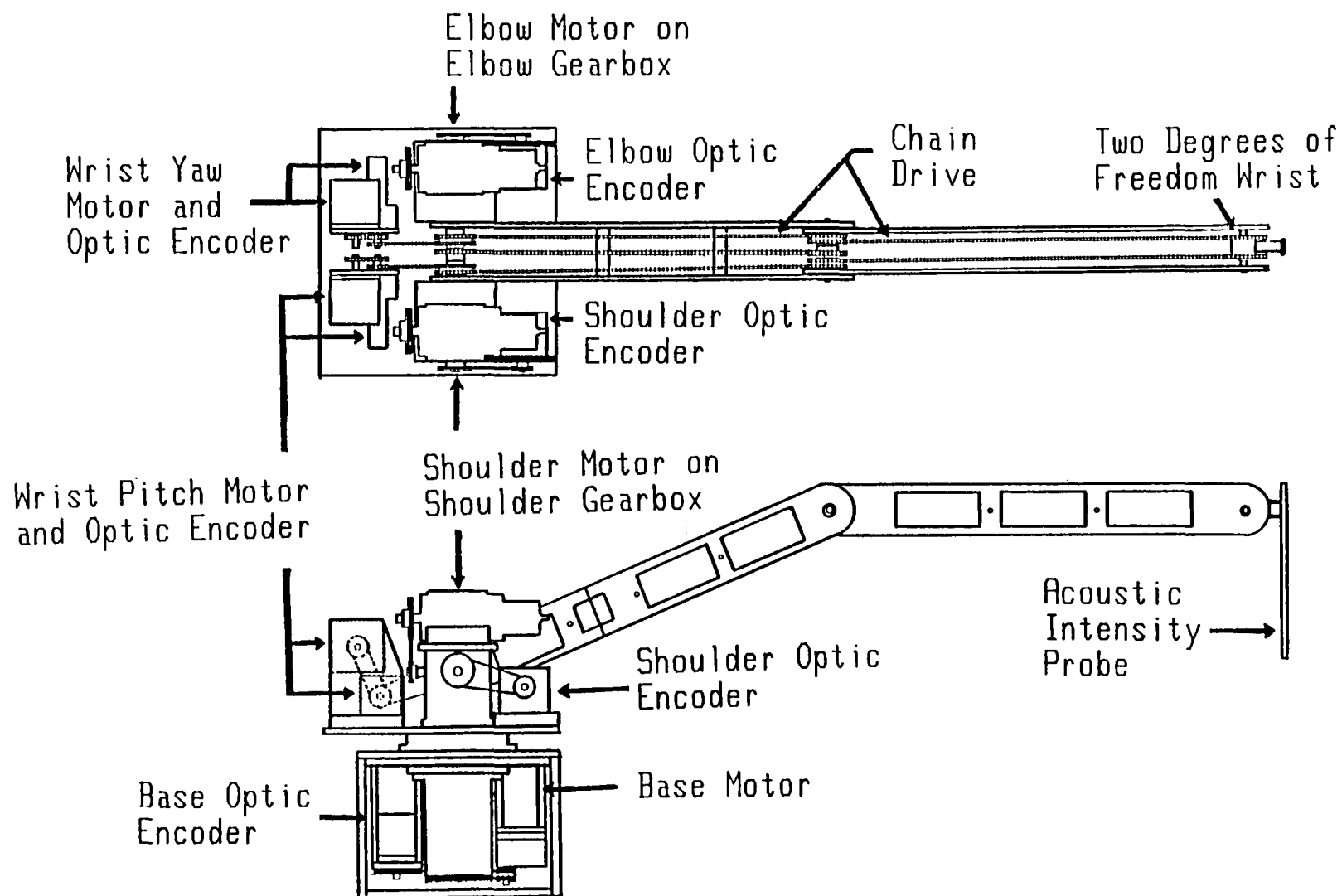
Figure 3-1. Schematic of instrumentation robot.

Since the transformation from joint rotation to rectangular coordinate translation is highly nonlinear, a computer program was written to evaluate the spacial resolution that would result from various optic encoders. Considering the worst case robot kinematic configuration, the model showed the point to point resolution is no greater than 7.5 mm with ten bit encoders. In the normal working space of the robot the resolution is approximately 2.5 mm. These values are acceptable for the acoustic intensity application of the robot and the additional cost of higher precision encoders is certainly not warranted.

3.3 KINEMATICS AND DYNAMICS

The spacial control of a robotic manipulator requires a solution of the inverse kinematic problem. That is, the position and the orientation of the end effector is given and the angles at all the joints must be determined. This is the opposite of most kinematic problems. Most industrial robot controllers use mini-computers to solve this problem for six degree-of-freedom manipulators. The usual technique is to iterate with the position equations until sufficienct accuracy is obtained for the angles. The instrumentation robot uses only five degrees-of-freedom with motion limited to the front hemisphere, and a microcomputer for the controller. Consequently, an exact solution technique was developed that makes use of the isosceles triangle formed by the first two links of the robot.

The angle definitions and the vector terminology for the solution can be seen in Figure 3-2. The solution begins by assuming the coordinates of point 5, (x_5, y_5, z_5), and the direction
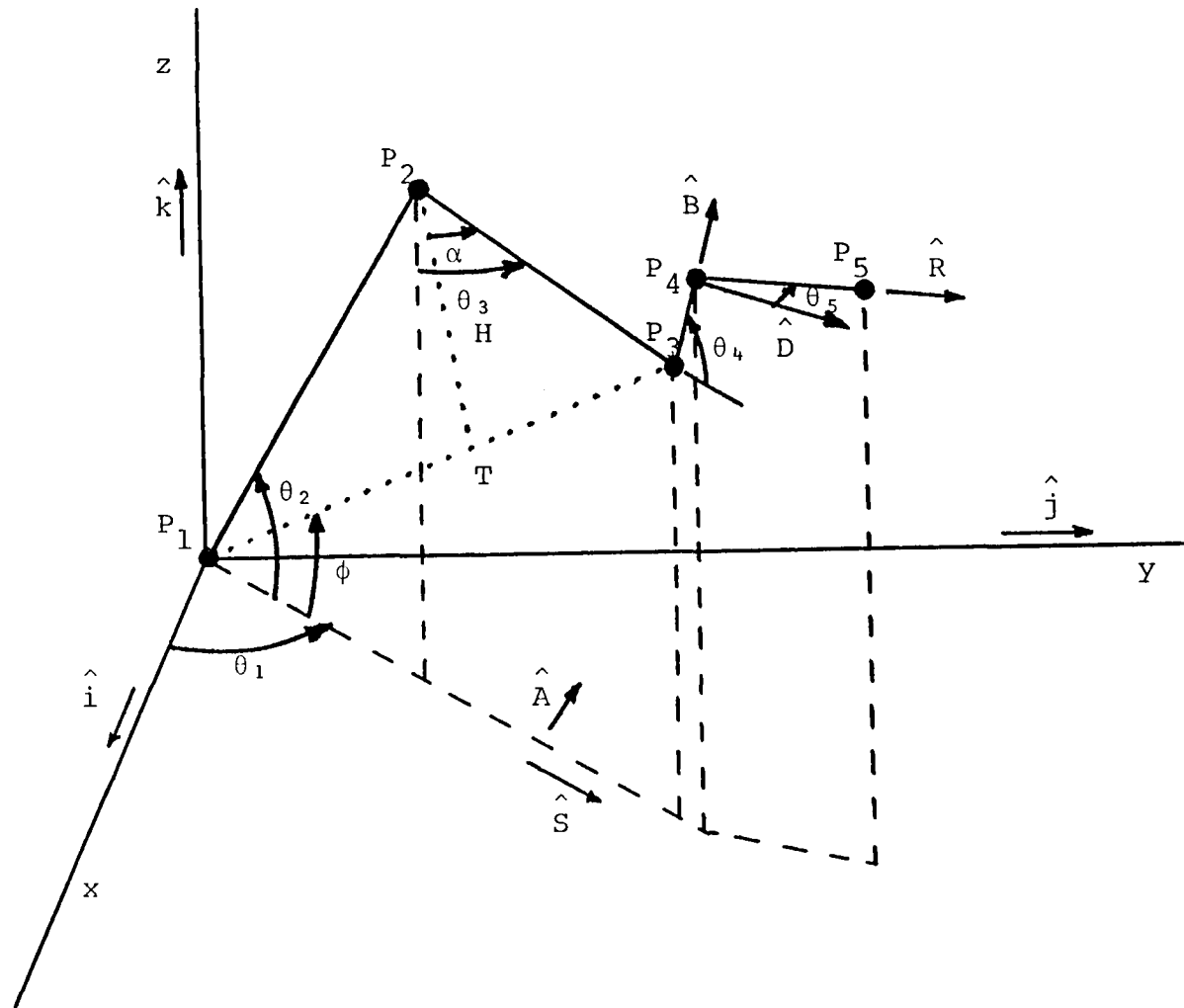
13

Figure 3-2. Robot geometry showing notation for the kinematics solution. The dashed lines show the projection of the joints P_2 through P_5 and the robot members on the x-y plane. The caret notation indicates a unit vector.

14

cosines of the probe element, $(1,m,n)$, are known. These values
are known from the scan generation algorithm of RAIMS. Then point
4 coordinates are known

$$P_4 \sim (x_5-Rl, y_5-Rm, z_5-Rn) \sim (x_4, y_4, z_4) \qquad (3.1)$$

where R is the length of the probe. The projection of P_4 onto the
x-y plane defines the vector S and the vector V, also in the x-y
plane perpendicular to S.

$$S = x_4\hat{i} + y_4\hat{j} \qquad (3.2)$$
$$A = -y_4\hat{i} + x_4\hat{j} \qquad (3.3)$$

The vector B, along the axis of rotation of θ_5, can now be defined

$$B = R \times A \qquad (3.4)$$

and vector D, along the direction of the robot but in the plane of
rotation of the probe, can also be determined

$$D = A \times B. \qquad (3.5)$$

Vectors A, B, and D form an orthogonal coordinate system from
which angle θ_5 can be determined

$$C_1 = R \cdot \hat{A} \qquad (3.6)$$
$$C_2 = R \cdot \hat{D} \qquad (3.7)$$
$$\theta_5 = \arctan(C_1/C_2) \qquad (3.8)$$

Now, using B, point 3 can be identified

$$P_3 \sim (x_4 - W\hat{B}\cdot\hat{i}, \ y_4 - W\hat{B}\cdot\hat{j}, \ z_4 - W\hat{B}\cdot\hat{k}) \qquad (3.9)$$

15

$$P_3 \sim (x_3, y_3, z_3) \qquad\qquad (3.10)$$

where W is the length of wrist member. Knowing P_3 allows the determination of the base angle

$$\theta_1 = \arctan(y_3/x_3). \qquad\qquad (3.11)$$

An isosceles triangle is formed with vertices P_1, P_2, and P_3 where the base is

$$T = \sqrt{x_3^2 + y_3^2 + z_3^2} \qquad\qquad (3.12)$$

and the projection of P_3 onto the x-y plane gives

$$E = \sqrt{x_3^2 + y_3^2}. \qquad\qquad (3.13)$$

The height of the isosceles triangle is

$$H = \sqrt{L^2 - T^2/4} \qquad\qquad (3.14)$$

Now, intermediate results are obtained,

$$\phi = \arctan(z_3/E) \qquad\qquad (3.15)$$

$$\alpha = \arctan((T/2)/H) \qquad\qquad (3.16)$$

from which algebraic relationships for right triangles results in

$$\theta_2 = 90^\circ + \phi - \alpha \qquad\qquad (3.17)$$

$$\theta_3 = \phi + \alpha. \qquad\qquad (3.18)$$

Finally, using orthogonal projections of the wrist length, the last angle is found

$$C_4 = \mathbf{W} \cdot \hat{\mathbf{s}} \qquad\qquad (3.19)$$

$$C_3 = \mathbf{W} \cdot \hat{\mathbf{k}} \qquad\qquad (3.20)$$

16

$$\Theta_4 = \arctan(C_3/C_4). \qquad\qquad (3.21)$$

The robot kinematics can result in two possible solutions for any given set of coordinates and direction cosines for the probe. These two solutions correspond to the elbow joint above or below the robot. Due to clearance considerations, it is most desirable to have the elbow above the robot and this solution is consistently obtained when positive square roots are taken in equations (3.12, 3.13, 3.14). This is valid while P_3 remains in the front hemisphere of the robot, as it is constrained to.

The dynamics of the robot, with respect to the inertial torques, are not important. To evaluate the effect of inertial torque on motor loading, a program was written to calculate the inertial as well as the static torque. d'Alembert's Principle was used to calculate the torque required to translate the robot members and Euler's torque equation was used to calculate the torque for pure rotation. This approach required: 1) calculation of the absolute acceleration for the center of mass of each member in the robot, 2) calculation of the angular acceleration of each member in the robot, and 3) determination of the inertia dyadic for each member. To simplify calculations, the wrist and probe members were assumed to be point masses so they have no angular acceleration. The results showed the inertia torques are not important compared to the static torques unless the velocity is substantially increased above the design criteria. Appendix A contains the equations and the graphical output for this analysis.

4.0 DIGITAL CONTROL UNIT

4.1 RAIMS SCAN CONTROLS

Two types of scan algorithms can be used for acoustic intensity measurement: the point-to-point scan algorithm and the continuous scan algorithm.

In the point-to-point scan algorithm the acoustic transducer is directed to a prescribed point, remains stationary while the measurement is taken, and then moves to another measurement point. Accurate position control is necessary for valid measurements. The present control system uses ten bit optic encoders for position control. The ten bit encoders provide an average spatial resolution of .25 cm and repeatability of .25 cm. The worst case spatial resolution is .75 cm for the most extreme reach. These position control specifications are satisfactory for valid point-to-point measurements.

In the continuous scan algorithm, measurements are taken while the transducer is moving within a prescribed area. The measurements are processed by time and space-averaging techniques. The processed measurement is representative of the average acoustic intensity of the scanned area. Accurate position control is needed for well defined measurements of the area with respect to position. The present control system specifications for position are satisfactory for valid continuous scan measurements. Accurate velocity control is needed for well distributed measurements of the area with respect to time. For the ideal continuous scan, the transducer velocity should be constant. At present, the point-to-point scan algorithm and an open-loop

18

continuous scan algorithm have been tested.

4.2 DCU COMPONENTS

The digital control unit provides the interface between the desktop computer and the robot. It consists of an MPU board, an IEEE-488 interface, an optic encoder/analog motor driver interface, a feedback control board, and a power drive circuit. The GPIB interface allows the digital control unit to be connected to any computer controller with the capability of executing the operating system. Coordinate generation and robot motion "teaching" is done by the controller and this information is dumped to the digital control unit. The software of the DCU is written in assembly language for fast execution and requires little memory. Instructions and data from the controller are interpreted and the software ensures the robot motion is consistent with those commands.

4.3 DCU CONTROLLER

The present controller is a proportional controller of the form

$$G_c(s) = K_c = 34. \tag{4.1}$$

The electronics of the controller are shown in the schematic of Figure 4-1. The components of the controller are identified in Table 4.1.

The 5018 converts a digital, eight bit velocity command signal from the microprocessor to a $\pm 5V$ analog velocity command signal.

19
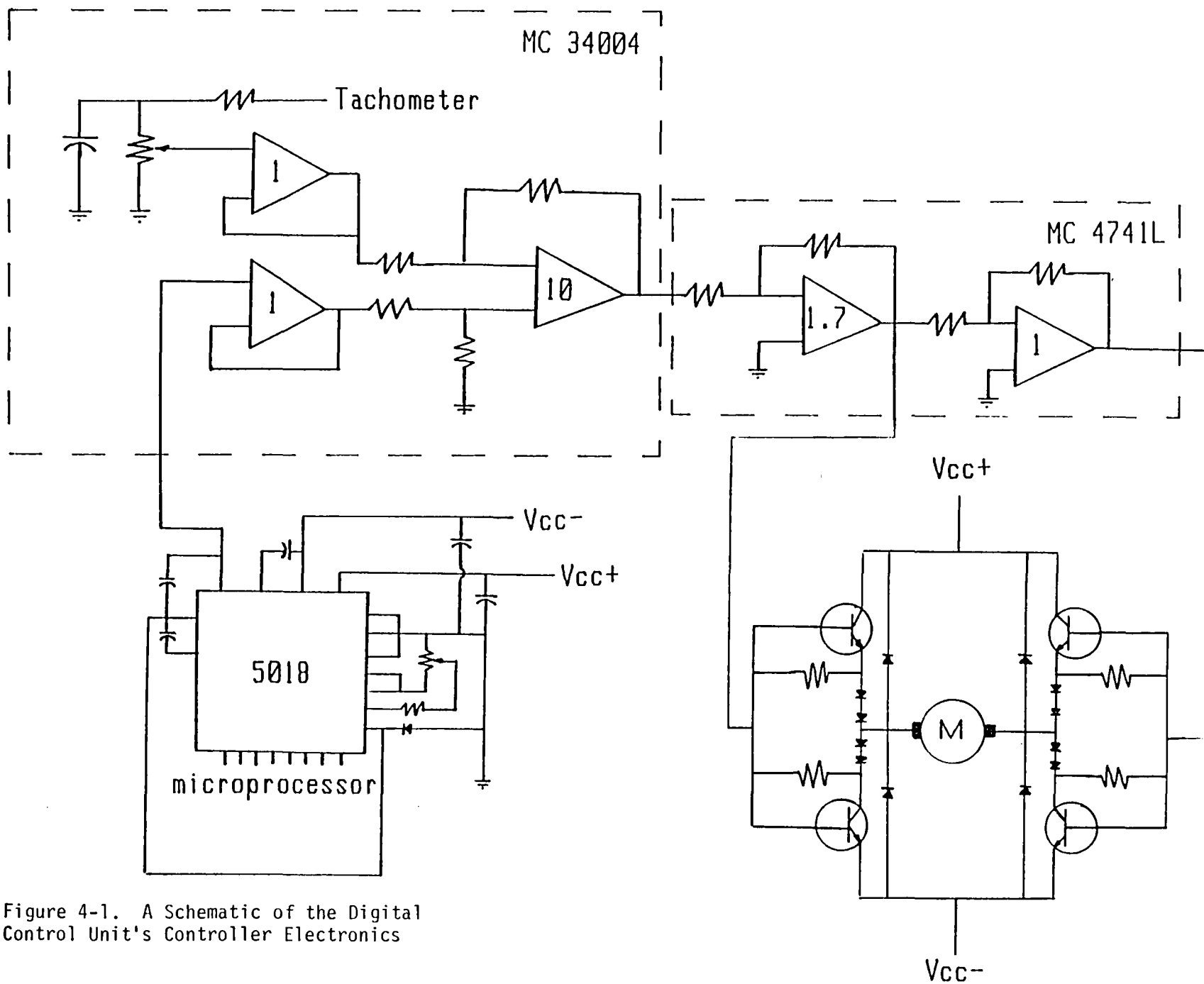
Figure 4-1. A Schematic of the Digital
Control Unit's Controller Electronics

Part Number	Description
5018	D/A Converter
MC 34004	Quad Op-Amp
MC 4741L	Quad Op-Amp
LM 317	Pos Voltage Regulator
LM 337	Neg Voltage Regulator

Table 4.1. The components of the digital control unit.

The MC 34004 receives the analog velocity command signal from the 5018. The MC 34004 compares the command signal to the analog tachometer signal and outputs a voltage signal equivlaent to ten times the difference of the input signal voltages.

The first op-amp of the MC 4741L receives the difference or the error signal from the MC 34004 and outputs an inverted signal equivalent to 1.7 times the error signal. The output signal of the first op-amp is inverted through the second op-amp of the MC 4741L. The output of the first op-amp is sent to the left side of the H-configuration motor control, and the output of the second op-amp is sent to the right side of the H-configuration.

The H-configuration motor control unit consists of two LM 317 positive voltage regulators and two LM 337 negative voltage regulators. Each side of the H-configuration has one LM 317 and one LM 337. Connected to the top and bottom of the H-configuration are the positive and negative motor voltage supplies, respectively.

The H-configuration controls the direction of the current and the magnitude of the voltage through the motor circuit, based

on the polarity and magnitude of the output voltages of the MC
4741L. The magnitude of the voltage across the motor is
equivalent to twice the magnitude of either output voltage of the
MC 4741L. For a positive voltage output of the first op-amp of
the MC 4741L, the LM 317 of the left side of the H-configuration
will open allowing a current with an equivalent positive voltage
to flow to the left side of the motor. Corresponding to the
positive voltage output of the first op-amp of the MC 4741L there
will be an equivalent negative voltage output of the second op-amp
which will be sent to the right side of the H-configuration. The
negative voltage signal will open the LM 337 of the right side
allowing an equivalent negative voltage on the right side of the
motor. The current will flow from the left side of the motor to
the right side with a voltage drop equivalent to twice the
magnitude of the applied voltage of either the LM 337 or the LM
317. For a negative voltage output of the first op-amp of the MC
4741L, the current will flow from the right side of the motor to
the left side resulting in an opposite motor rotation.

The overall gain of the controller is 34, based on a gain
of 10 for the MC 34004, 1.7 for the MC 4741L, and 2 for the H-
configuration.

4.4 DCU VELOCITY CONTROL

The RAIMS robot velocity control system utilizes
proportional control and tachometer feedback to control the
velocity of the armature-controlled DC motors. There are five
separate velocity control systems, one for each degree-of-freedom

or joint of the articulated robot arm.

There are several governing equations for the armature-controlled DC motor. For the voltage drop in the motor circuit

$$E_a = Ri + E_b + Lsi \qquad (4.1)$$

where E_a is the applied voltage from the controller, E_b is the motor back emf, i is the armature current, R is the armature resistance, and L is the armature inductance.

For the torque balance

$$T_m = Jsw_m + Bw_m + T_1 \qquad (4.2)$$

where T_m is the motor torque, T_1 is the load torque, w_m is the angular velocity of the motor, J is the mass moment of inertia, and B is the rotational damping.

The torque constant, K_m, relates the motor torque to armature current

$$T_m = K_m i \qquad (4.3)$$

and a velocity constant, K_b, relates the back emf to the angular velocity

$$E_b = K_b w_m. \qquad (4.4)$$

In state equation form, these equations reduce to

$$s \left\{ \begin{matrix} i \\ w_m \end{matrix} \right\} = \begin{bmatrix} -R/L & -K_b/L \\ K_m/J & -B/J \end{bmatrix} \left\{ \begin{matrix} i \\ w_m \end{matrix} \right\} + \begin{bmatrix} 1/L & \emptyset \\ \emptyset & -1 \end{bmatrix} \left\{ \begin{matrix} E_a \\ T_1 \end{matrix} \right\} \qquad (4.5)$$

$$w_m = [\emptyset \quad 1] \left\{ \begin{matrix} i \\ w_m \end{matrix} \right\} \qquad (4.6)$$

The block diagram for the velocity control system is shown in Figure 4-2.

The transfer function for the motor angular velocity and the input velocity command signal for zero load torque is

$$\frac{w_m(s)}{V_c(s)} = \frac{K_c K_m}{(sL+R)(sJ+B) + (K_t K_c + K_b) K_m} \tag{4.7}$$

The transfer function for the motor angular velocity and the load torque for the case of zero command velocity input is

$$\frac{w_m(s)}{T_l(s)} = \frac{sL + R}{(sL+R)(sJ+B) + (K_t K_c + K_b) K_m} \tag{4.8}$$

The response of the electrical components of the DCU have been experimentally verified by transfer function analysis. These tests show the analysis to be accurate and the response of this DCU to be linear to high frequencies.

5.0 ACOUSTIC INTENSITY

The indirect method for calculating acoustic intensity was selected. A major reason for this decision was the computational flexibility afforded by this approach. To minimize the error in estimating acoustic intensity using the indirect method, the design of a multi-element probe was investigated. This probe consists of three pairs of phased-matched microphones. The spacings between the microphone pairs were adjusted to meet the conditions necessary for reliable acoustic intensity measurements.

Load Torque

$$V_c \rightarrow \boxed{\Sigma} \rightarrow \boxed{K_c} \rightarrow \boxed{\Sigma} \rightarrow \boxed{1/(sL+R)} \rightarrow \boxed{K_m} \rightarrow \boxed{\Sigma} \rightarrow \boxed{1/(sJ+B)} \rightarrow W_m$$

$\boxed{K_b}$

$\boxed{K_t}$
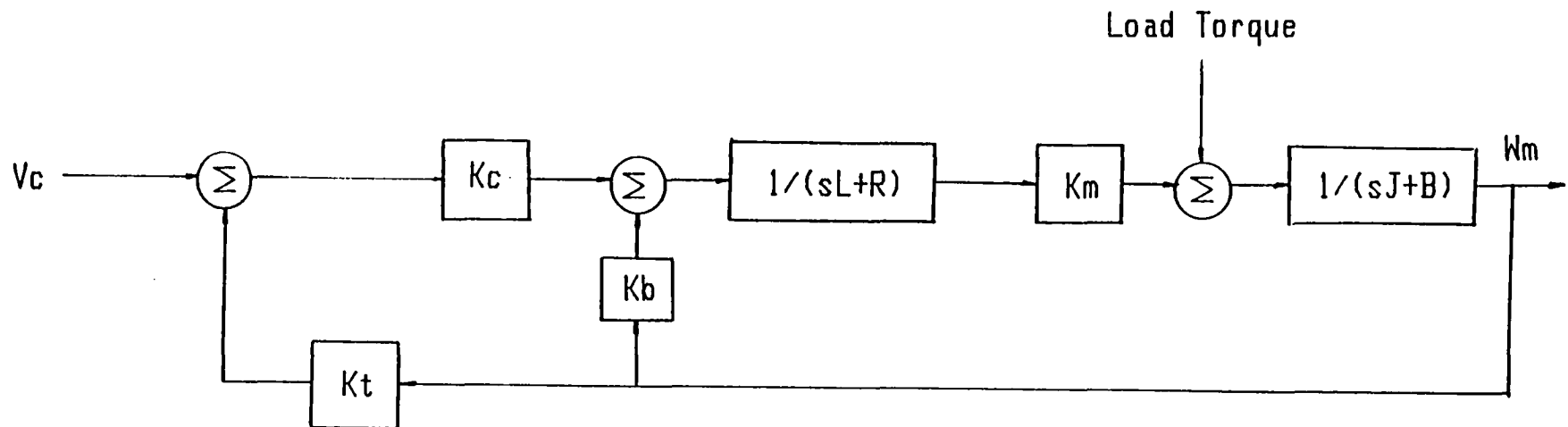
Block Diagram of Motor Driver System

Figure 4-2.   Instrumentation robot velocity control system.

5.1 BACKGROUND

Acoustic intensity is the time-averaged product of the instantaneous pressure and particle velocity.

$$I = \overline{P(t) \cdot U(t)} \qquad (5.1)$$

Since it is a vector quantity, acoustic intensity measurements can be used to measure the directional characteristics of an acoustic field. Only the resistive properties of the acoustic field are measured using this technique. The reactive part of the sound field has zero acoustic intensity because sound pressure and the reactive part of particle velocity are 90 degrees out of phase. Acoustic intensity measurements are not affected by standing waves or other reactive fields. These characteristics make acoustic intensity measurement a practical tool for locating and analyzing noise sources in complex reverberant environments.

Because of the difficulty in measuring particle velocity, the first acoustic intensity meters (Ref. 14) had limited use. However, the development of digital instruments has provided suitable computational power for calculating acoustic intensity through a direct (Ref. 12, 15) and indirect (Ref. 2, 3) method. Both acoustic intensity measurement techniques are basedon a two microphone measurement of the acoustic field. Orientating the microphones in the "r" direction, one in front of the other, particle velocity and sound pressure can be calculated from the sound pressure, $P_1(t)$ and $P_2(t)$, recorded by the two microphones. The following equations are used to estimate particle velocity and sound pressure in the "r" direction for a point in the acoustic

field.

$$U(t) = - \frac{1}{\rho \Delta r} (P_2 - P_1) dt \qquad (5.2)$$

$$P(t) = \{P_1(t) + P_2(t)\}/2 \qquad (5.3)$$

The direct method of sound intensity measurement uses a digital circuit to calculate acoustic intensity based on equations (5.2) and (5-3). The direct method determines acoustic intensity using the following equation.

$$\hat{I}_r = - \frac{1}{\rho \Delta r} \overline{\{(P_1 + P_2) \ (P_2 - P_1) dt\}} \qquad (5.4)$$

A dedicated acoustic intensity system using the direct method is commercially available.

The indirect method calculates sound intensity by using a two channel spectrum (FFT) analyzer interfaced to a calculator/computer. The analyzer computes the cross-spectrum from the two pressure measurements, $P_1(t)$ and $P_2(t)$. From this reading, the imaginary part of the cross-spectrum is used in the following equation to determine the acoustic intensity.

$$\hat{I}_r = - \int_0^\infty \frac{IM(G_{12}(f))}{2 \pi f \rho \Delta r} df \qquad (5.5)$$

A calculator or computer is necessary for this system. For the interested reader a complete development of the direct and indirect method for calculating acoustic intensity has been presented in several papers (Ref. 2, 3, 4, 6, 12, 15).

Studies (Ref. 3, 6, 15, 16, 17) using both techniques,

27

direct and indirect, have documented certain limitations on the accuracy of measuring acoustic intensity. Errors in estimating acoustic intensity involve microphone spacing, distance from noise source, type of noise source, frequency band, phase characteristics of the microphones and measuring system and directional characteristics of the microphones. RAIMS is designed to meet the conditions necessary for reliable acoustic intensity measurements. This is accomplished by adjusting system components and parameters to minimize these errors.

5.2 ARRAY PROBE DESIGN

The intensity probe used in RAIMS should measure acoustic intensity within 1 dB error for the frequency range from 50 to 10,000 Hz. Based on Thompson's research (Ref 16), the RAIMS probe would require at least three pairs of phased matched microphones. Microphone spacing for each pair was determined by the following equations proposed by Thompson.

$$0.1 \leq \kappa \Delta r \leq 1.3$$

$$0.0 \leq \Delta r/r \leq 0.5$$

where,
Δr = spacing between microphones
r = distance from noise source to center point between the microphones
κ = wave number

An alternative transducer arrangement would consist of a single pair of phase-matched microphones mechanically positioned by a drive system. A small stepper motor could be used to vary the microphone spacing, optimizing the intensity measurement for each frequency band.

The RAIMS robot is designed to operate with a maximum end effector load of approximately one kilogram. This is a major consideration when selecting the probe's microphones. At present, several probe designs are under consideration.

6.0 RAIMS SYSTEM SOFTWARE

A series 200 Hewlett Packard desktop computer controls and processes data from the DCU and the HP-3582A spectrum analyzer. A flow chart of the RAIMS operating system is shown in Figure 6-1. The RAIMS operating system is a composite of several subprograms. The first subprogram presents basic system operating conditions including necessary hardware and input information. A subroutine of the information subprogram is used to calibrate the acoustic intensity probe transducers, HP-3582A spectrum analyzer and the robot arm. The HP-3582A spectrum analyzer and an acoustic tube with an anechoic termination are necessary equipment for operating the transducer calibration software. The subroutine for calibrating the instrumentation robot involves driving the robot arm to several mechanical stops. During this process the position of the robot is measured by the robot's optic encoders and passed through the DCU to the computer system for evaluation. All calibration data is stored in the system's mass storage unit and is used to initialize the system.

Two scan types can be selected for analyzing the acoustic field. Both perform point to point position control. The scan types can be either pre-programmed scans or programmable scans controlled by the series 200 computer keyboard. The pre-
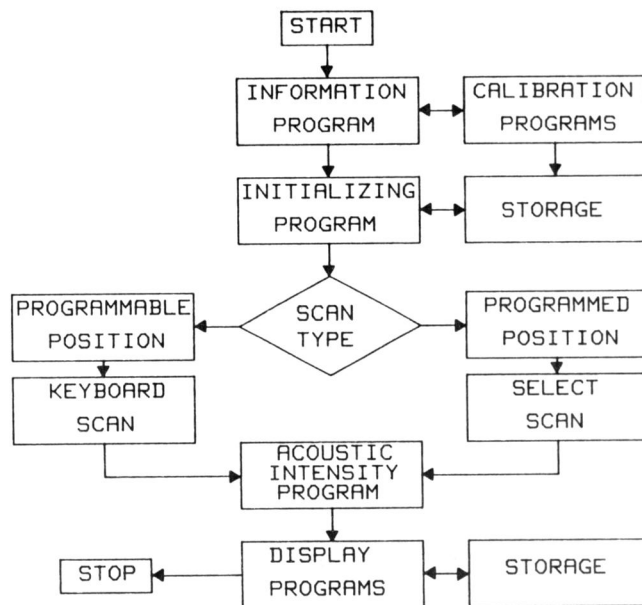
Figure 6-1. Flow chart of RAIMS operating system.
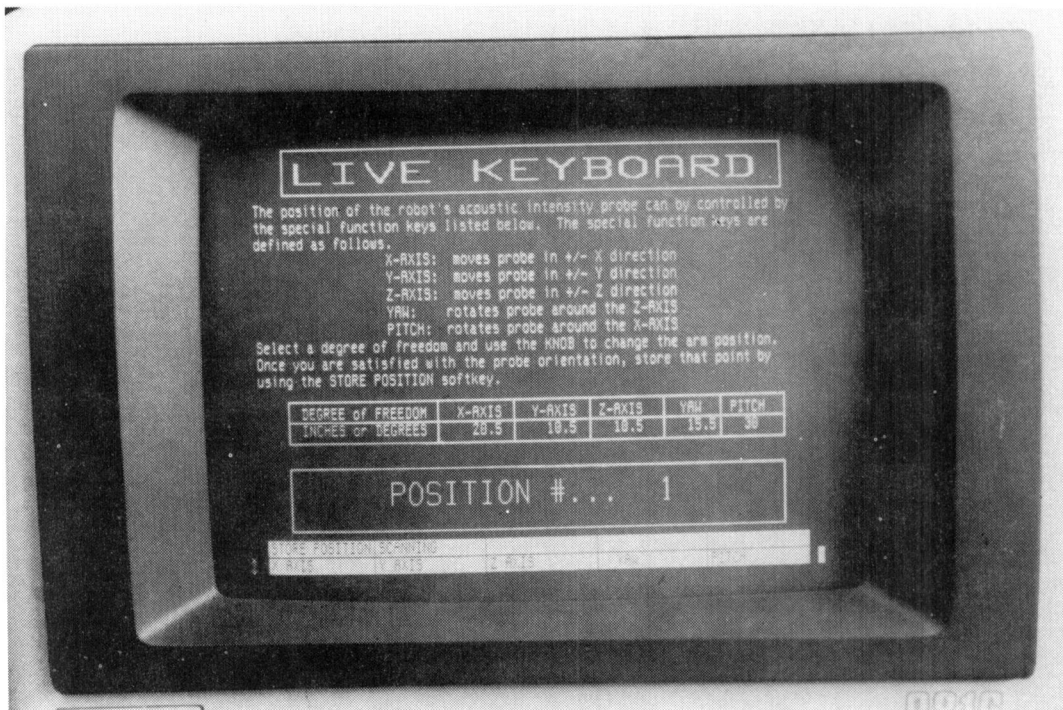
Figure 6-2. Illustration of "Live Keyboard" display on desktop computer.

30

programmed scans include planes, lune (spherical) sections, and
cylinders. The system operator selects certain pre-programmed
scan parameters such as position, orientation and area of the
plane scan. The programmable scans allow the system operator to
select over 800 points for acoustic intensity analysis by either
walking the robot arm through the scan or programming a scan point
by point. An example of the "live keyboard" control of the
instrumentation robot arm is shown in Figure 6-2.

After selecting and programming the scan information, the
system automatically measures the acoustic intensity and stores
the data for the complete test. The acoustic intensity subprogram
positions the robot arm, auto-scales the HP-3582A to collect sound
pressure data, retrieves the cross-spectrum data and calculates
the acoustic intensity while moving the robot arm to the next
measurement point. A display subprogram presents the data for
each measurement.

Due to the potentially large quantity of data generated by
RAIMS, two display subprograms were developed. Both are written
for the HP 200 series desktop computer.

The local data display subprogram output in Figure 6-3,
documents the acoustic intensity calculated at the past probe
position. This display is updated as new intensity data is
collected. Past acoustic intensity data is not lost during the
updating process because all data collected by RAIMS is stored.

To enhance the information of the local acoustic intensity
measurements, a color-coded display of the acoustic intensity
field is generated by the acoustic color-graphics subprogram.

RAIMS
NASA/LEWIS

Measurement Site .... TEST SPECIMEN #1

Probe Location :

Xaxis ...	20.5
Yaxis ...	10.5
Zaxis ...	10.5
Yaw	15.5
Pitch ...	30

Position Number 1

Octave	31.5	63	125	250	500	1K	2K	4K	8K	16K	Lin
IL in dB	45	60	52	49	48	0	0	0	0	0	66

Frequency Response of Acoustic Intensity
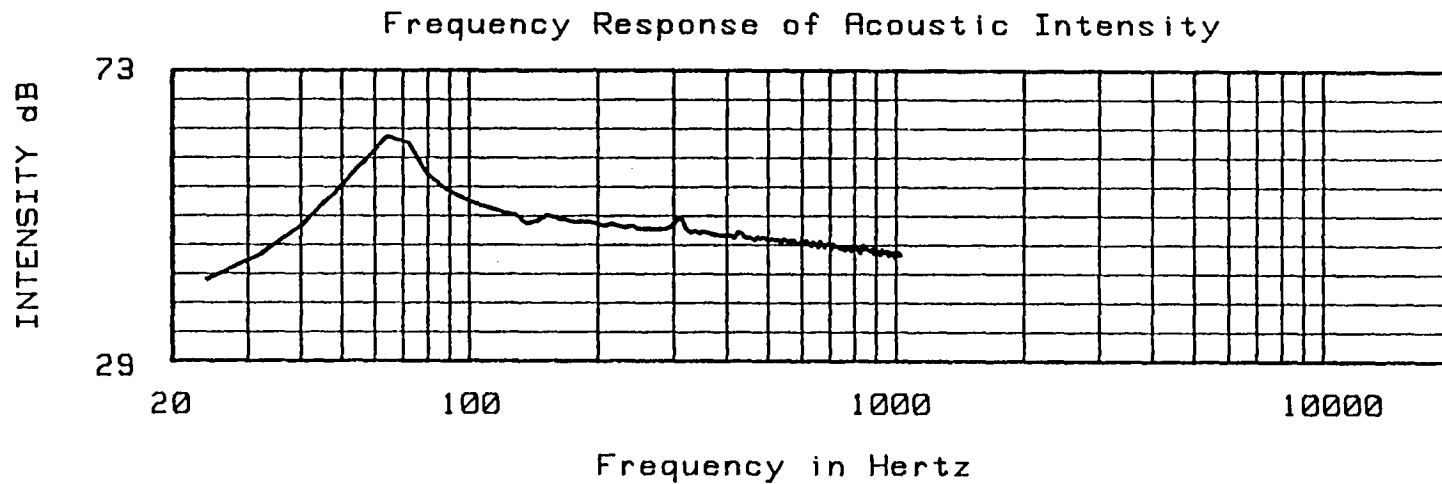
Figure 6-3. Typical output display of local acoustic intensity data.

This subprogram superimposes color-coded acoustic intensity information on the surface of a grid model of the test specimen. As the acoustic intensity scan progresses, the grid model becomes completely annotated with color-coded data. The acoustic color graphics subprogram has many graphical control features to assist the operator evaluate the acoustic intensity information. These features include a zoom factor to enlarge the model on the screen, a view vector to rotate the test specimen and a surface element adjustment to change the size and shape of the model's grid work. Figure 6-4 illustrates a grid model for a helicopter transmission test specimen.

7.0 SPEAKER SYSTEM TESTS

The accuracy and repeatability of detecting a noise source using RAIMS were evaluated using a speaker system. The system consisted of four 7.6 centimeter diameter speakers. An 800 Hz signal was used to drive the second speaker in the system. RAIMS was programmed to generate a 75 centimeter by 60 centimeter planar scan fo the array 15 centimeters from the surface. A measurement was taken every .75 centimeter along the scan line. The planar scan consisted of 48 lines. Figure 7-1 shows the instrumentation robot scanning the speaker system during this test. The results are as follows.

7.1 RAIMS ACCURACY

The .75 centimeter resolution planar scan detected the

OH 58

HELICOPTER

TRANSMISSION
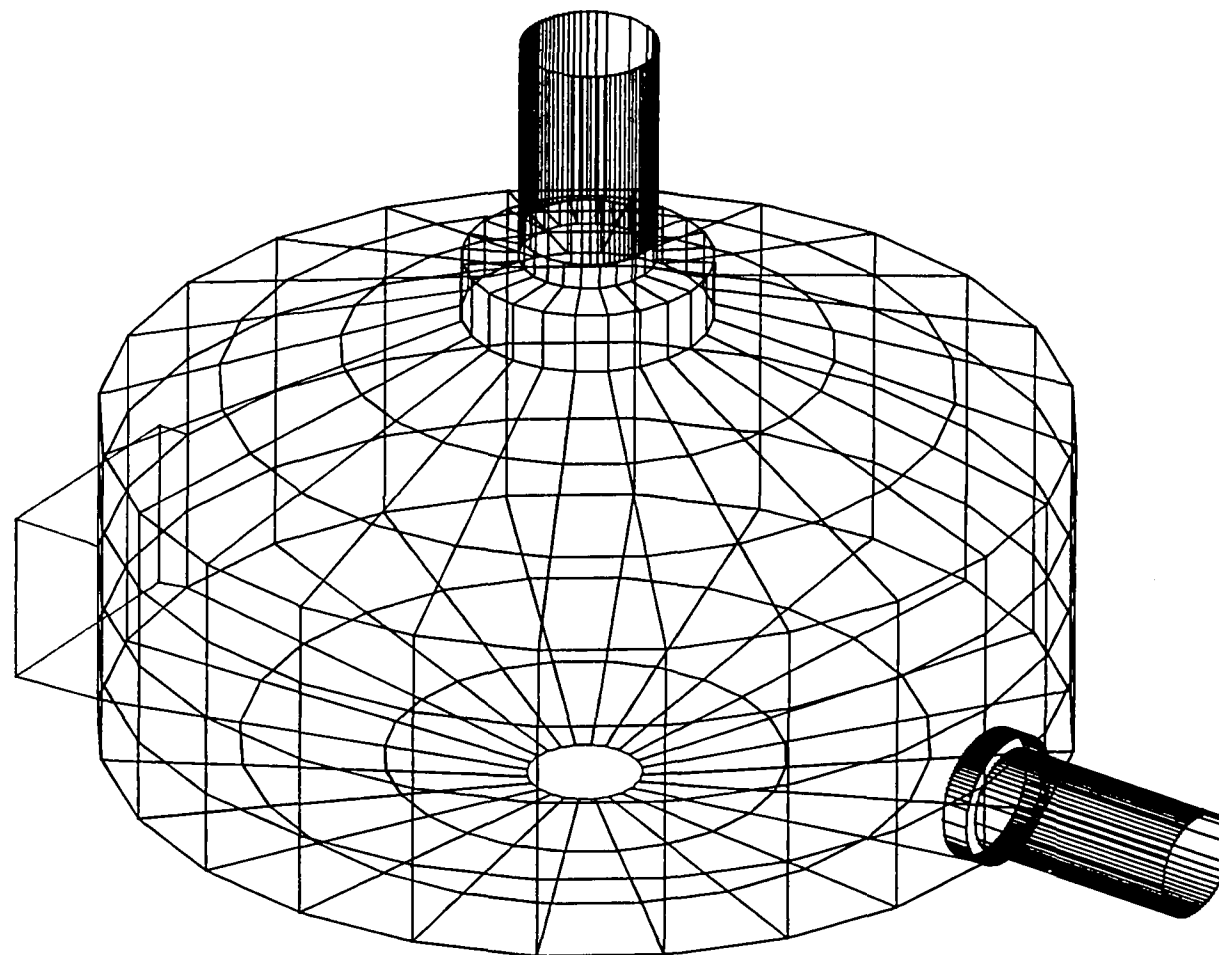
Figure 6-4.   Grid model of helicopter transmission used in the color-coded acoustic intensity data display.
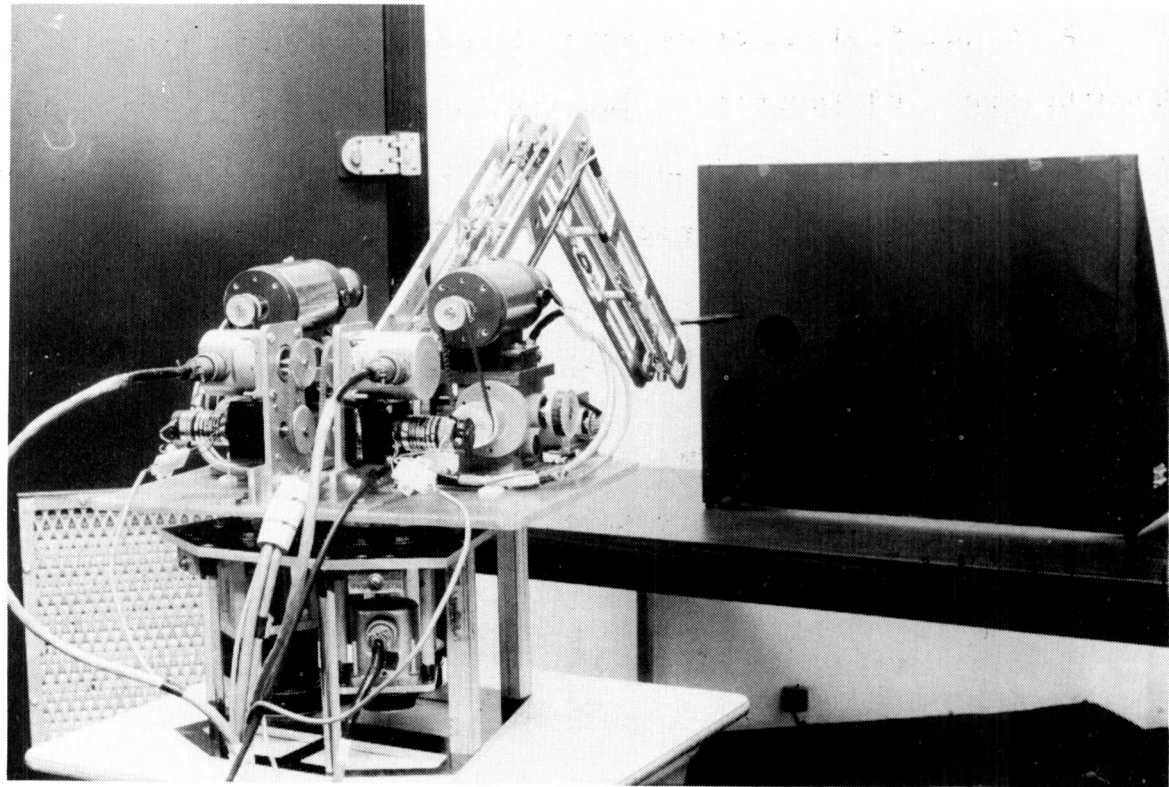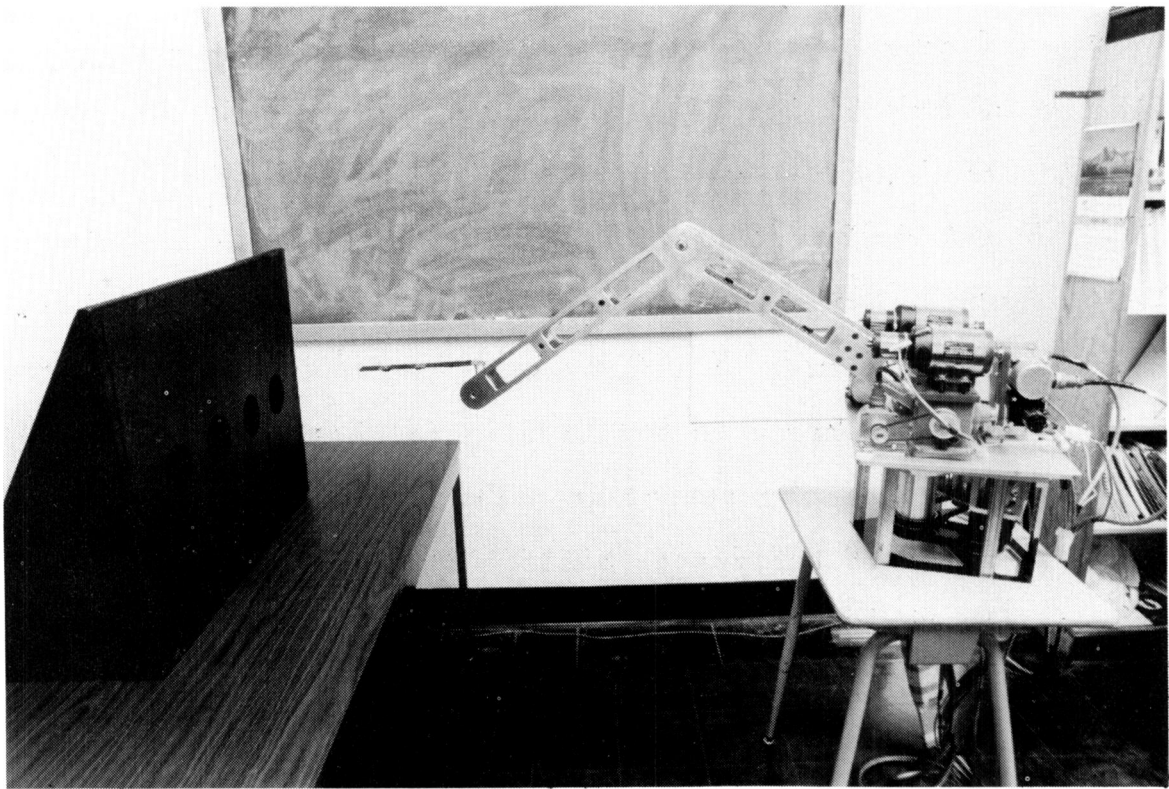
Figure 7-1. Instrumentation robot scans the speaker system.

35

single noise source in the array. The acoustic intensity generated by the 7.6 centimeter speaker dropped from .75 to 1.5 dB over the surface of the speaker. The maximum intensity was located at the center of the speaker. Figure 7-2 is a contour map of the acoustic intensity measured across a 15 centimeter wide by 75 centimeter long area of the speaker system centered over the speaker array. Accuracy in positioning the probe for intensity mapping is of major importance in noise identification. A 1.25 centimeter error in horizontal positioning the probe over the center of the speaker would cause a .7 dB reduction in sound intensity. This is illustrated in Figure 7-3.

7.2 RAIMS REPEATABILITY

A unique feature of RAIMS is the accuracy in repeating an intensity scan and locating noise sources. The resulting acoustic intensity scans did not change by more than ±5% in the region of high intensity during a repeat analysis of the speaker array. Acoustic intensity data for two scans of the same zone on the speaker array surface are shown in Figure 7-4.

7.3 SPACE-AVERAGING TECHNIQUE

The space averaging technique developed by Chung (Ref 5) consisted of collecting data from the intensity probe while uniformly scanning a surface area. Both time and space averaging of the intensity data are accomplished in this procedure. According to Chung (Ref 5), this technique reduces the number of measurements required for an "accurate" acoustic intensity test.

Magnitude of
Acoustic Intensity

15 cm

#1 #2 #3 #4

75 cm

Section of
Speaker System
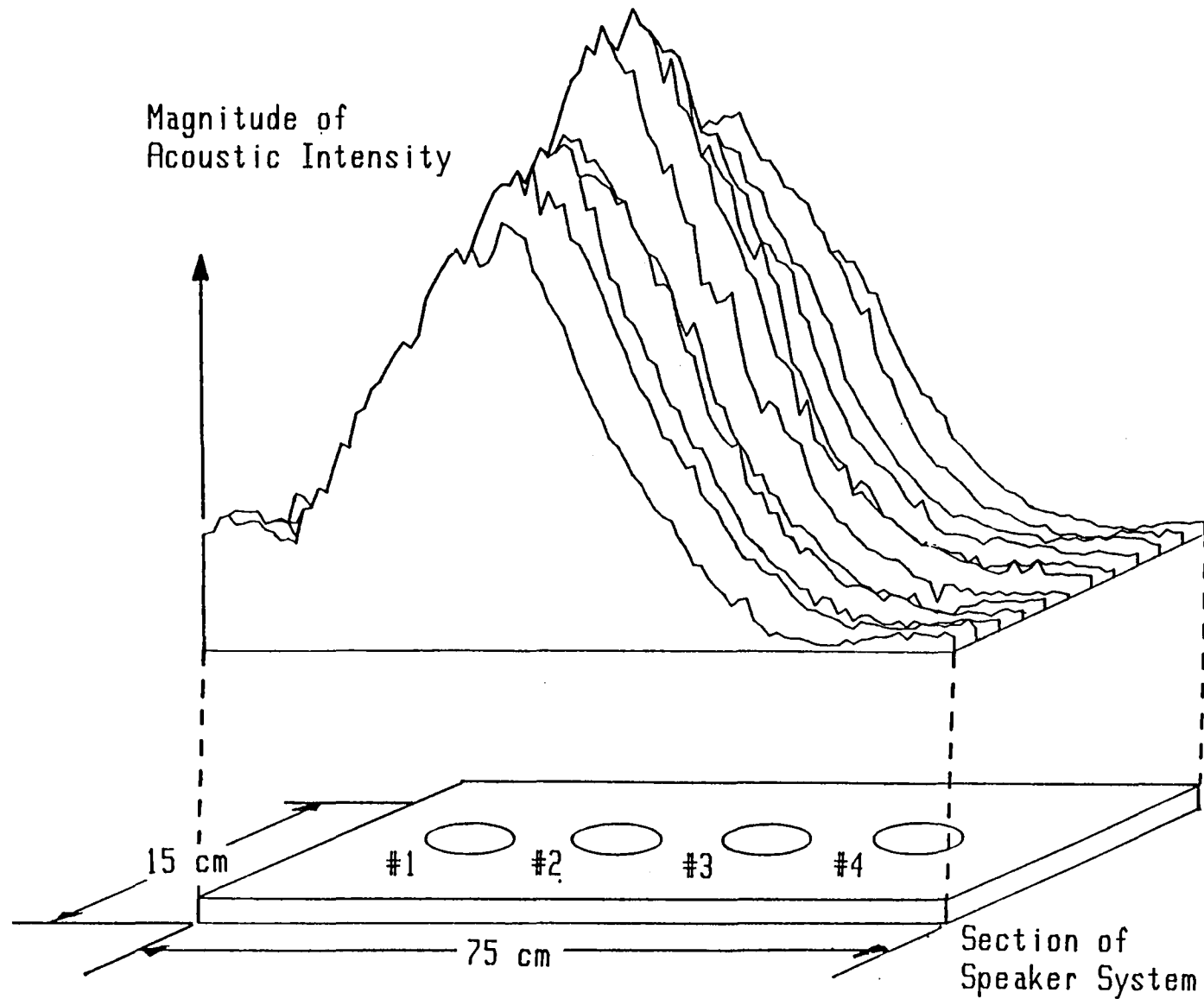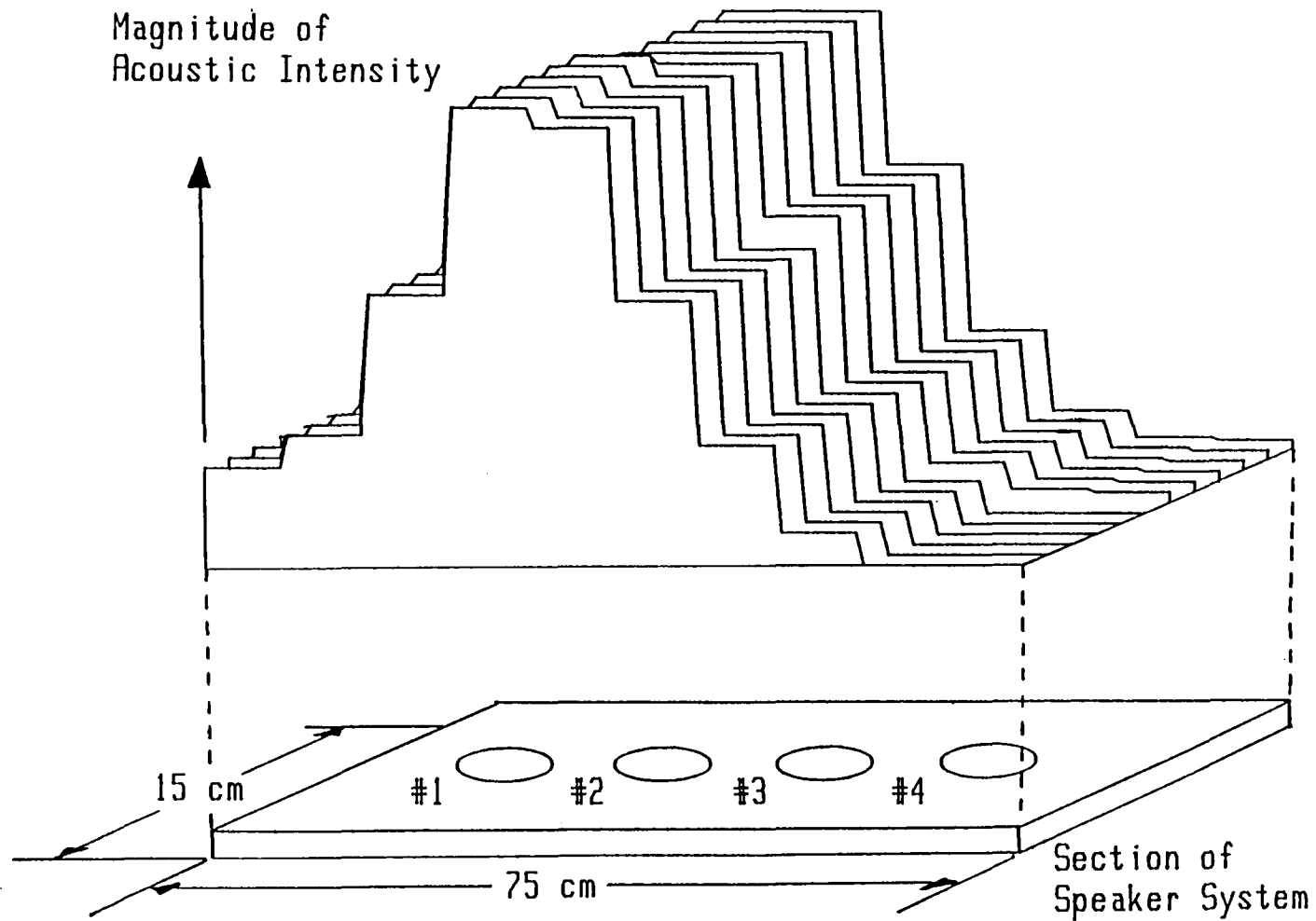
Figure 7-2. An acoustic intensity contour map of a 15 by 75 centimeter area of
the speaker system produced using RAIMS. Speaker # 2 was generating an 800 Hz
sound during this scan. RAIMS determined the acoustic intensity of .75 cm
intervals along twelve scan lines in the near field.
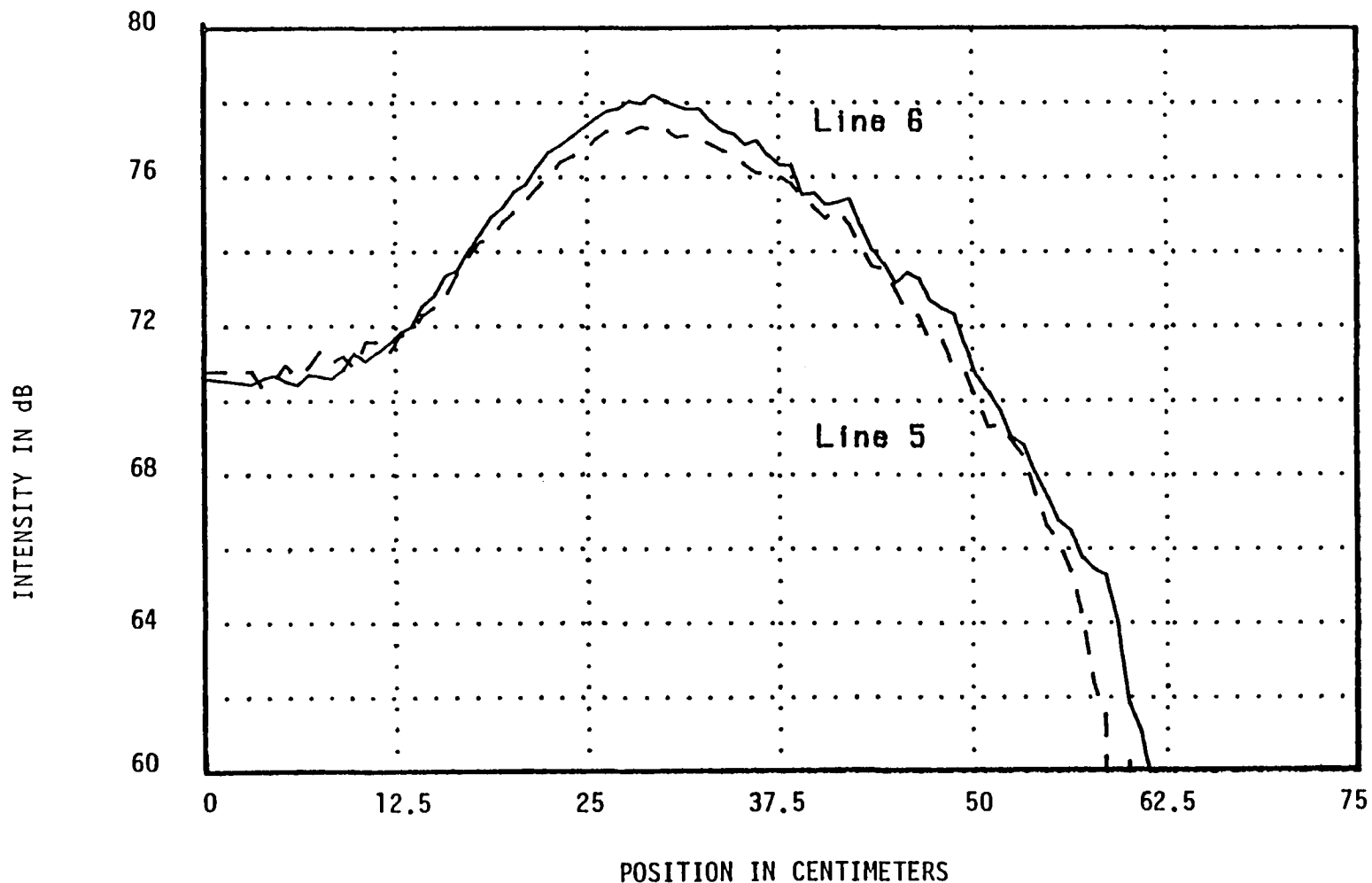
Figure 7-3. Two acoustic intensity plots for a scan across the speaker system are generated by RAIMS. Line 6 is intensity data for a scan passing over the center of the transmitting speaker while line 5 is 1.25 cm off center. Intensity levels below 60 dB were not considered ue to the noise level of the probe.
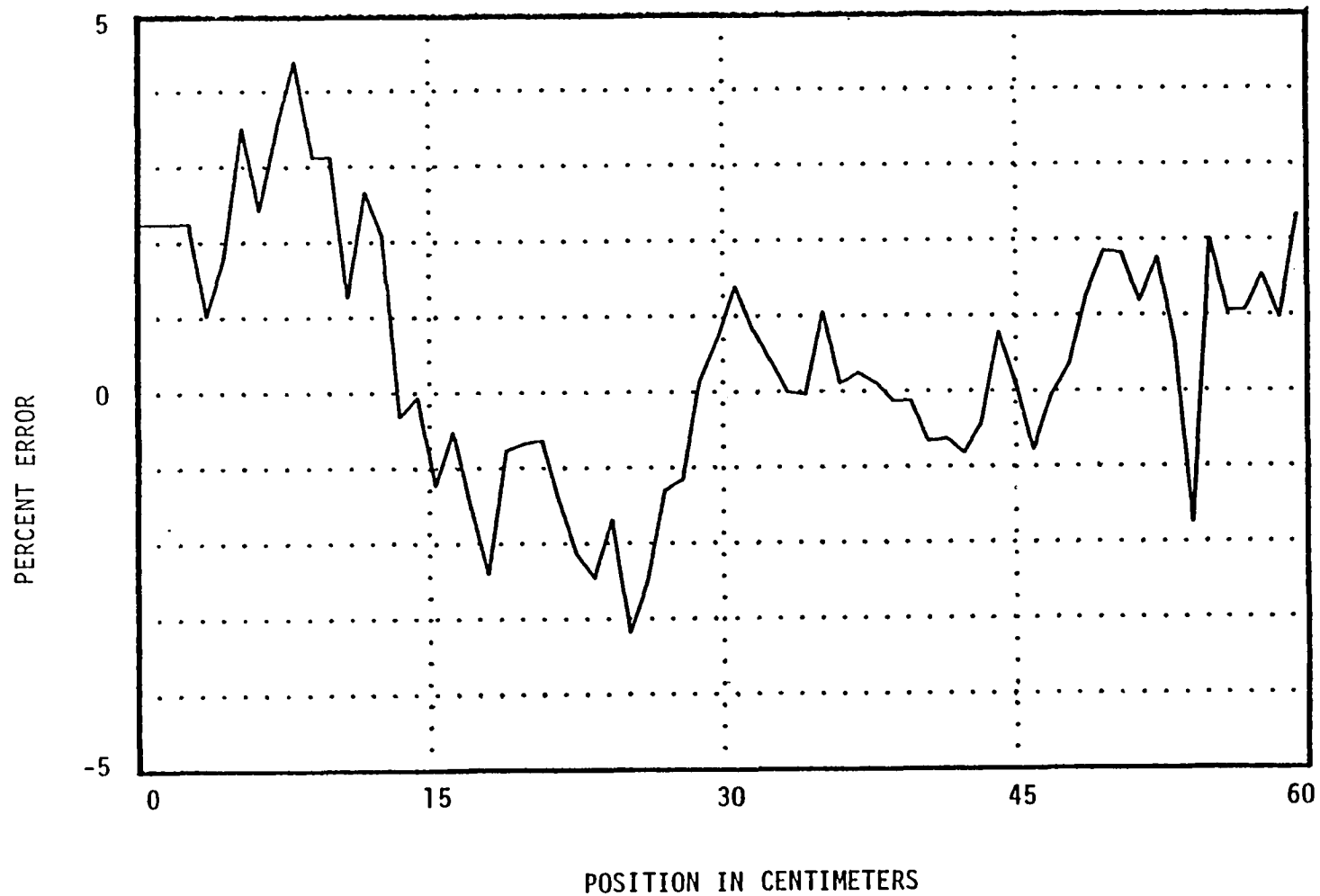
Figure 7-4. Percent error in repeatability while scanning across the center speaker row. Percent error beyond 60 cm was not calculated due to low sound levels.

RAIMS was programmed to perform a space-time averaging analysis of the speaker system. As configured in the previous measurements, only one speaker was generating sound. An .800 Hz tone was used for this test. From the 15 centimeter by 75 centimeter section of the speaker system, twenty, 7.5 cm by 7.5 cm areas were defined. The robot manipulator collected intensity data from each section for about one minute while scanning the area in increments of 1.25 cm. This scan was semi-continuous by programming the arm to proceed from point to point with no pause. Results of this test are illustrated in Figure 7-5. Comparing the high resolution point to point acoustic intensity contour map in Figure 7-2 with the acoustic intensity contour map generated by using the space-averaging technique shows that the spatial accuracy of locating the noise source in the speaker system was reduced by using this technique.

7.4 CONCLUSIONS

1)   The Robotic Acoustic Intensity Measurement System substantially reduced the labor involved in collecting acoustic intensity data.

2)   RAIMS improved the spatial resolution of acoustic intensity maps and the location of a noise source.

3)   RAIMS demonstrated good repeatability in obtaining acoustic intensity data due to its position accuracy.

Magnitude of
Acoustic Intensity

15 cm

#1   #2   #3   #4

75 cm

Section of
Speaker System

Figure 7-5. An acoustic intensity contour map of a 15 by 75 centimeter area of the speaker system produced using RAIMS in a space averaging mode. Speaker # 2 was generating an 800 Hz sound during this scan as in the first RAIMS test.

8.0 GENERAL VIBRATION CHARACTERISTICS OF THE BELL HELICOPTER OH-58 TRANSMISSION

A survey of general vibration characteristics of the Bell OH-58 helicopter transmission was conducted to determine dominant spectral information to be observed during RAIMS studies. An array of twelve accelerometers were used in this study. Nine accelerometers were coupled to the helicopter transmission housing while three additional accelerometers monitored vibration levels generated by the 85° bevel gearbox and the closing end gearbox. Vibration levels were recorded while the transmission drive system was running at the operating points cited in table 1. Frequency data was obtained from 10 Hz to 10,000 Hz which is the calibrated range of the accelerometers used. The following results were concluded from this study.

The dominant closed end gearbox frequencies* are:

1) 720 Hz
2) 1600 Hz
3) 2320 Hz
4) 3040 Hz

The dominant 85° bevel gearbox frequencies* are

1) 1600 Hz
2) 3040 Hz

Some dominant helicopter transmission frequencies* are:

1) 1920 Hz
2) 3840 Hz
3) 5120 Hz
4) 5760 Hz
5) 8000 Hz
6) 8640 Hz
7) 9200 Hz

*Bandwidth of 120 Hz.

42

	Input	Output
Speed (RPM)	6060	~~370.4~~ 347.5
Load (in-lbs)	3086	~~52410~~ 53116
Power (HP)	~~501.4~~ 296.7	~~287.7~~ 292.9

Table 8-1. Operating conditions of the Bell OH-58 helicopter transmission.

The vibration data is spatially presented in relation to the accelerometer position on the helicopter transmission in figures 8-1 through 8-3. Figures 8-4 and 8-5 illustrate the vibration data in a three-dimensional format. Appendix B contains a series of graphic illustrations locating the positions of acceleration readings on the helicopter transmission. Vibration data for both the 0-2500 Hz bandwidth and 0-10,000 Hz bandwidth is also included in this appendix.

Several sound pressure readings were recorded during the vibration tests. The results, shown in figures 8-6 and 8-7, indicate that the sensing elements used in the RAIMS system have the appropriate sensitivity and bandwidth to detect the noise characteristics of the helicopter transmission system.

The results of this study will serve as a reference during the acoustic intensity tests conducted on the Bell OH-58 helicopter transmission.

Acceleration data in g's at position #9

Acceleration data in g's at position #8

ACCELEROMETER LOCATIONS

FRONT-TOP VIEW

Acceleration data in g's at position #6

Acceleration data in g's at position #7
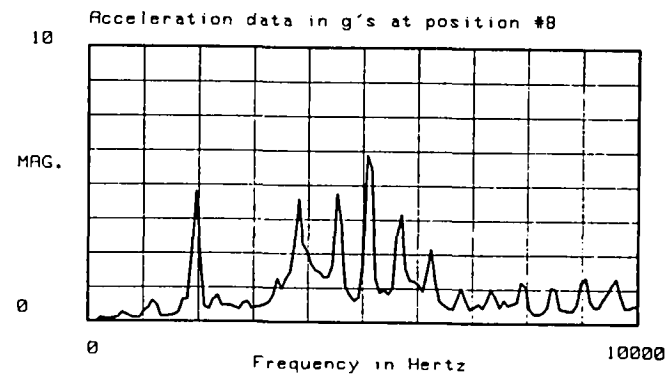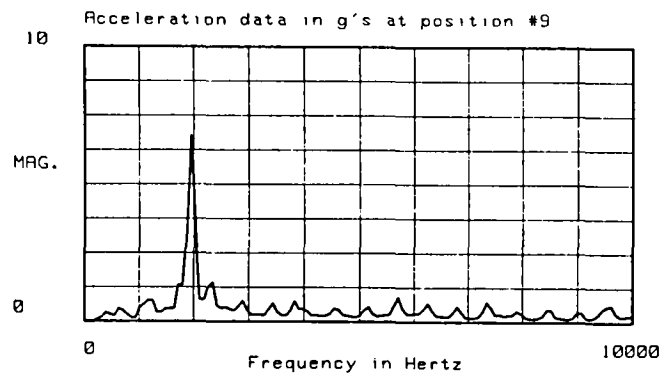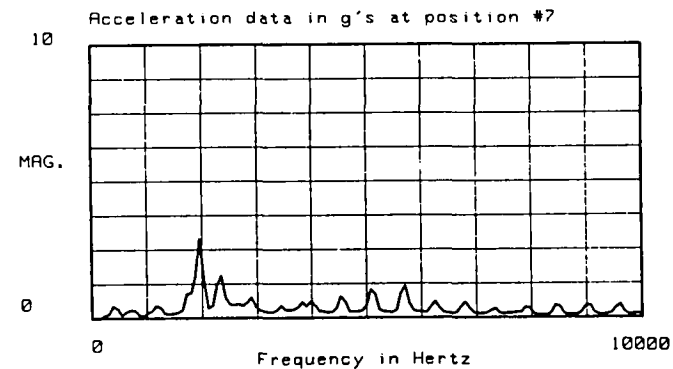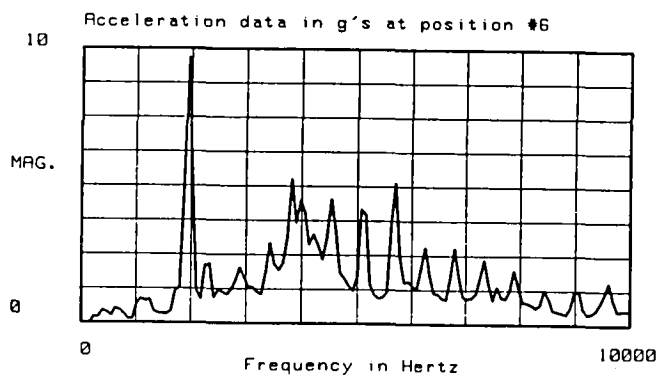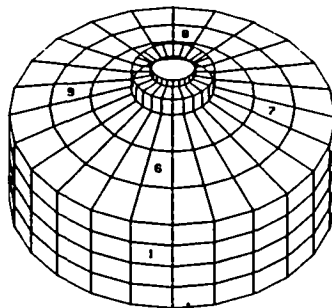
Figure 8-1. Four frequency response spectrums of the RMS g-level of vibration for the top section of the helicopter transmission are presented. The helicopter transmission graphic illustrates the position of the accelerometers.
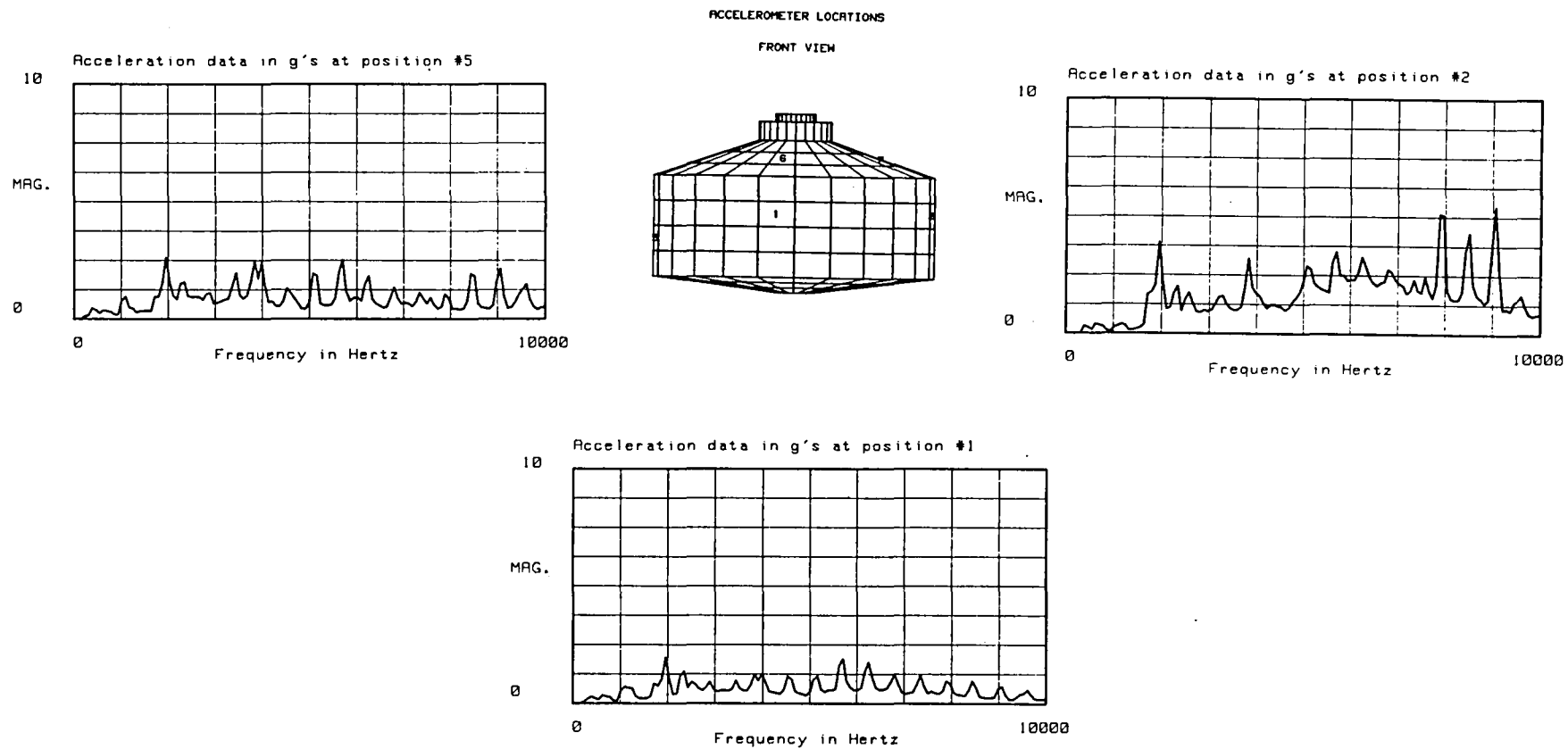
Figure 8-2. Three frequency response spectrums of the RMS g-level of vibration for the front section of the helicopter transmission are presented. The helicopter transmission graphic illustrates the position of the accelerometers.

ACCELEROMETER LOCATIONS

BACK VIEW

Acceleration data in g's at position #3

10

MAG.

0

0   10000

Frequency in Hertz

Acceleration data in g's at position #4

10

MAG.

0

0   10000

Frequency in Hertz
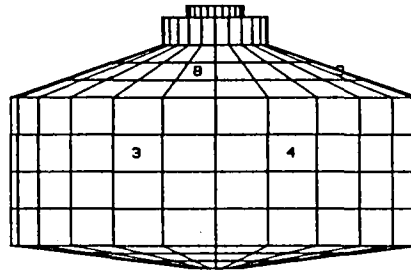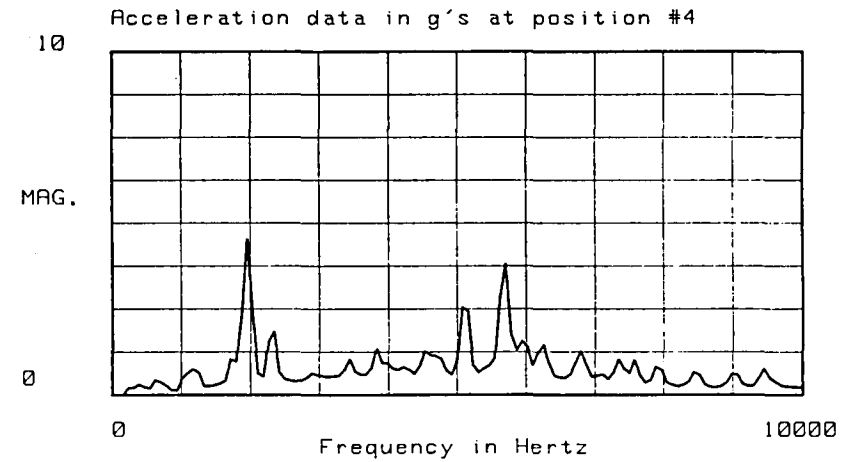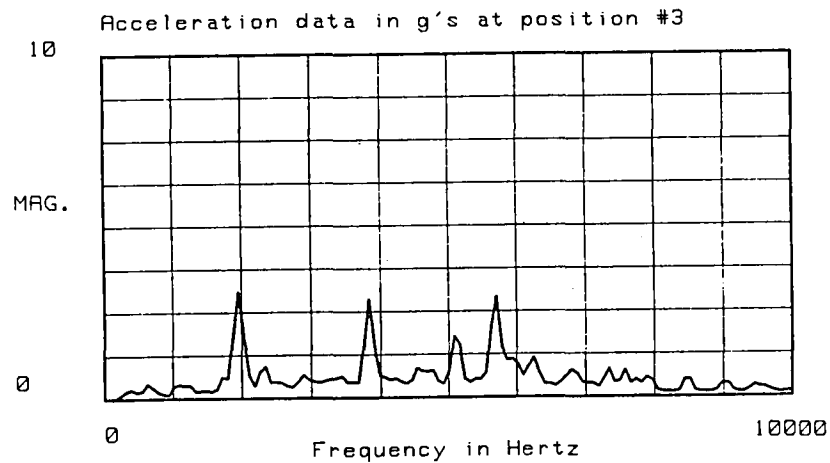
Figure 8-3. Two frequency response spectrums of the RMS g-level of vibration for the back section
of the helicopter transmission are presented. The helicopter transmission graphic
illustrates the position of the accelerometers.

ACCELEROMETER DATA FOR THE

BELL OH58 HELICOPTER TRANSMISSION
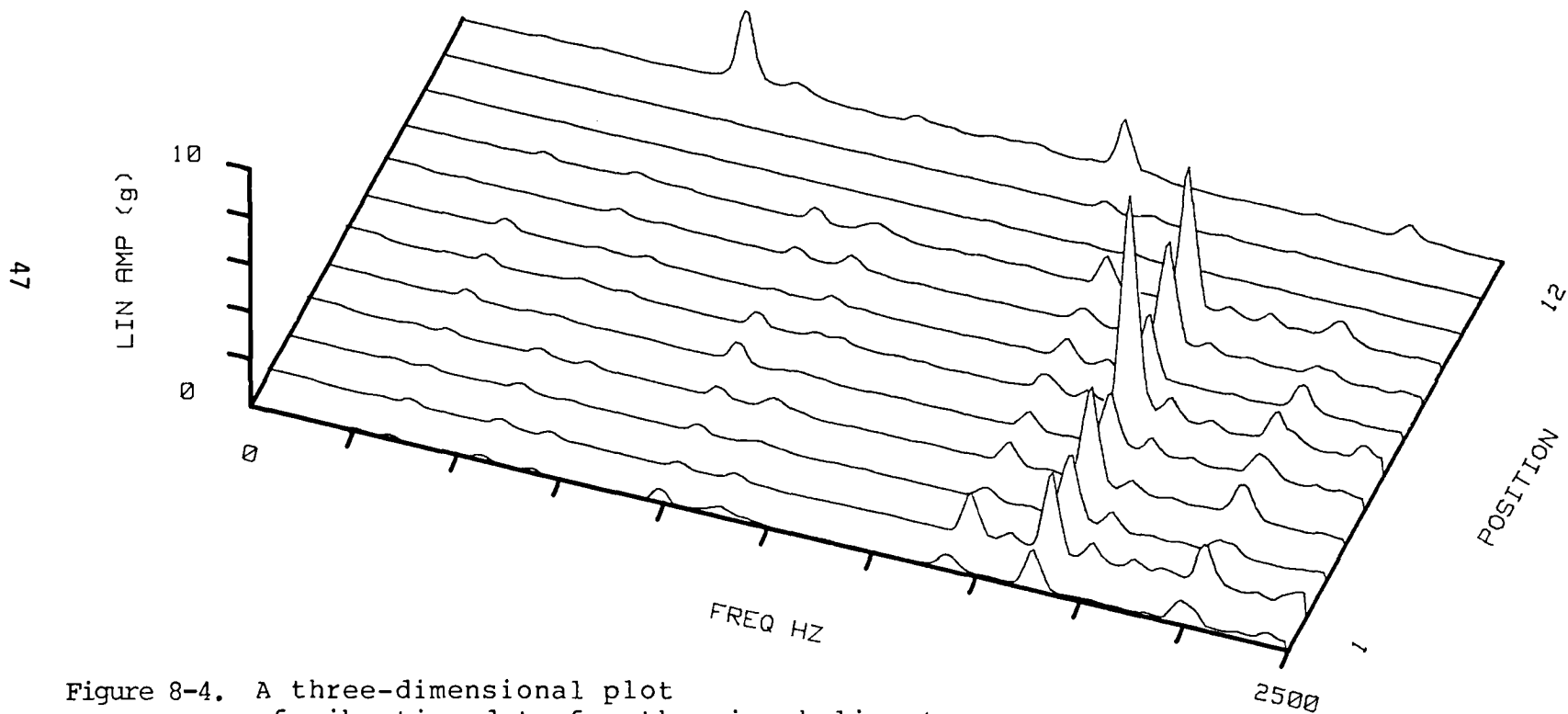
Figure 8-4. A three-dimensional plot
of vibration data for the nine helicopter
transmission locations, two 85° bevel gearbox locations
and one closed end gearbox location. Position numbers 1 through 9 correspond
to the helicopter transmission as cited in Appendix A. Position 10 and 11 are
located on the 85° bevel gearbox and position 12 is the closed end gearbox site.

ACCELEROMETER DATA FOR THE

BELL OH58 HELICOPTER TRANSMISSION
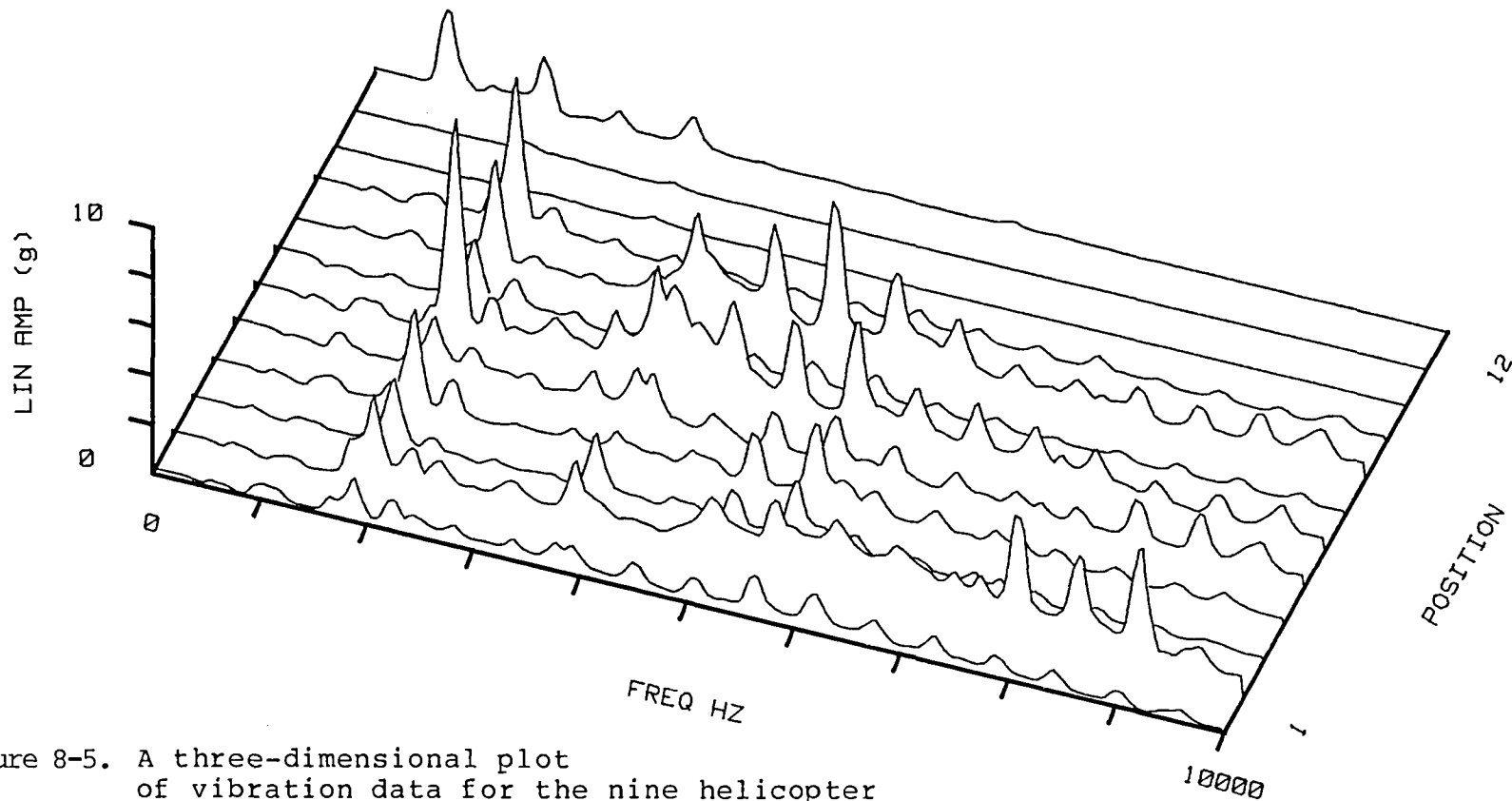
Figure 8-5. A three-dimensional plot
of vibration data for the nine helicopter
transmission locations, two 85° bevel gearbox locations
and one closed end gearbox location. Position numbers 1 through 9 correspond
to the helicopter transmission as cited in Appendix A. Position 10 and 11 are
located on the 85° bevel gearbox and position 12 is the closed end gearbox site.

ACCELEROMETER DATA FOR THE

BELL OH58 HELICOPTER TRANSMISSION

POSITION 13: SOUND PRESSURE (B&K)
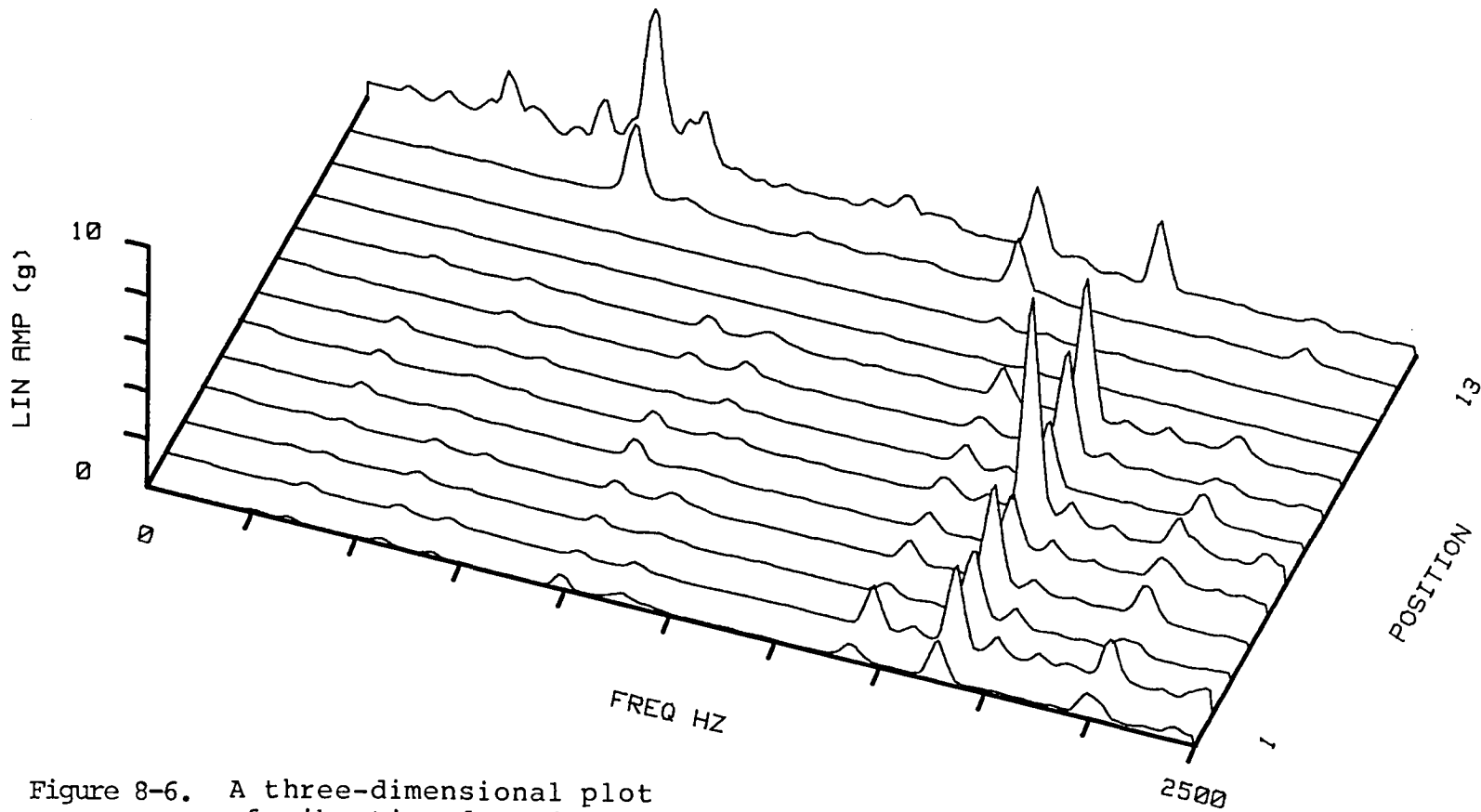
Figure 8-6. A three-dimensional plot
of vibration data for the twelve
locations measured in this test. Position 13
is the frequency response of the sound pressure in the test cell.

ACCELEROMETER DATA FOR THE
BELL OH58 HELICOPTER TRANSMISSION
POSITION 13:   SOUND PRESSURE
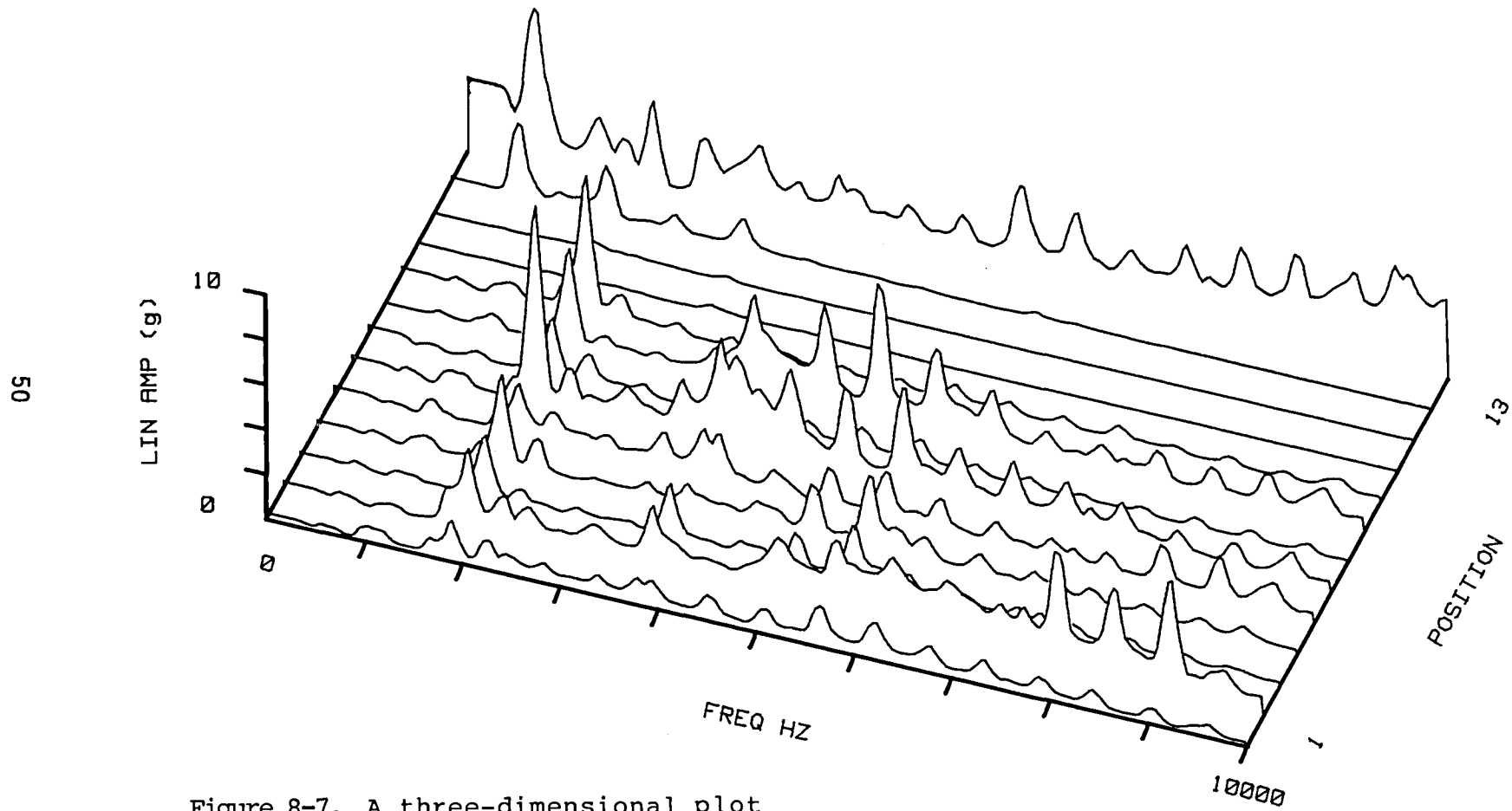
Figure 8-7. A three-dimensional plot
of vibration data for the twelve
locations measured in this test.   Position 13
is the frequency response of the sound pressure in the test cell.

REFERENCES

1) Alfredson, R. A., "A New Technique for Noise Source Identification on Multi-cylinder Automotive Engine," Proceedings of Noise-Con 77, 1977, pp 307-318.

2) Fahy, F. J., "Measurements of Acoustic Intensity using the Cross-Spectral Density of Two-Microphone Signals," Journal of the Acoustical Society of America, Vol. 62, No. 4, 1977, pp 1057-1059.

3) Chung, J. Y., "Cross-Spectral Method of Measuring Acoustic Intensity Without Error Caused by Instrumentation Phase Mismatch," Journal of the Acoustical Society of America, Vol. 64, No. 6, 1978, pp 1613-1616.

4) Chung, J. Y., Pope, J., "Practical Measurement of Acoustic Intensity - The Two-Microphone Cross-Spectral Method," Proceedings of INTER-NOISE 78, 1978, pp 893-900.

5) Chung, J. Y., Pope, J., and Feldmaier, D. A., "Application of Acoustic Intensity Measurements to Engine Noise Evaluation," General Motors Research Laboratories Publication GMR-2905, January, 1979.

6) Chung, J. Y., Blaser, D. A., "Recent Developments in the Measurements of Acoustic Intensity using the Cross-Spectral Method," S.A.E. Technical Paper #810396, February, 1981.

7) Fahy, F. J., "Measurements with an Intensity Meter of the Acoustic Power of a Small Machine in a Room." Journal of Sound and Vibration, Vol. 57, No. 3, 1978, pp 311-322.

8) Lambert, J. M., "The Application of a Modern Intensity-Meter to Industrial Problems: Example of in-situ sound power determination," Proceedings of INTER-NOISE 79, 1979, pp 227-231.

9) Gade, S., Wulff, H., and Ginn, K. B., "Sound Intensity Measurement Inside Aircraft," B & K Application Note 1982.

10) Gade, S., Wulff, H., and Ginn, K. B., "Sound Power Determination Using Sound Intensity Measurements, Part 1," B & K Application Note 1982.

11) Gade, S., Wulff, H., and Ginn, K. B., "Sound Power Determination Using Sound Intensity Measurements, Part 2," B & K Application Note 1982.

12) Fahy, F. J., "A Technique for Measuring Intensity with a Sound Level Meter," Noise Control Engineering, Vol. 9, 1977, pp 155-169.

13) Gade, S., "Sound Intensity (Part II. Instrumentation & Applications)," B & K Technical Review, No. 4, 1982.

14)   Olson, H. F., "System Response to the Energy Flow of Sound Waves," U.S. Patent No. 1,892,644, 1932.

15)   Gade, S., "Sound Intensity (Part I Theory)," B & K Technical Review, No. 3, 1982.

16)   Thompson, J. K., Tree, D. R., "Finite Difference Approximation Errors in Acoustic Intensity Measurements," Journal of Sound and Vibration, Vol. 75, No. 2, 1981, pp 229-238.

17)   Pavic, G., "Measurement of Sound Intensity," Journal of Sound and Vibration, Vol. 51, No. 4, 1977, pp 533-545.

APPENDIX A

Computer Simulation of Kinematics and Dynamics
of Proposed Robot Designs

As a design aid, the dynamic and kinematic solutions to the robot arm model were programmed into a computer system to analyze robot position, velocity, acceleration, and torque. A Hewlett-Packard 21MX computer system interfaced to a Lexidata color display system was used in this study. One section of the program graphically represented robot arm positions as generated by the kinematics solution. Figure A-1 illustrates the information provided by this analysis. Various scan algorithms for mapping acoustic intensity were also simulated in this study. The color graphics added a third dimension to the presentation of acoustic intensity data, as shown in figure A-2. The Lexidata system was also used to display dynamic characteristics of the robot arm design. Figures A-3 through A-6 are examples of typical output displays.

The kinematic and dynamic solution to the robot geometry problem presented in figure 3-2 is outlined below. Nomenclature for this analysis is given at the end.

UPPER ARM: B_1

$$\frac{R\ B_1}{\omega} = \dot{\theta}_2 \hat{n}_{21} + S_2 \dot{\theta}_1 \hat{n}_{22} + C_2 \dot{\theta}_1 \hat{n}_{23}$$

$$\frac{R\ B_1}{\omega} = C_1 \dot{\theta}_2 \hat{N}_1 + S_1 \dot{\theta}_2 \hat{N}_2 + \dot{\theta}_1 \hat{N}_3$$

$$\frac{R\ B_1}{\alpha} = \ddot{\theta}_2 \hat{n}_{21} + (C_2 \dot{\theta}_1 \dot{\theta}_2 + S_2 \ddot{\theta}) \hat{n}_{22} + (-S_2 \dot{\theta}_1 \dot{\theta}_2 + C_2 \ddot{\theta}_1) \hat{n}_{23}$$

$$\frac{R\ B_1}{\alpha} = (-S_1 \dot{\theta}_1 \dot{\theta}_2 + C_1 \ddot{\theta}_2) \hat{N}_1 + (C_1 \dot{\theta}_1 \dot{\theta}_2 + S_1 \ddot{\theta}_2) \hat{N}_2 + \ddot{\theta}_1 \hat{N}_3$$

$$\frac{R\ G}{A} = \frac{\overline{\frac{dV}{dt}}^{R\ G_1}}{} = [(C_1 S_2 \dot{\theta}_1 \dot{\theta}_2 + S_1 C_2 \dot{\theta}_2^2 + S_1 S_2 \ddot{\theta}_2 + S_1 C_2 \dot{\theta}_1^2$$

$$+ C_1 S_2 \dot{\theta}_1 \dot{\theta}_2 - C_1 C_2 \ddot{\theta}_1)\frac{1}{2}\ DARM - 0.5(-S_1 \dot{\theta}_1^2$$

$$+ C_1 \ddot{\theta}_1]\hat{N}_1$$

$$+ [(-C_1 C_2 \dot{\theta}_1^2 + S_1 S_2 \dot{\theta}_1 \dot{\theta}_2 - S_1 C_2 \ddot{\theta}_1 + S_1 S_2 \dot{\theta}_1 \dot{\theta}_2 - C_1 C_2 \dot{\theta}_2^2$$

$$- C_1 S_2 \ddot{\theta}_2)\frac{1}{2}\ DARM - 0.5(C_1 \dot{\theta}_1^2 + S_1 \ddot{\theta}_1)]\hat{N}_2$$

$$+ [(-S_2 \dot{\theta}_2^2 + C_2 \ddot{\theta}_2)\frac{1}{2}\ DARM]\hat{N}_3$$

FOREARM: B_2

$$\frac{RB_2}{\omega} = \dot{\gamma}\ \hat{n}_{31} + S_{23}\dot{\theta}_1\hat{n}_{32} + C_{23}\dot{\theta}_1\hat{n}_{33}$$

$$\frac{RB_2}{\omega} = C_1\dot{\gamma}\hat{N}_1 + S_1\dot{\gamma}\hat{N}_2 + \dot{\theta}_1\hat{N}_3$$

$$\frac{RB_2}{\alpha} = \ddot{\gamma}\hat{n}_{31} + (C_{23}\dot{\theta}_1\dot{\gamma} + S_{23}\ddot{\theta}_1)\ \hat{n}_{32} + (-S_{23}\dot{\theta}_1\dot{\gamma} + C_{23}\ddot{\theta}_1)\ \hat{n}_{33}$$

$$\frac{RB_2}{\alpha} = (-S_1\dot{\theta}_1\dot{\gamma} + C_1\ddot{\gamma})\ \hat{N}_1 + (C_1\dot{\theta}_1\dot{\gamma} + S_1\ddot{\gamma})\ \hat{N}_2 + \ddot{\theta}_1\hat{N}_3$$

$$\frac{RG_2}{A} = [(C_1S_2\dot{\theta}_1\dot{\theta}_2 + S_1C_2\dot{\theta}_2{}^2 + S_1S_2\ddot{\theta}_2 + S_1C_2\dot{\theta}_1{}^2 + C_1S_2\dot{\theta}_1\dot{\theta}_2 - C_1C_2\ddot{\theta}_1)$$

$$\text{DARM} + 0.5S_1\dot{\theta}_1{}^2 - 0.5C_1\ddot{\theta}_1 + (C_1S_{23}\dot{\theta}_1\dot{\gamma} + S_1C_{23}\dot{\gamma}^2 + S_1S_{23}\ddot{\gamma}$$

$$+ S_1C_{23}\dot{\theta}_1{}^2 + C_1S_{23}\dot{\theta}_1\dot{\gamma} - C_1C_{23}\ddot{\theta}_1)\tfrac{1}{2}\ \text{DARM}]\ \hat{N}_1$$

$$+ [(-C_1C_2\dot{\theta}_1{}^2 + S_1S_2\dot{\theta}_1\dot{\theta}_2 - S_1C_2\ddot{\theta}_1 + S_1S_2\dot{\theta}_1\dot{\theta}_2 - C_1C_2\dot{\theta}_2{}^2 - C_1S_2\ddot{\theta}_2)$$

$$\text{DARM} - 0.5(C_1\dot{\theta}_1{}^2 + S_1\ddot{\theta}_1) + (-C_1C_{23}\dot{\theta}_1{}^2 + S_1S_{23}\dot{\theta}_1\dot{\gamma}$$

$$- S_1C_{23}\ddot{\theta}_1 + S_1S_{23}\dot{\theta}_1\dot{\gamma} - C_1C_{23}\dot{\gamma}^2 - C_1S_{23}\ddot{\gamma})\ \tfrac{1}{2}\ \text{DARM}]\ \hat{N}_2$$

$$+ [(-S_2\dot{\theta}_2{}^2 + C_2\ddot{\theta}_2)\ \text{DARM} + (-S_{23}\dot{\gamma}^2 + C_{23}\ddot{\gamma})\tfrac{1}{2}\ \text{DARM}]\ \hat{N}_3$$

<u>WRIST</u>: B_3

Assume point mass: no angular velocity

no angular acceleration

Assume mass is at end of forearm,

$$\frac{R}{A}B_3 = \quad C_1S_2\dot\theta_1\dot\theta_2 + S_1C_2\dot\theta_2^2 + S_1S_2\ddot\theta_2 + S_1C_2\dot\theta_1^2 - C_1C_2\ddot\theta_1)$$

$$Darm + 0.5(S_1\dot\theta_1^2 - C_1\ddot\theta_1) + (C_1S_{23}\dot\theta_1\dot\gamma + S_1C_{23}\dot\gamma^2$$

$$+ S_1S_{23}\ddot\gamma + S_1C_{23}\dot\theta_1^2 + C_1S_{23}\dot\theta_1\dot\gamma - C_1C_{23}\ddot\theta_1)\ Darm]\ N_1$$

$$+ [(-C_1C_2\dot\theta_1^2 + S_1S_2\dot\theta_1\dot\theta_2 - S_1C_2\ddot\theta_1 + S_1S_2\dot\theta_1\dot\theta_2 - C_1C_2\dot\theta_2^2 - C_1S_2\ddot\theta_2)$$

$$Darm - 0.5(C_1\dot\theta_1^2 + S_1\ddot\theta_1) + (-C_1C_{23}\dot\theta_1^2 + S_1S_{23}\dot\theta_1\dot\gamma - S_1C_{23}\ddot\theta_1$$

$$+ S_1S_{23}\dot\theta_1\dot\gamma - C_1C_{23}\dot\gamma^2 - C_1S_{23}\ddot\gamma)\ Darm]\ N_2$$

$$+ [(-S_2\dot\theta_2^2 + C_2\ddot\theta_2)\ Darm + (-S_{23}\dot\gamma^2 + C_{23}\ddot\gamma)\ Darm]\ N_3$$

<u>PAYLOAD</u>: P

Assume point mass: no angular velocity

no angular acceleration

Assume mass is at end of payload arm,

$$\frac{R\ P}{A_1} = [0.5(S_1\dot{\theta}_1^2 - C_1\ddot{\theta}_1)] + [2C_1S_2\dot{\theta}_1\dot{\theta}_2 + S_1C_2\dot{\theta}_2^2$$

$$+ S_1S_2\ddot{\theta}_2 + S_1C_2\dot{\theta}_1^2 - C_1C_2\ddot{\theta}_1 + 2C_1S_{23}\dot{\theta}_1\dot{\gamma}$$

$$+ S_1C_{23}\dot{\gamma}^2 + S_1S_{23}\ddot{\gamma} + S_1C_{23}\dot{\theta}_1^2 - C_1C_{23}\ddot{\theta}_1] \text{ DARM}$$

$$+ [C_1S_{234}(\dot{\gamma} + \dot{\theta}_4)\dot{\theta}_1 + S_1C_{234}(\dot{\gamma} + \dot{\theta}_4)^2 + S_1S_{234}(\ddot{\gamma} + \ddot{\theta}_4)$$

$$+ S_1C_{234}\dot{\theta}_1^2 + C_1S_{234}\dot{\theta}_1(\dot{\gamma} + \dot{\theta}_4) - C_1C_{234}\ddot{\theta}_1] \text{ WLEN}$$

$$+ [2C_1S_{234}C_5\dot{\theta}_1(\dot{\gamma} + \dot{\theta}_4) + S_1C_{234}C_5(\dot{\gamma} + \dot{\theta}_4)^2 -$$

$$2S_1S_{234}S_5\dot{\theta}_5(\dot{\gamma} + \dot{\theta}_4) + S_1S_{234}C_5(\ddot{\gamma} + \ddot{\theta}_4)$$

$$+ 2S_1C_5\dot{\theta}_1\dot{\theta}_5 + C_1S_5\dot{\theta}_5^2 - C_1C_5\ddot{\theta}_5 + C_1S_5\dot{\theta}_1^2$$

$$+ S_1S_5\ddot{\theta}_1 + 2C_1C_{234}S_5\dot{\theta}_1\dot{\theta}_5 + S_1C_{234}C_5\dot{\theta}_5^2$$

$$+ S_1C_{234}S_5\ddot{\theta}_5 + S_1C_{234}C_5\dot{\theta}_1^2 - C_1C_{234}C_5\ddot{\theta}_1] \text{ PLEN}$$

$$\frac{R}{A_2}P = [0.5(-c_1\dot{\theta}_1{}^2 - s_1\ddot{\theta}_1)] + [-c_1c_2\dot{\theta}_1{}^2 + 2s_1s_2\dot{\theta}_1\dot{\theta}_2 - s_1c_2\ddot{\theta}_1$$

$$- c_1c_2\dot{\theta}_2{}^2 - c_1s_2\ddot{\theta}_2 - c_1c_{23}\dot{\theta}_1{}^2 + 2s_1s_{23}\dot{\theta}_1\dot{\gamma} - s_1c_{23}\ddot{\theta}_1$$

$$- c_1c_{23}\dot{\gamma}^2 - c_1s_{23}\ddot{\gamma}] \text{ DARM}$$

$$+ [-c_1c_{234}\dot{\theta}_1{}^2 + 2s_1s_{234}\dot{\theta}_1(\dot{\gamma} + \dot{\theta}_4) - s_1c_{234}\ddot{\theta}_1 - c_1c_{234}(\dot{\gamma} + \dot{\theta}_4)^2$$

$$- c_1s_{234}(\ddot{\gamma} + \ddot{\theta}_4)] \text{ WLEN}$$

$$+ [s_1c_5\dot{\theta}_1{}^2 + c_1s_5\dot{\theta}_1\dot{\theta}_5 - c_1c_5\ddot{\theta}_1 + s_1c_{234}c_5\dot{\theta}_1\dot{\theta}_5$$

$$+ c_1s_{234}c_5\dot{\theta}_5(\dot{\gamma} + \dot{\theta}_4) + c_1c_{234}s_5\dot{\theta}_5{}^2 - c_1c_{234}c_5\ddot{\theta}_5$$

$$- c_1c_{234}c_5\dot{\theta}_1{}^2 + 2s_1s_{234}c_5\dot{\theta}_1(\dot{\gamma} + \dot{\theta}_4) + s_1c_{234}s_5\dot{\theta}_1\dot{\theta}_5$$

$$- s_1c_{234}c_5\ddot{\theta}_1 - c_1c_5\dot{\theta}_1\dot{\theta}_5 + s_1s_5\dot{\theta}_5{}^2 - s_1c_5\ddot{\theta}_5$$

$$- c_1c_{234}c_5(\dot{\gamma} + \dot{\theta}_4)^2 + c_1s_{234}\dot{\theta}_5(\dot{\gamma} + \dot{\theta}_4) - c_1s_{234}c_5$$

$$(\ddot{\gamma} + \ddot{\theta}_4)] \text{PLEN}$$

$$\frac{R\_P}{A_3} = [-S_2\dot{\theta}_2{}^2 + C_2\ddot{\theta}_2 - S_{23}\dot{\gamma}^2 + C_{23}\ddot{\gamma}] \text{ DARM}$$

$$+ [-S_{234}(\dot{\gamma} + \dot{\theta}_4)^2 + C_{234}(\ddot{\gamma} + \ddot{\theta}_4)] \text{ WLEN}$$

$$+ [(-S_1C_1S_5 + C_{234}C_5 + C_1S_1C_5)(\ddot{\gamma} + \ddot{\theta}_4)$$

$$+ (S_1{}^2 - C_1{}^2)(S_5\dot{\theta}_1 - C_5\dot{\theta}_1)(\dot{\gamma} + \dot{\theta}_4) - S_1C_1\dot{\theta}_5(\dot{\gamma} + \dot{\theta}_4)$$

$$- S_{234}C_5(\dot{\gamma} + \dot{\theta}_4)^2 - 2C_{234}S_5(\dot{\gamma} + \dot{\theta}_4) - C_1S_1S_5\dot{\theta}_5$$

$$(\dot{\gamma} + \dot{\theta}_4) - S_{234}C_5\dot{\theta}_5{}^2 - S_{234}S_5\ddot{\theta}_5] \text{ PLEN}$$

DARM - length of upper arm and forearm

WLEN - length of wrist segment

PLEN - length of payload segment

NOMENCLATURE

$\bar{A}_i$ — Acceleration of mass center in direction i

B_i — Rigid body number i designation

C_i — Abbreviation for $\cos(\theta_i)$

C_{ij} — Abbreviation for $C_iC_j - S_iS_j$

C_{ijk} — Abbreviation for $C_iC_{jk} - S_iS_{jk}$

G_i — Point of mass center of body i

$\hat{N}_i$ — Unit vector in reference frame R in direction i

$\hat{n}_{ij}$ — Unit vector in reference frame i in direction j

R — Inertial reference frame designation

S_i — Abbreviation for $\sin(\theta_i)$

S_{ij} — Abbreviation for $S_iC_j + C_iS_j$

S_{ijk} — Abbreviation for $C_iC_{jk} - S_iS_{jk}$

$\underline{{}^R\alpha^{B_i}}$ — Angular acceleration of body B_i in reference frame R

γ — Abbreviation for $\theta_2 + \theta_3$

θ_i — Angular displacement of joint i

$\underline{{}^R\omega^{B_i}}$ — Angular velocity of body B_i in reference frame R

60

VIEW ORIENTATION-
The robot, located at the origin,
is viewed from a point in space
defined by x=2, y=1, z=0.

HEAD LOCATION -
The coordinates of the transducer
in space: x = -10.9, y=-14.8,
z=0.0 inches.

ANGULAR POSITIONS -
Partial listing of the angle
solution.

NOISE SOURCE
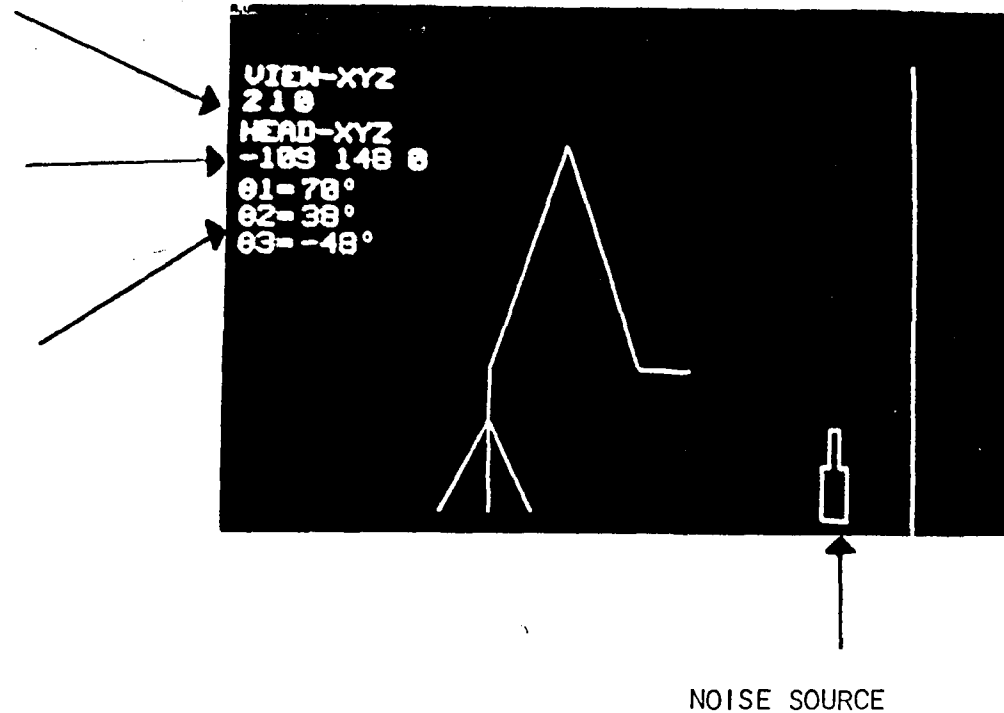
Figure A-1 Output display from lexidata system of the stick figure robot arm on a tripod with the acoustic
           intensity probe. Simulation was used to analyze various kinematic solutions for proposed robot
           designs.
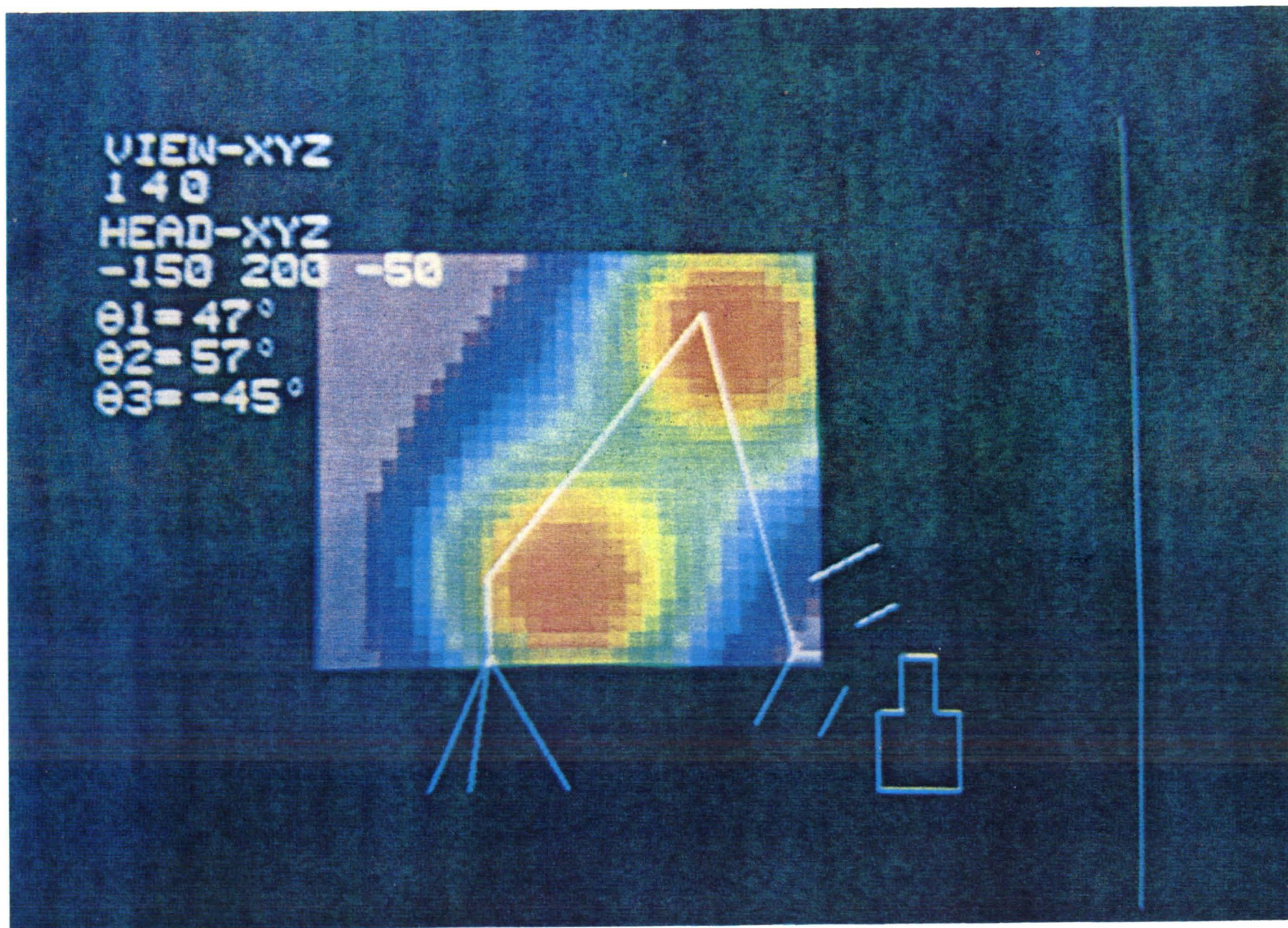
Figure A-2, Simulation of robot scanning an acoustic field.

6. 00   IN/SEC

	POINT A	POINT B
X=	-30. 00	X= 30. 00
Y=	20. 00	Y= 20. 00
Z=	5. 00	Z= 5. 00

THETA 1
THETA 2
THETA 3
THETA 4
THETA 5

TIME (SEC)
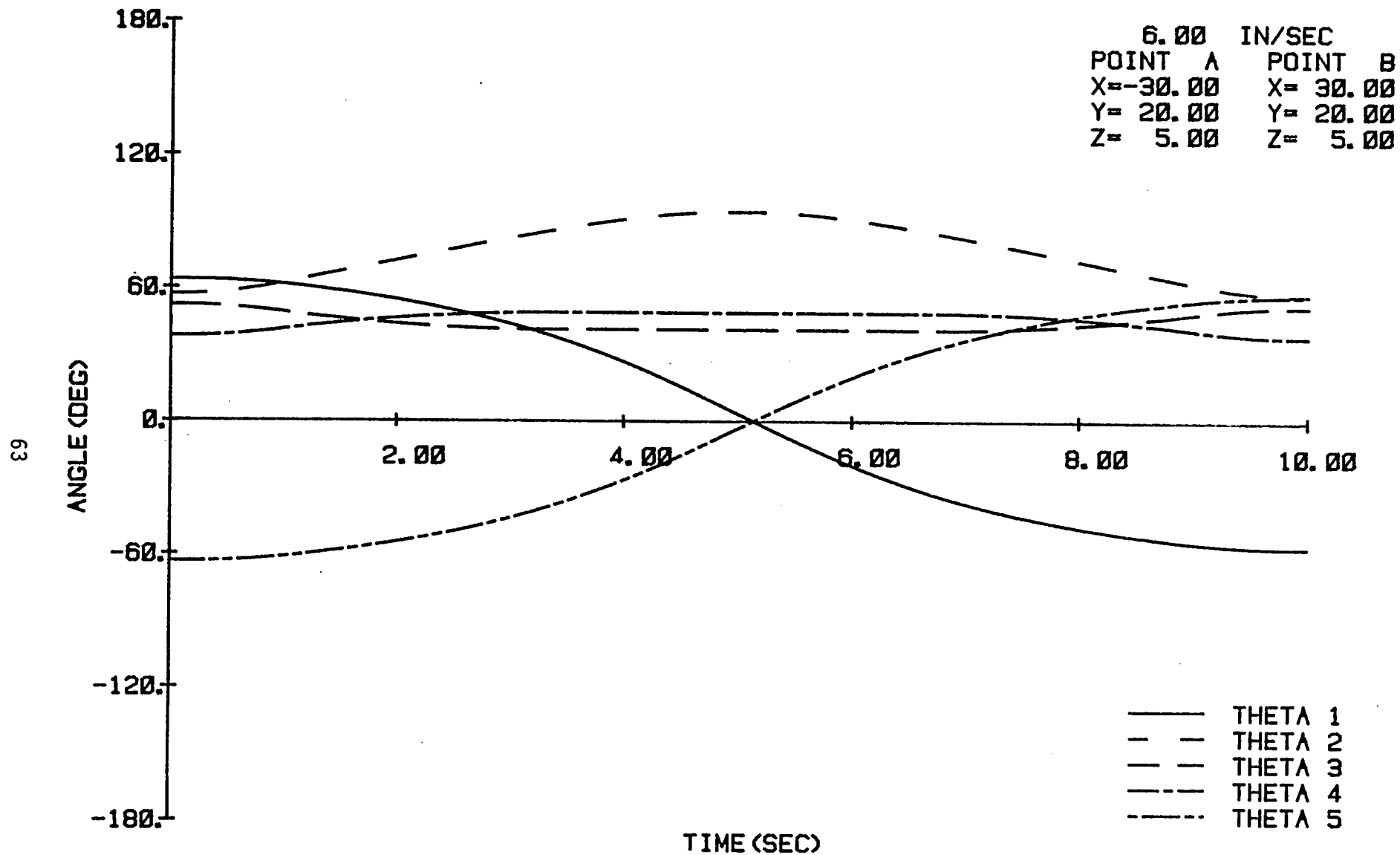
Figure A-3 Analytically Determined Angles θ_1, θ_2, θ_3, θ_4, and θ_5 Versus Time for an End Effector Velocity of 6 in/sec from Point A to Point B.
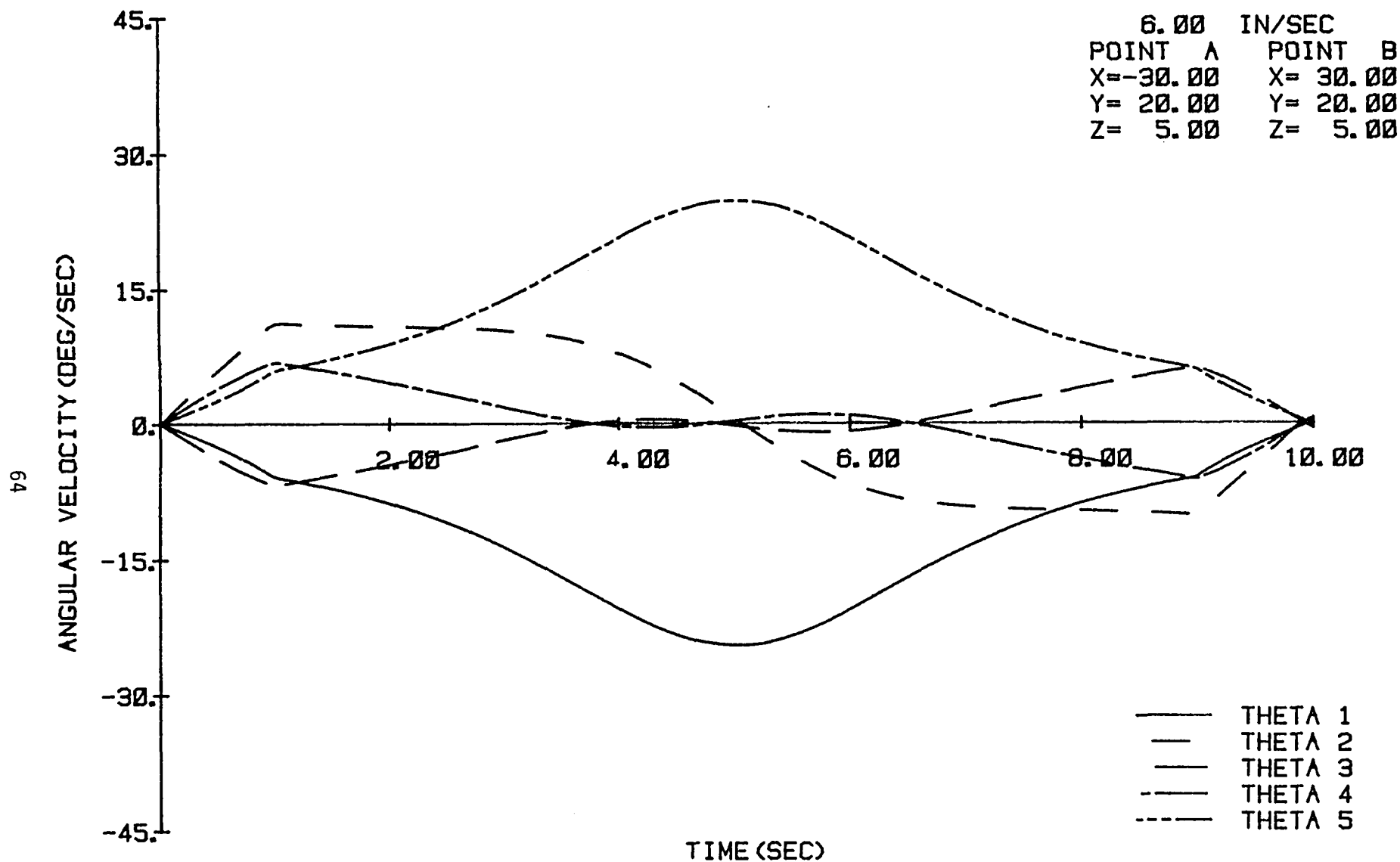
Figure A-4 Analytically determined Angular Velocity Versus Time.
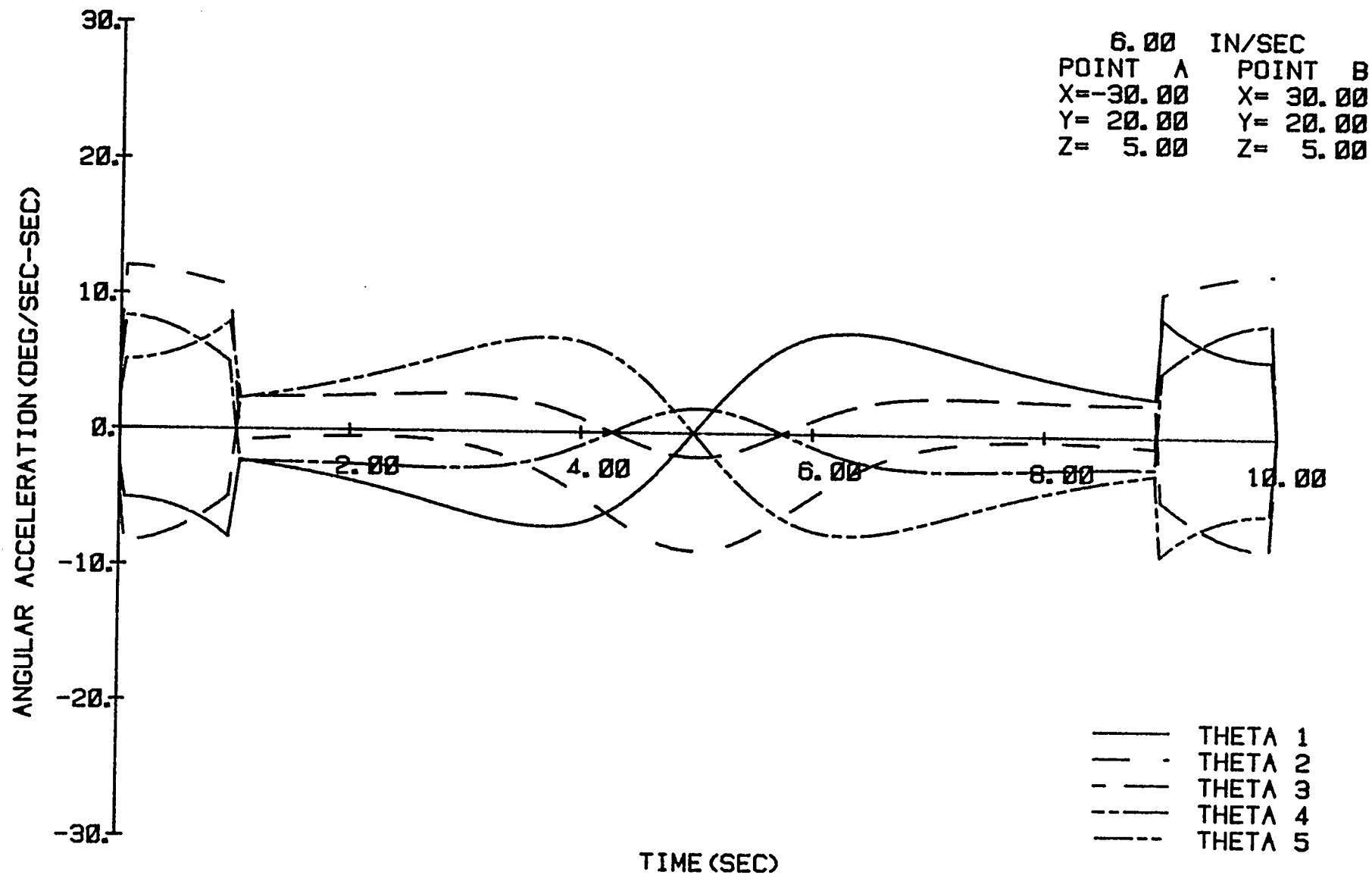
Figure A-5 Analytically Determined Angular Acceleration Versus Time.
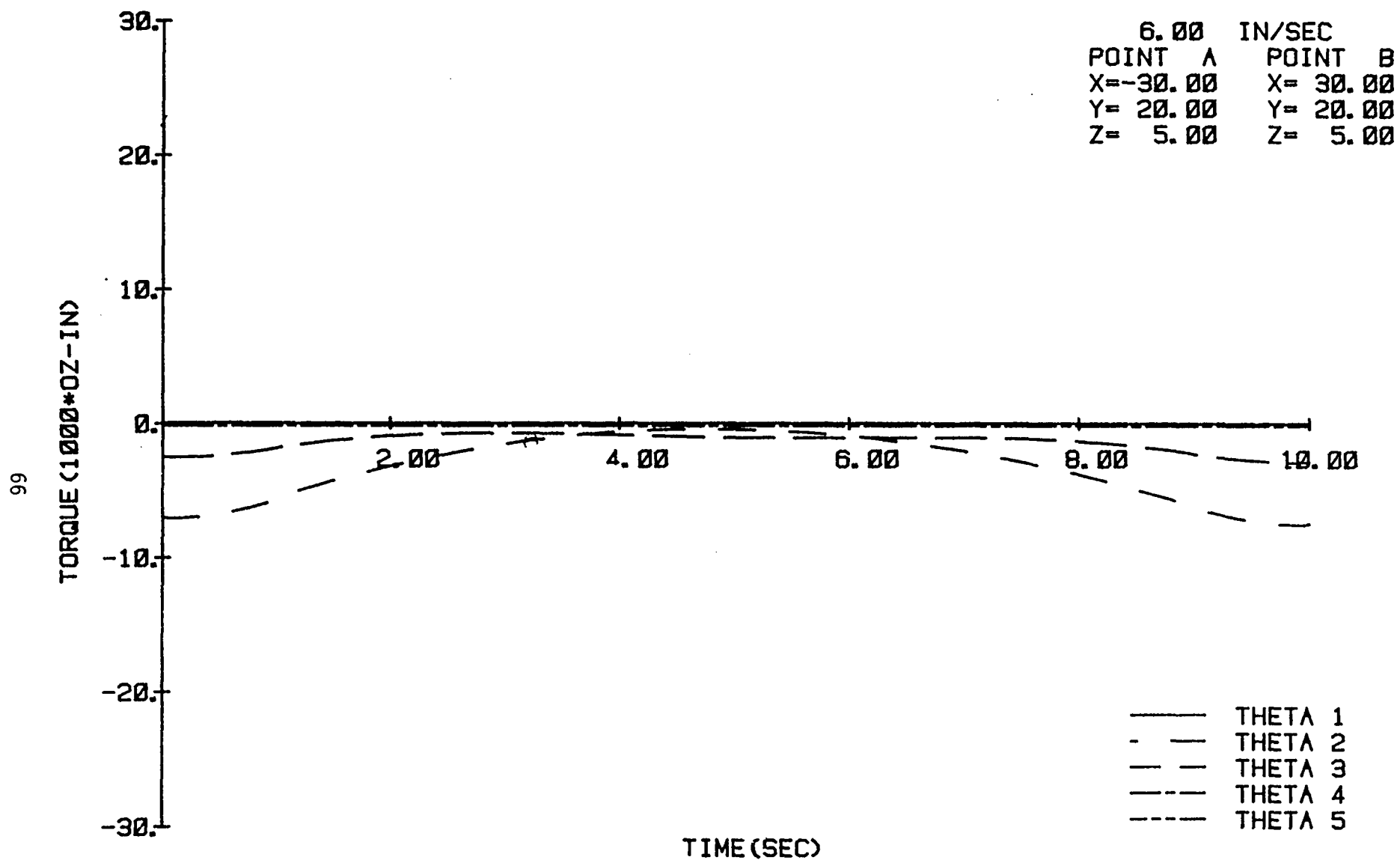
Figure A-6 Analytically determined torque versus time.

ACCELEROMETER LOCATIONS
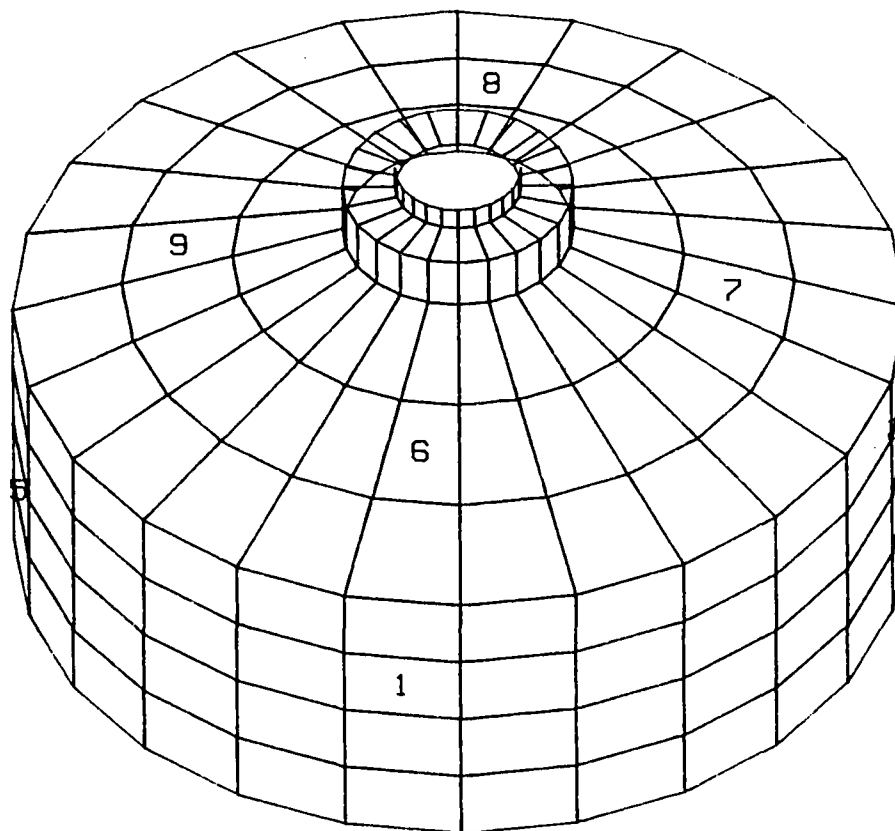
FRONT-TOP VIEW

Figure B-1. Accelerometer positions on the OH-58 transmission.

ACCELEROMETER LOCATIONS

TOP VIEW (FRONT ↑)
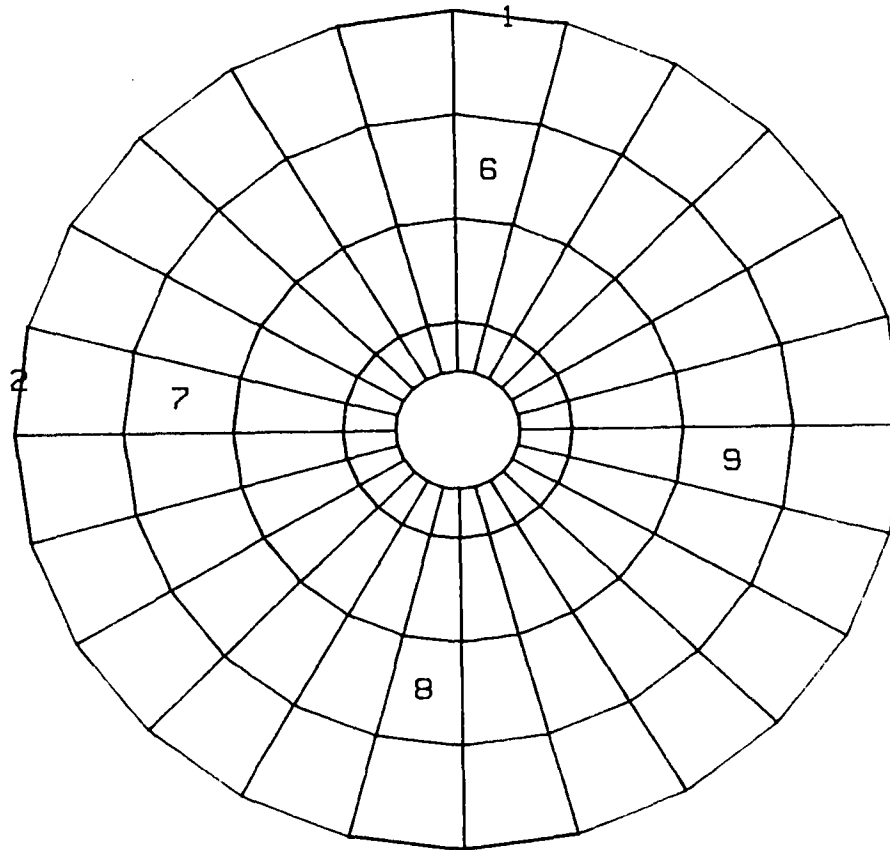
Figure B-2. Accelerometer positions on the top of the OH-58 transmission.

ACCELEROMETER LOCATIONS

FRONT VIEW
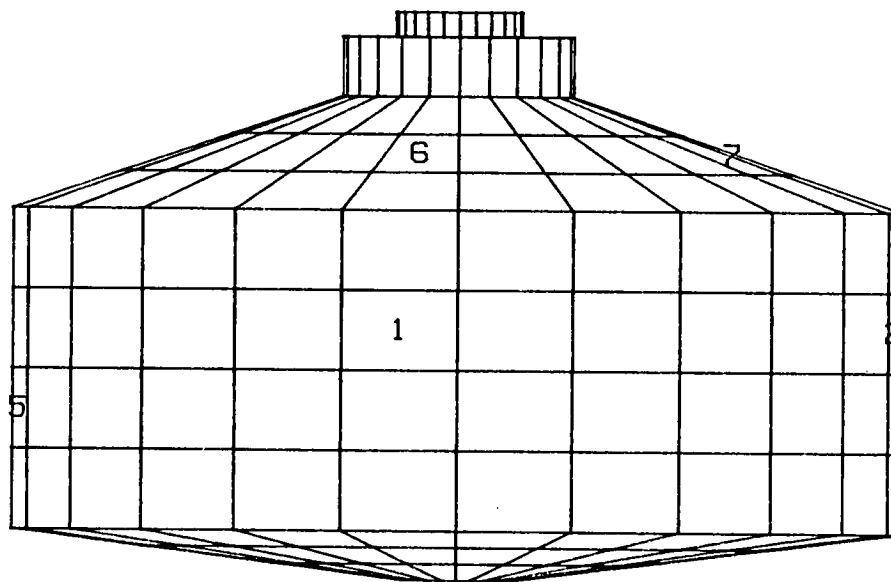
Figure B-3. Accelerometer positions on the front of the OH-58 transmission.

ACCELEROMETER LOCATIONS

RIGHT SIDE VIEW
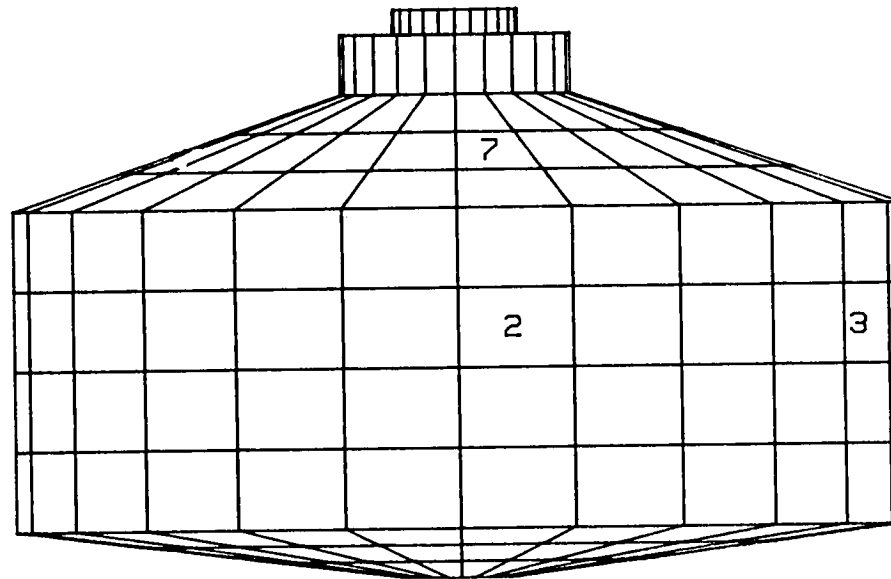
Figure B-4. Accelerometer positions on the right side of the OH-58 transmission.

ACCELEROMETER LOCATIONS

LEFT SIDE VIEW
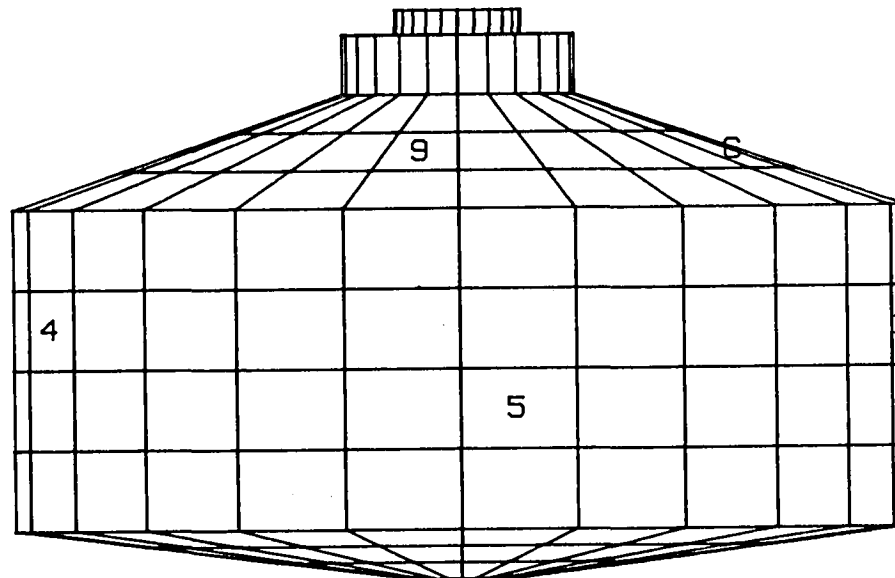
Figure B-5. Accelerometer positions on the left side of the OH-58 transmission.

ACCELEROMETER LOCATIONS

BACK VIEW
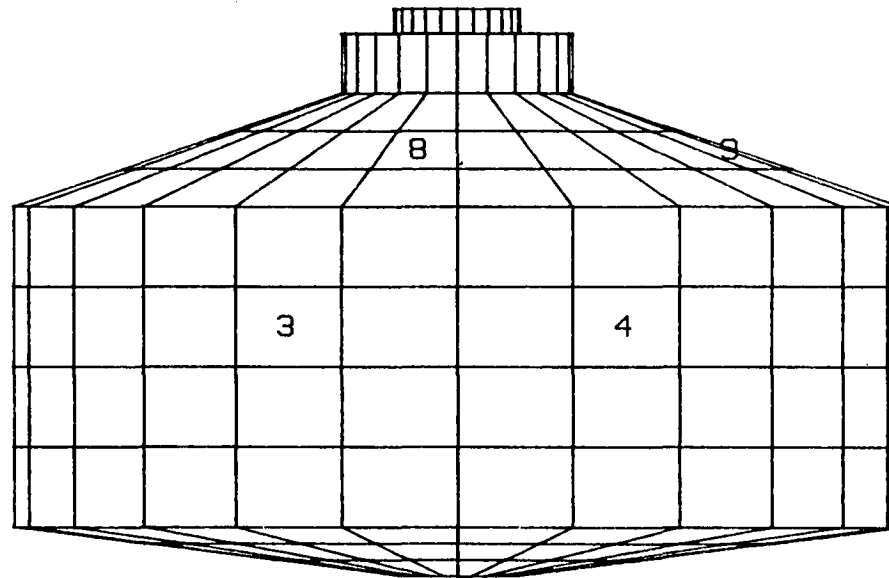
Figure B-6. Accelerometer positions on the back side of the OH-58 transmission.
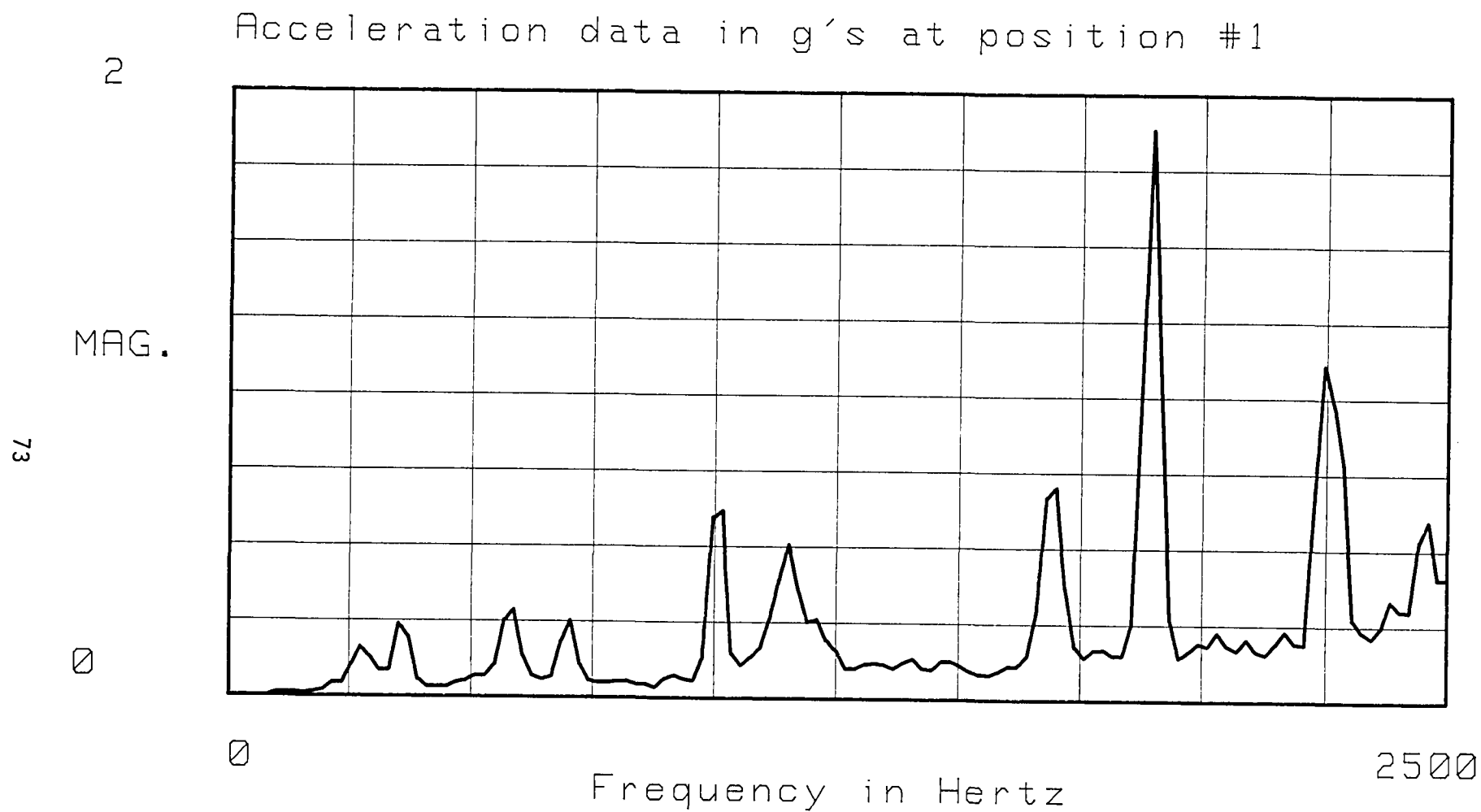
Figure B-7. Acceleration data in g's at position #1.
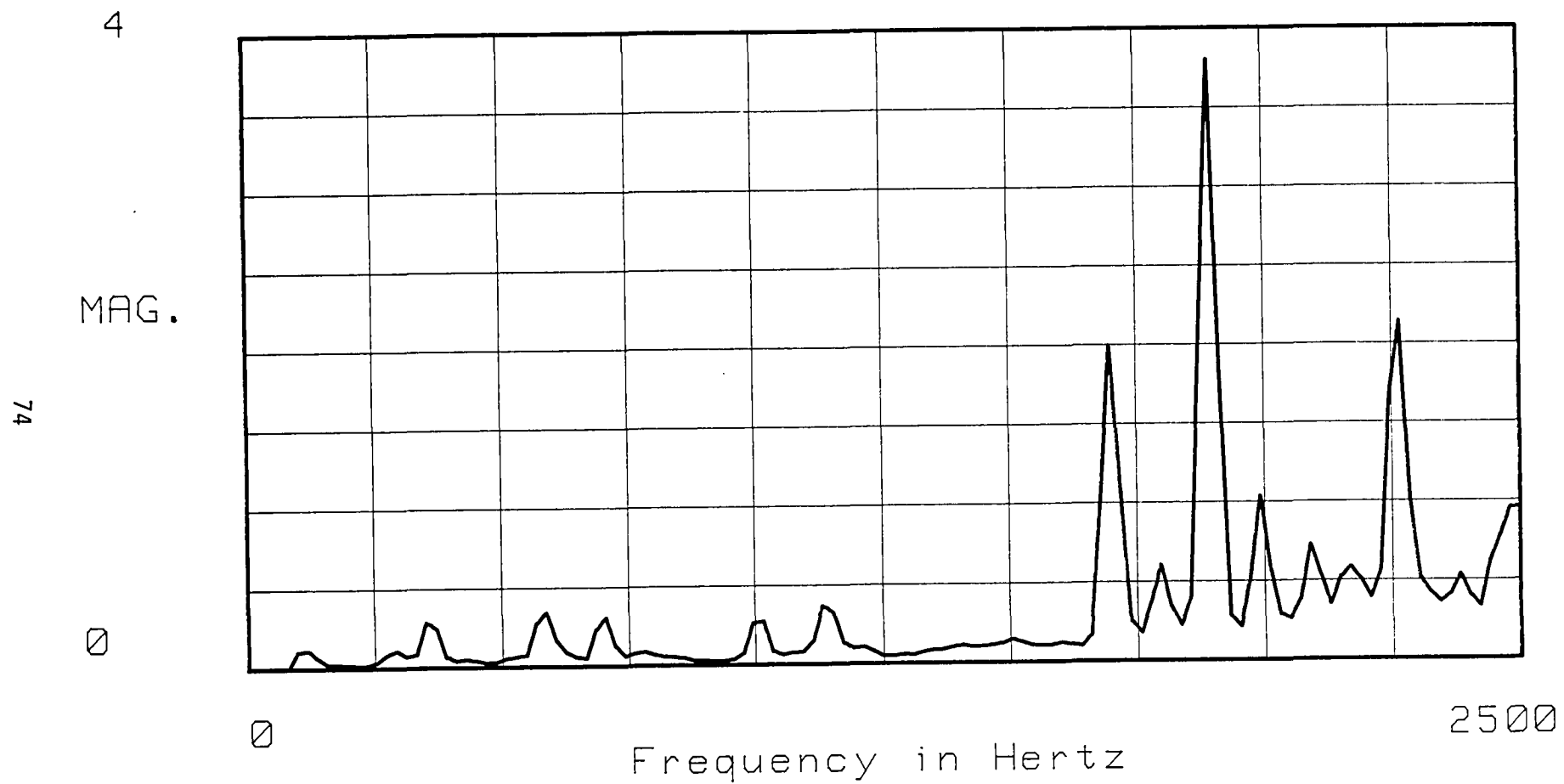
Figure B-8. Acceleration data in g's at position #2.

Acceleration data in g's at position #3

3

MAG.

0

0   2500

Frequency in Hertz

75
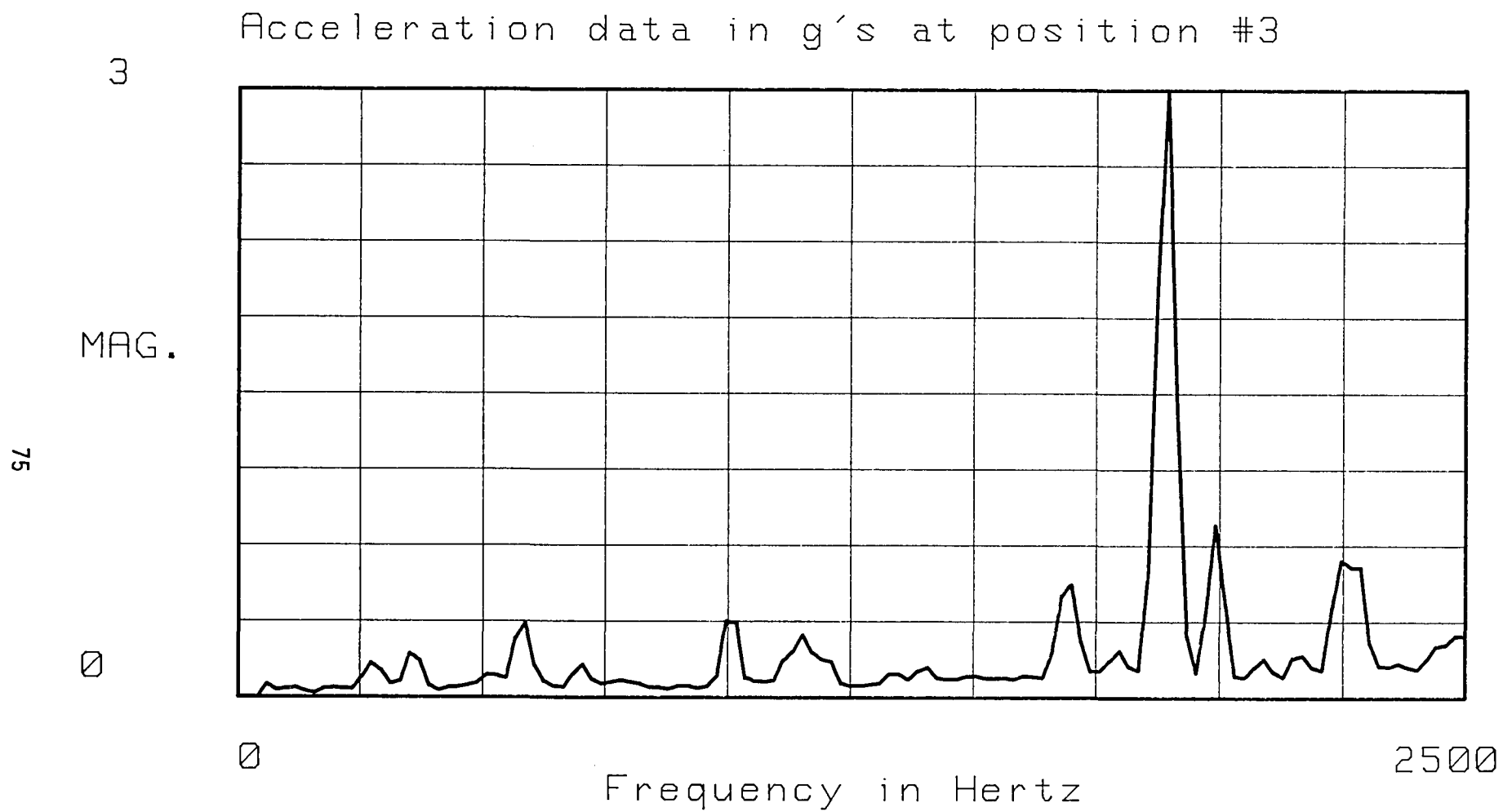
Figure B-9. Acceleration data in g's at position #3.
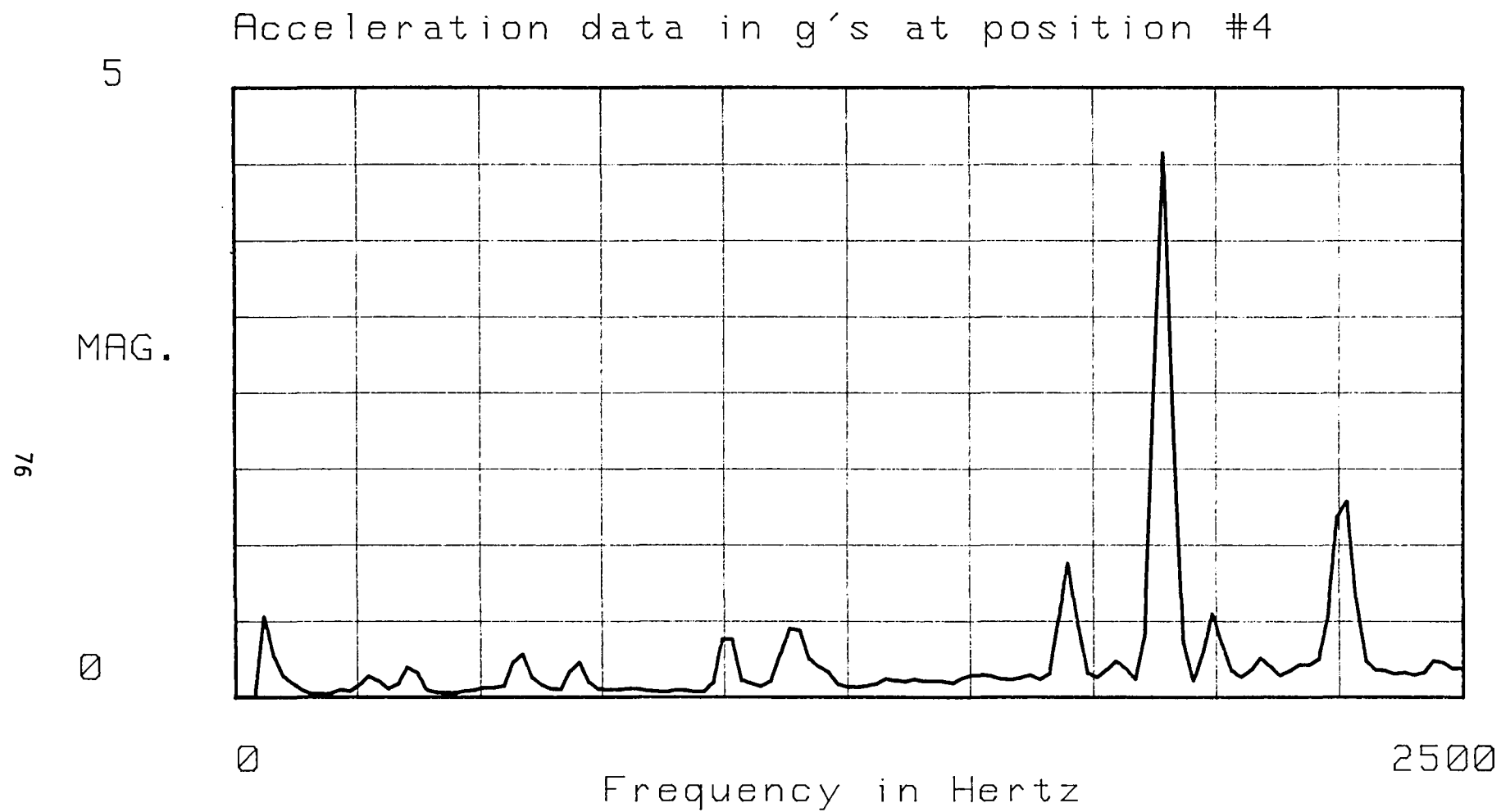
Figure B-10. Acceleration data in g's at position #4.
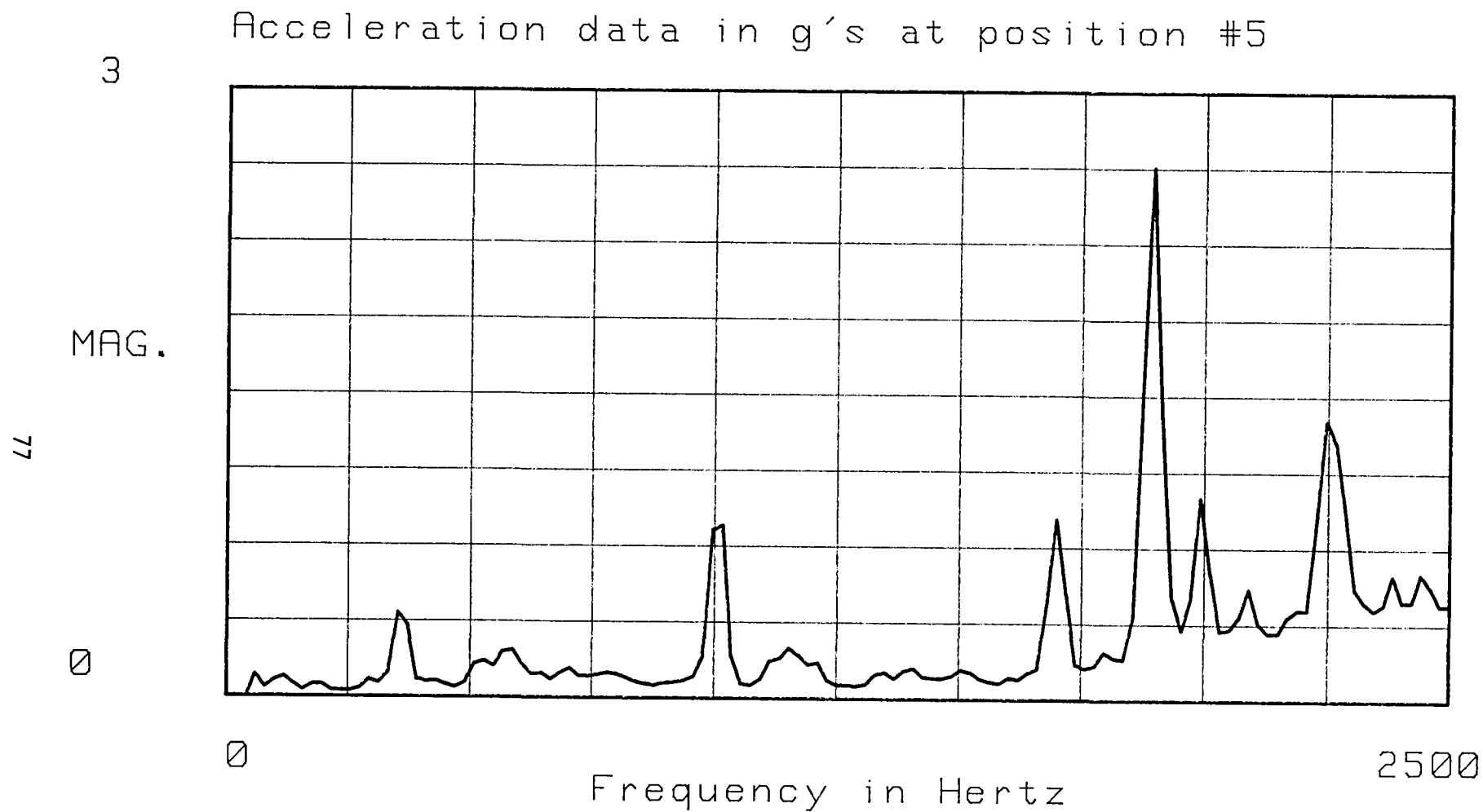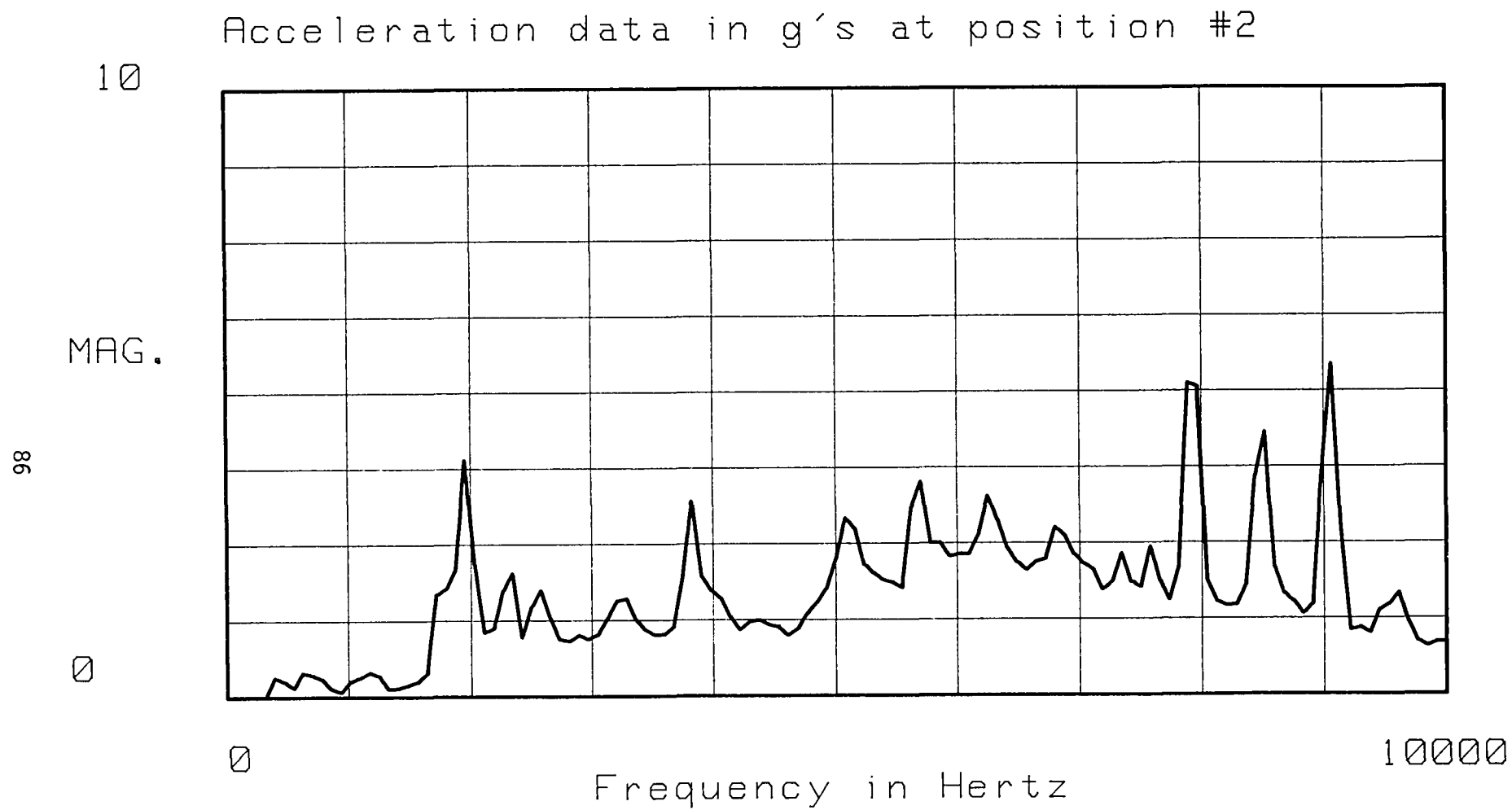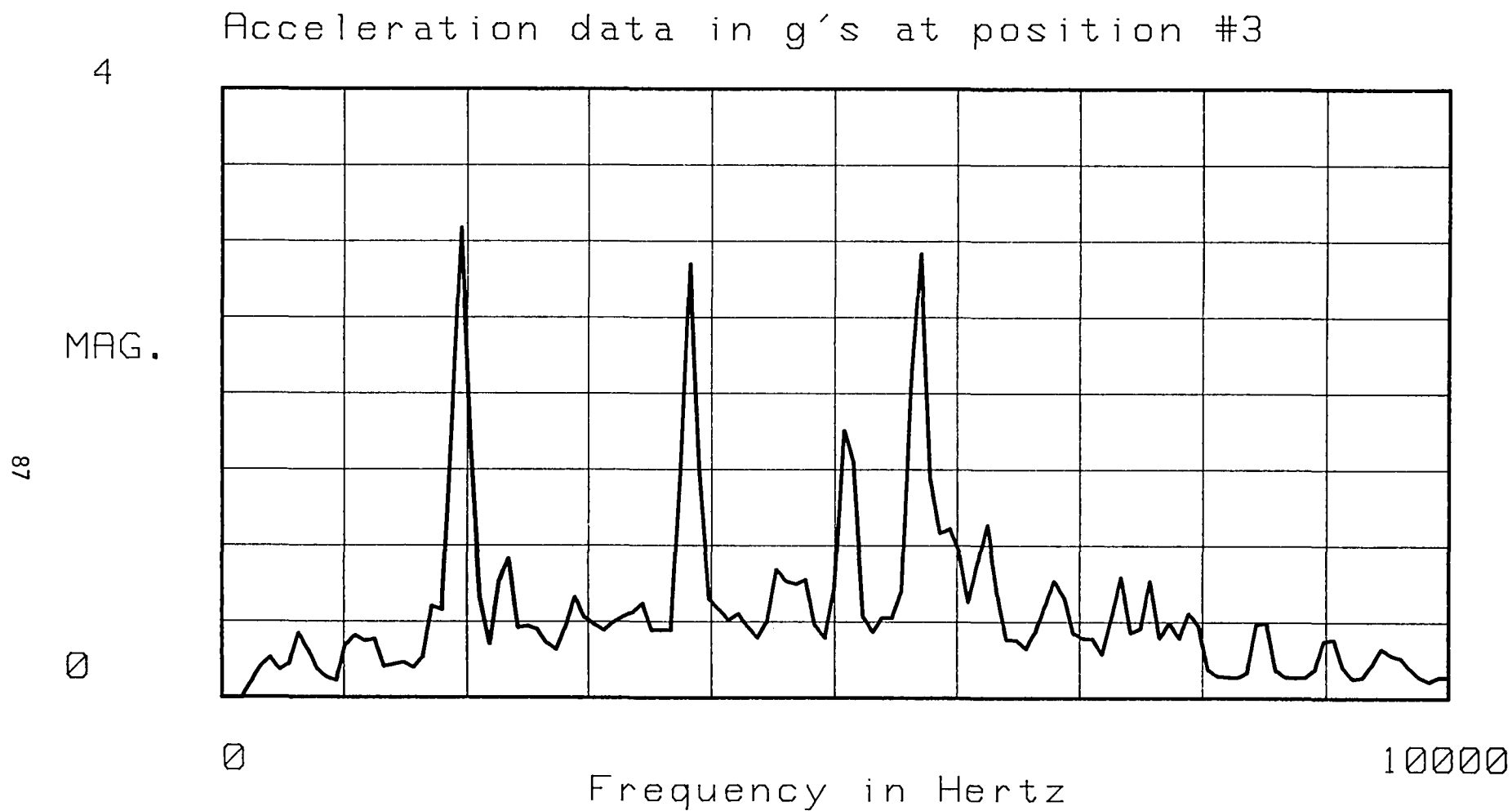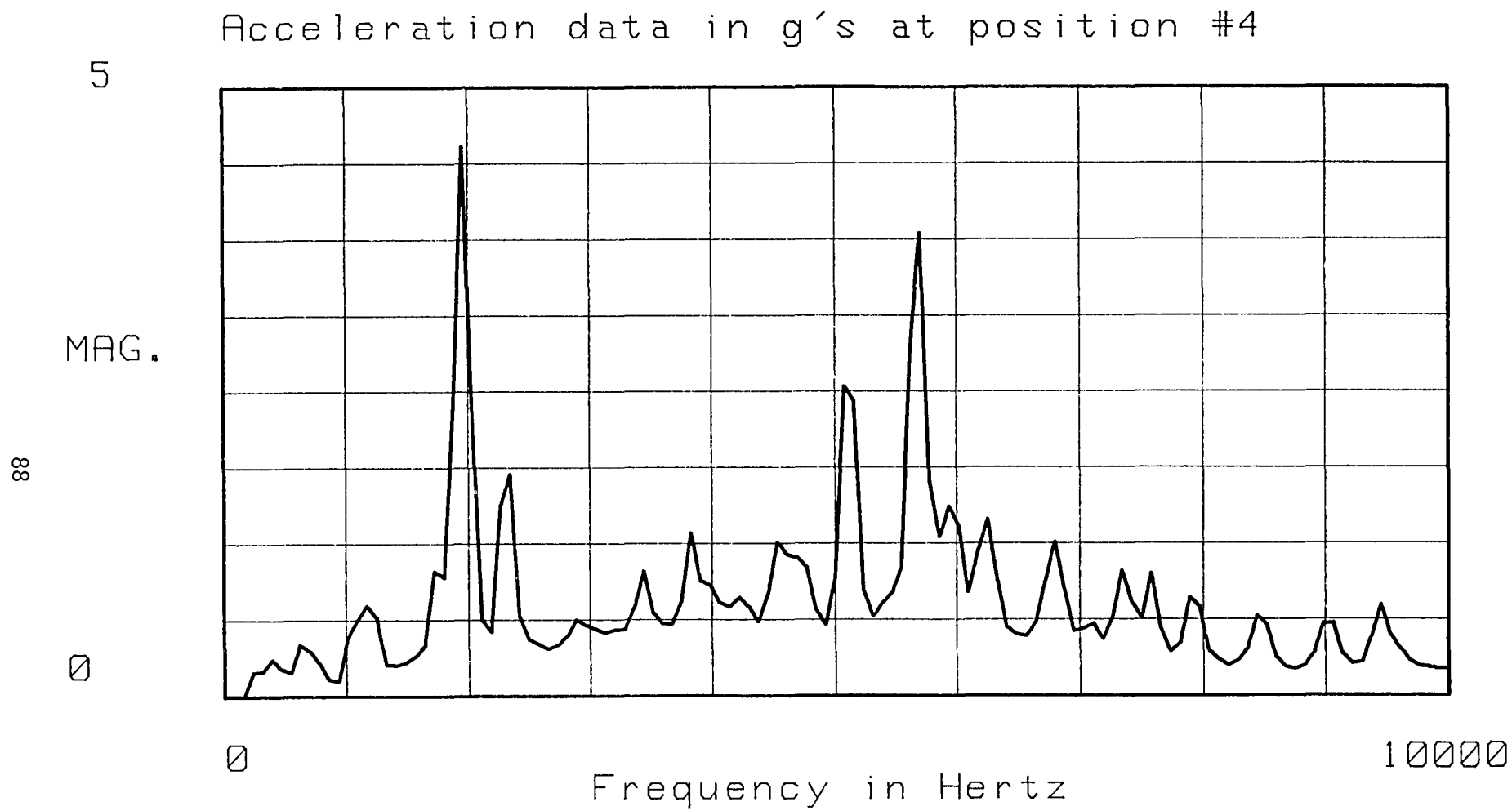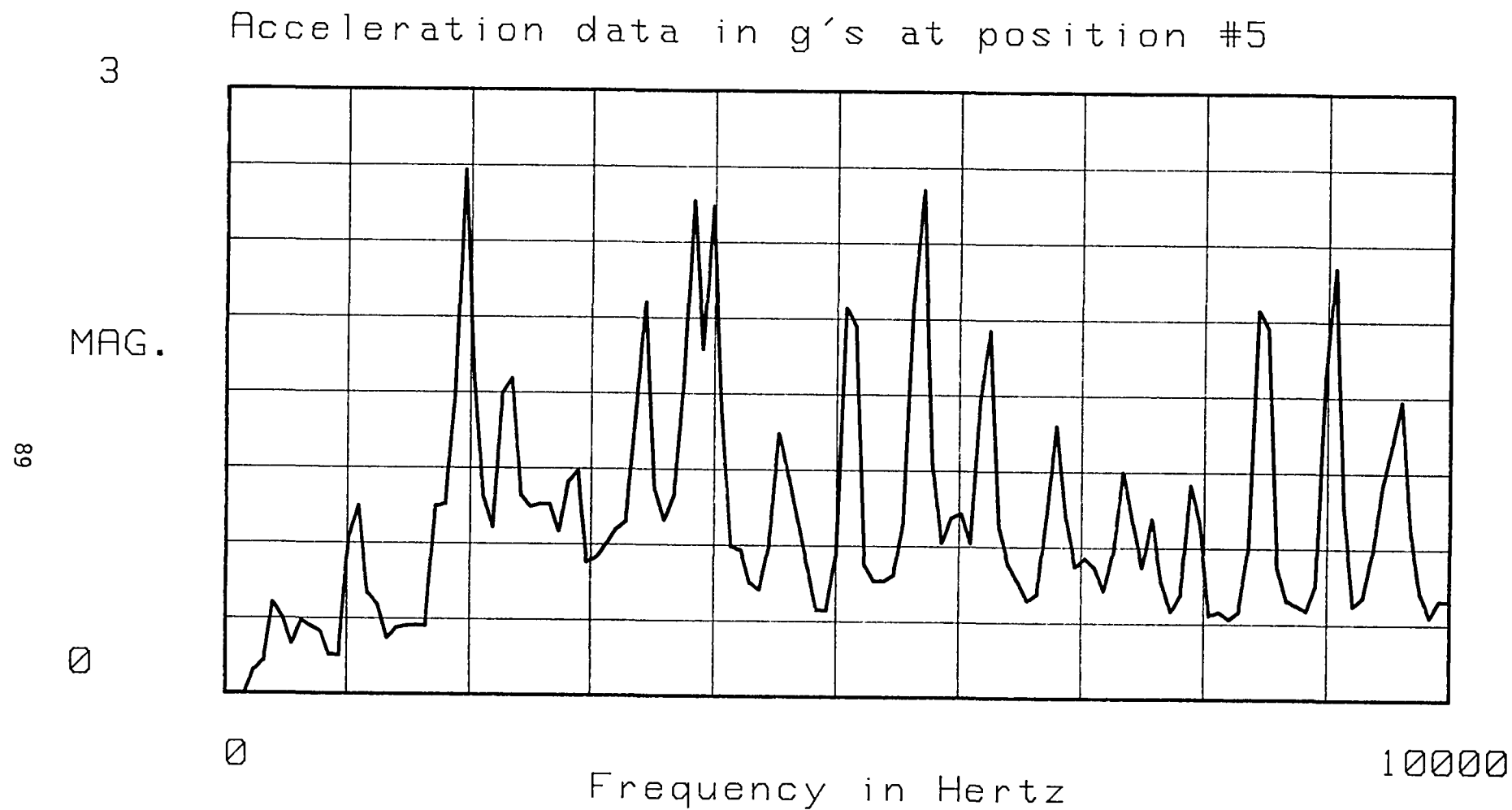
Figure B-11.   Acceleration data in g's at position #5.

Acceleration data in g's at position #6
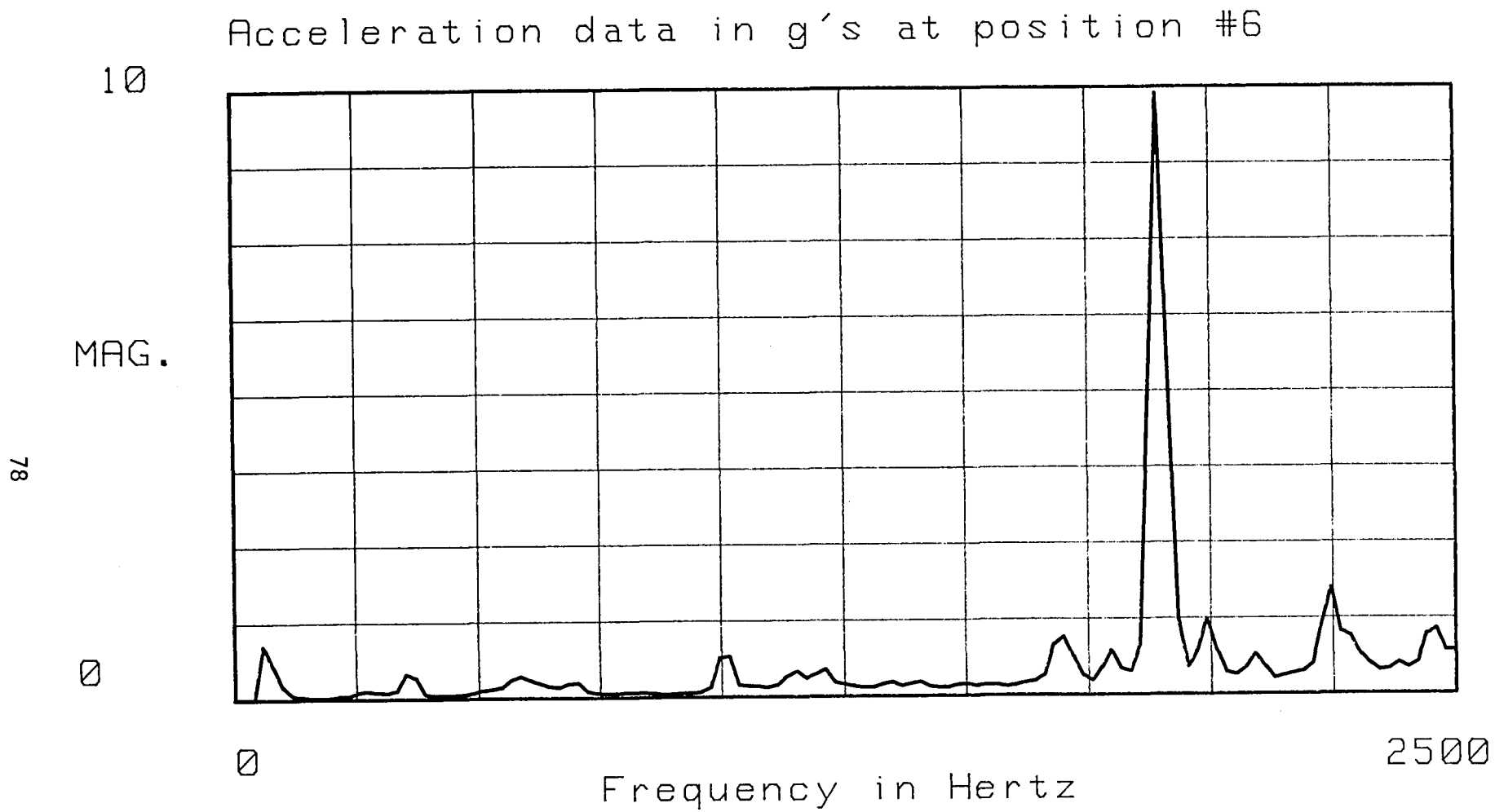
Figure B-12.   Acceleration data in g's at position #6.

Acceleration data in g´s at position #7
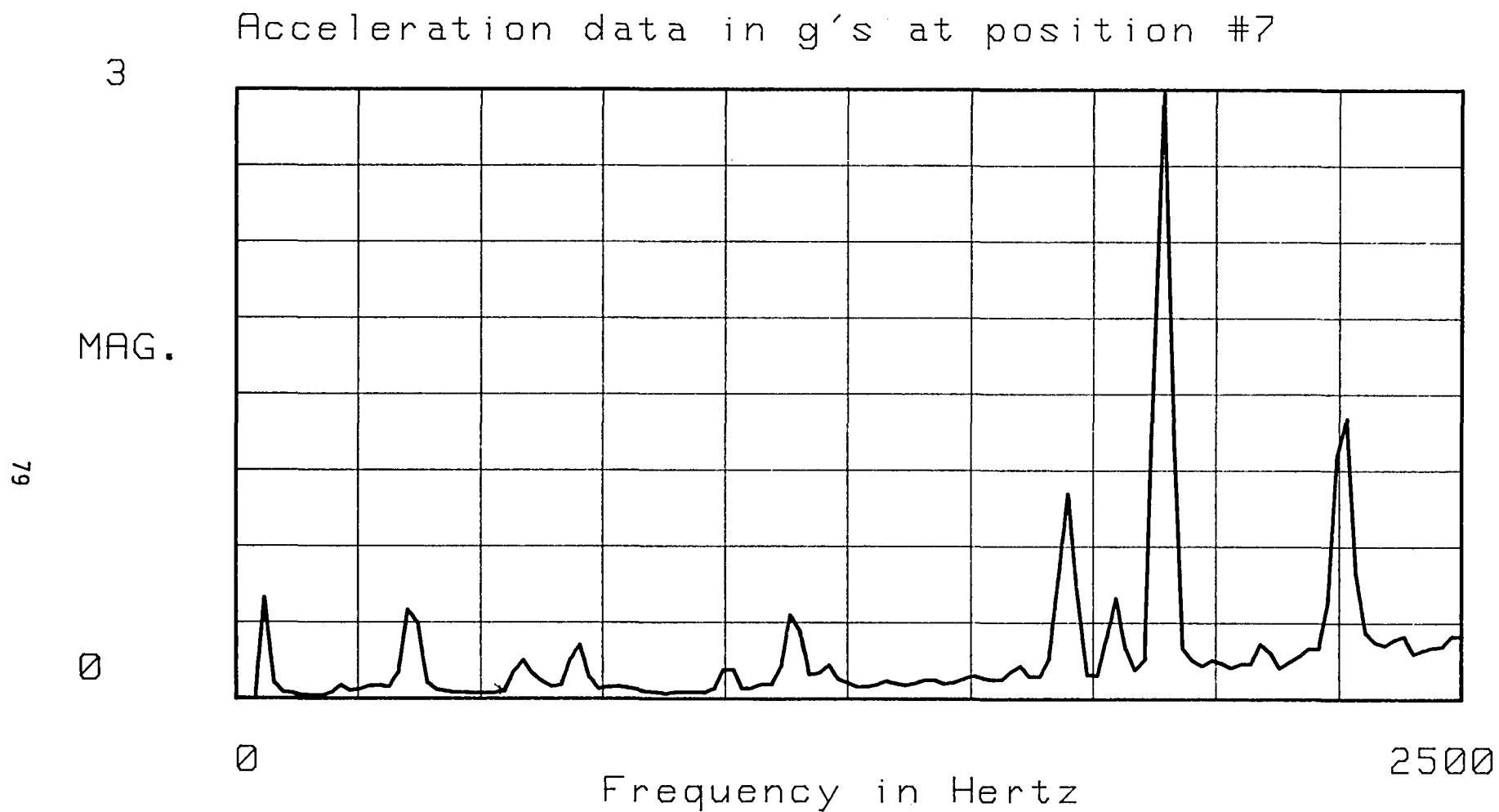
Figure B-13. Acceleration data in g's at position #7.
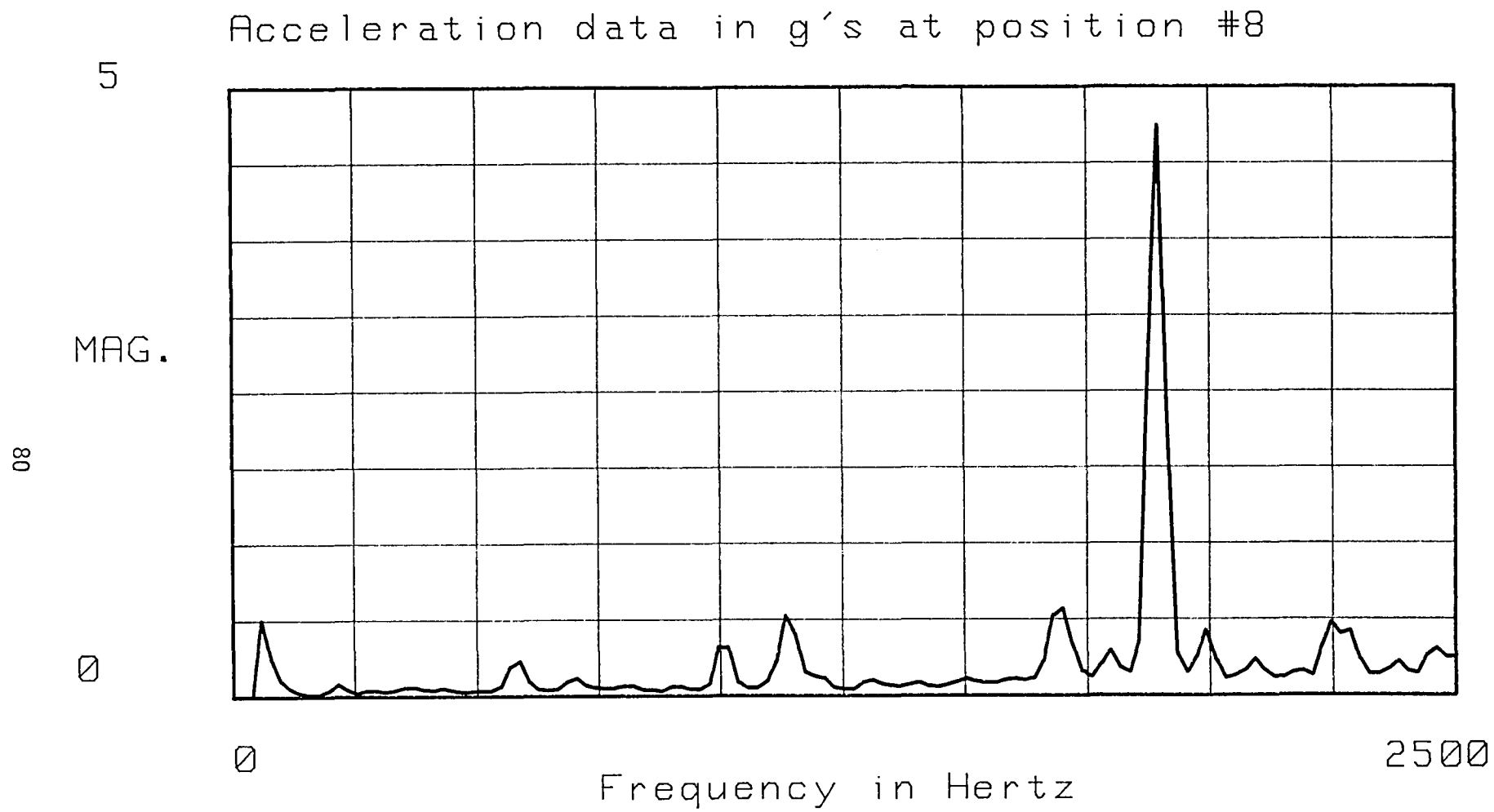
Figure B-14. Acceleration data in g's at position #8.
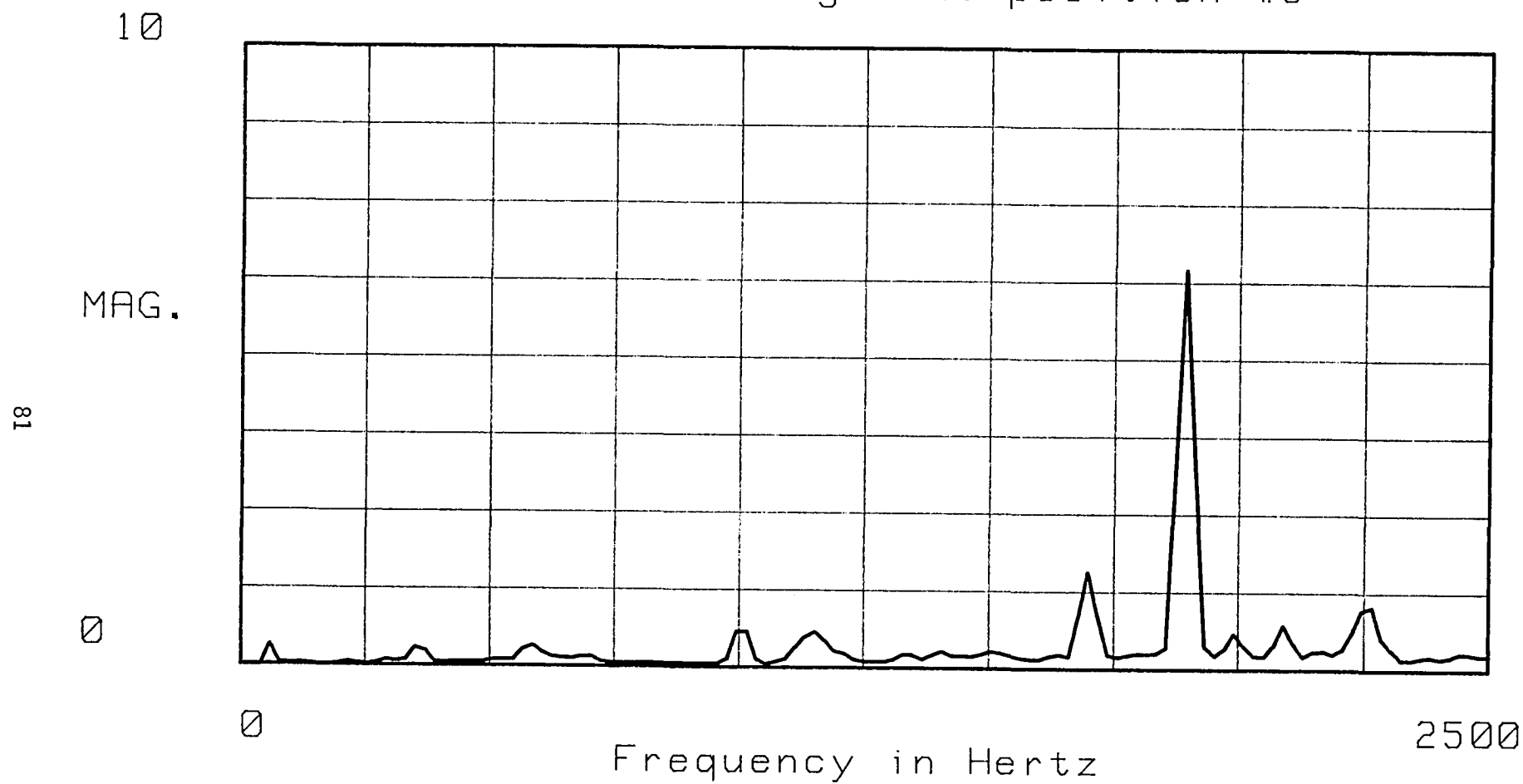
Figure B-15. Acceleration data in g's at position #9.
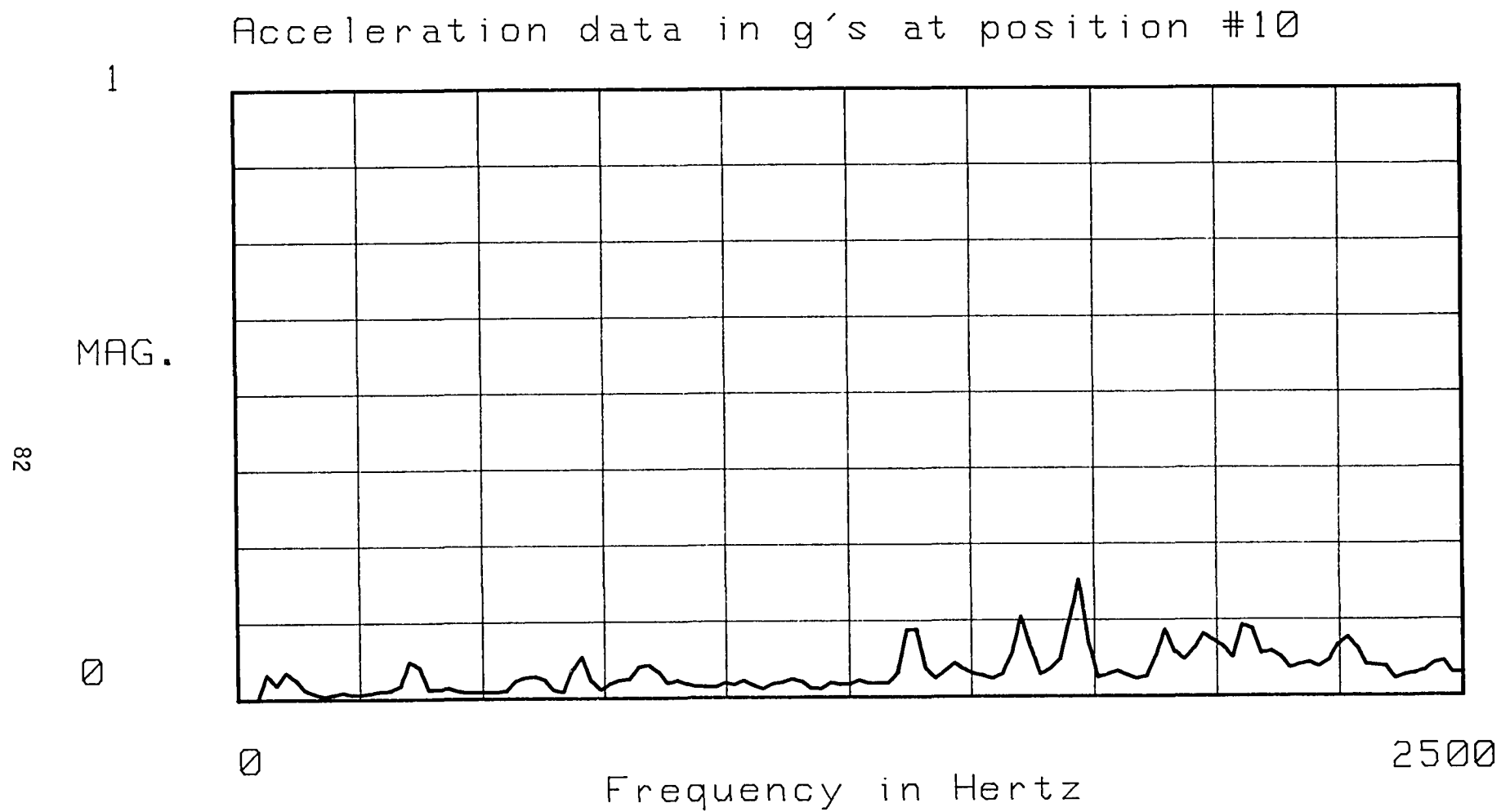
Figure B-16. Acceleration data in g's at position #10.

Acceleration data in g's at position #11

1

MAG.

0

0   2500

Frequency in Hertz
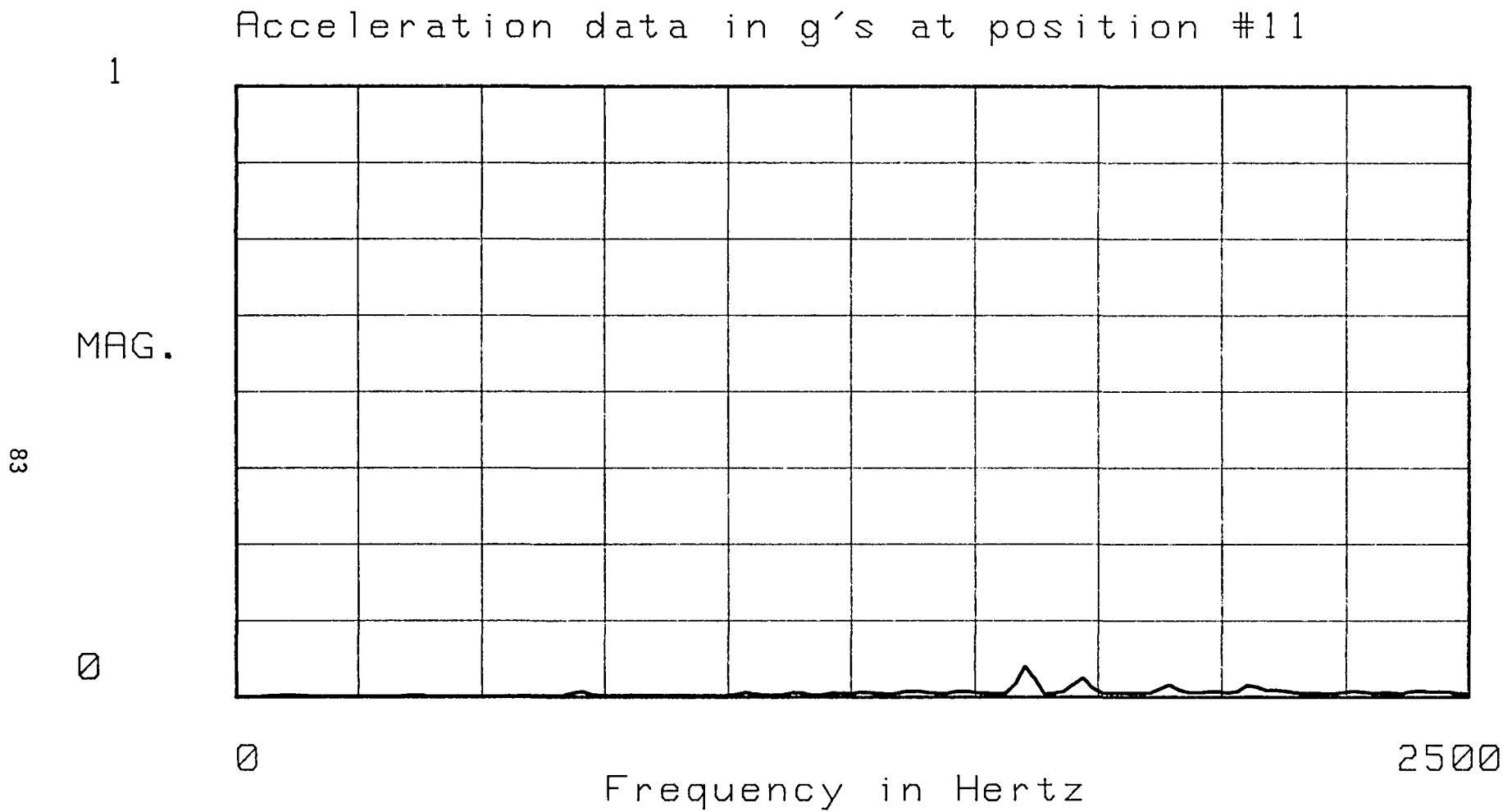
Figure B-17. Acceleration data in g's at position #11.
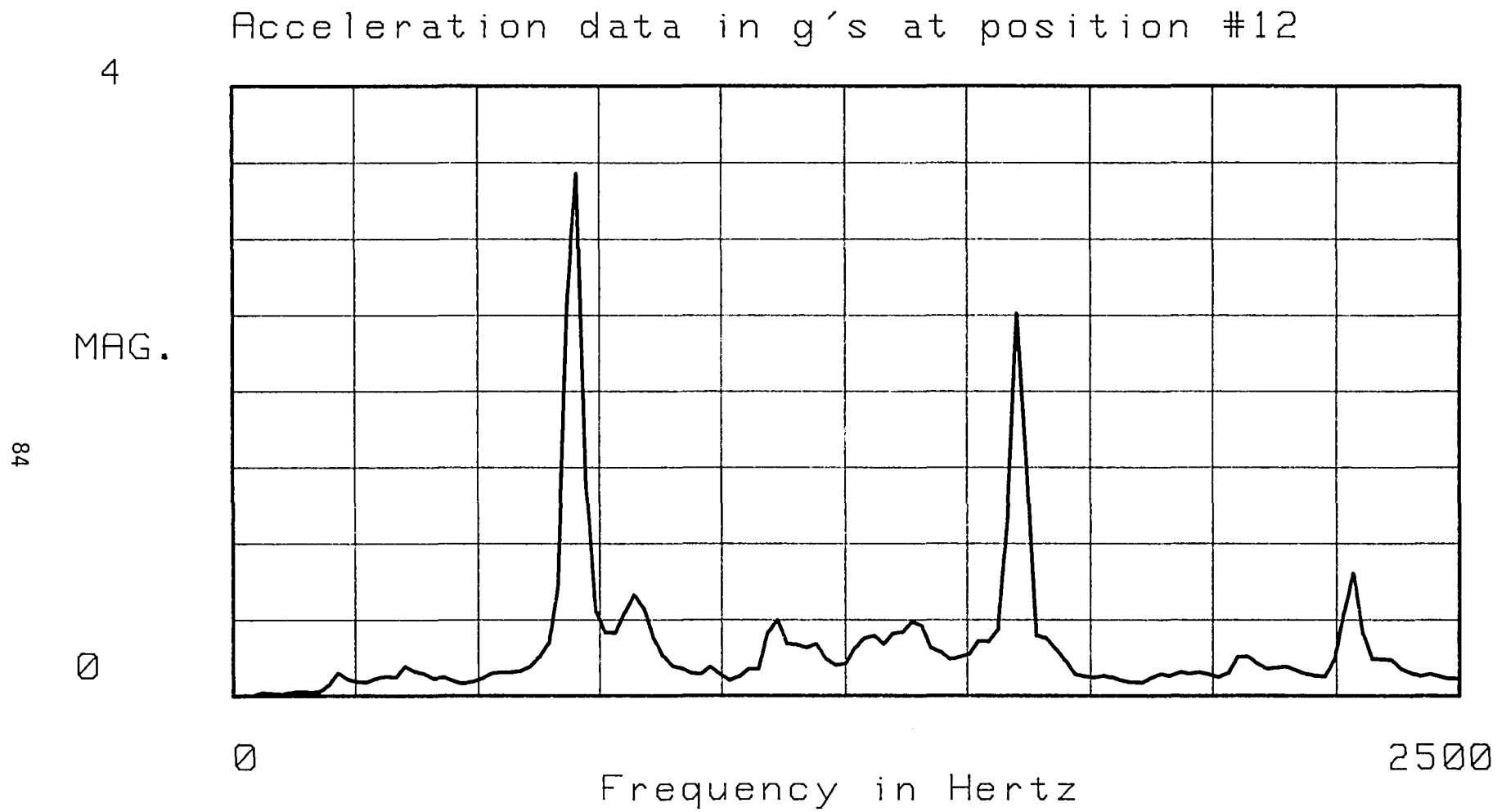
Figure B-18.   Acceleration data in g's at position #12.

Acceleration data in g's at position #1

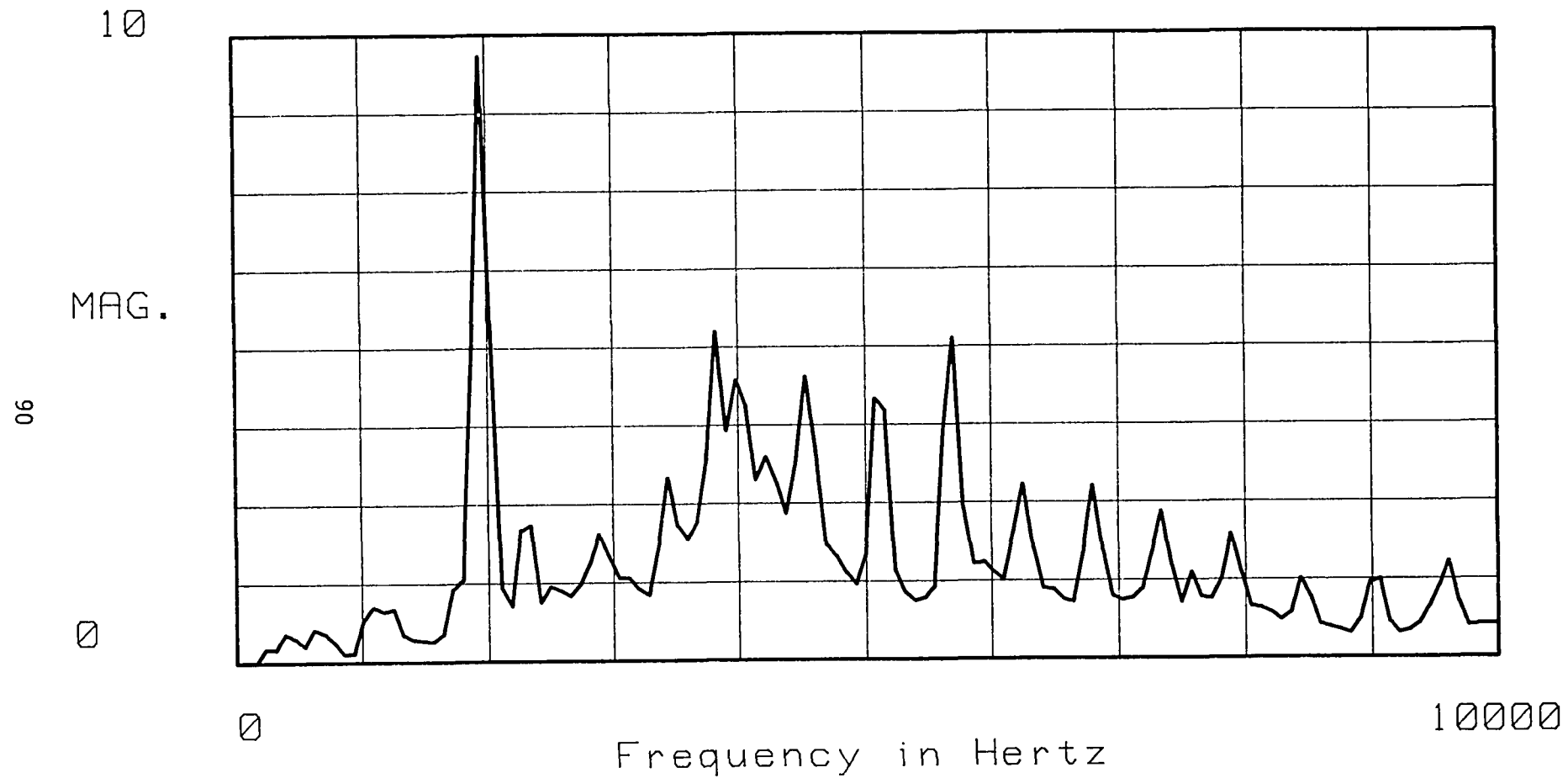2

MAG.

0

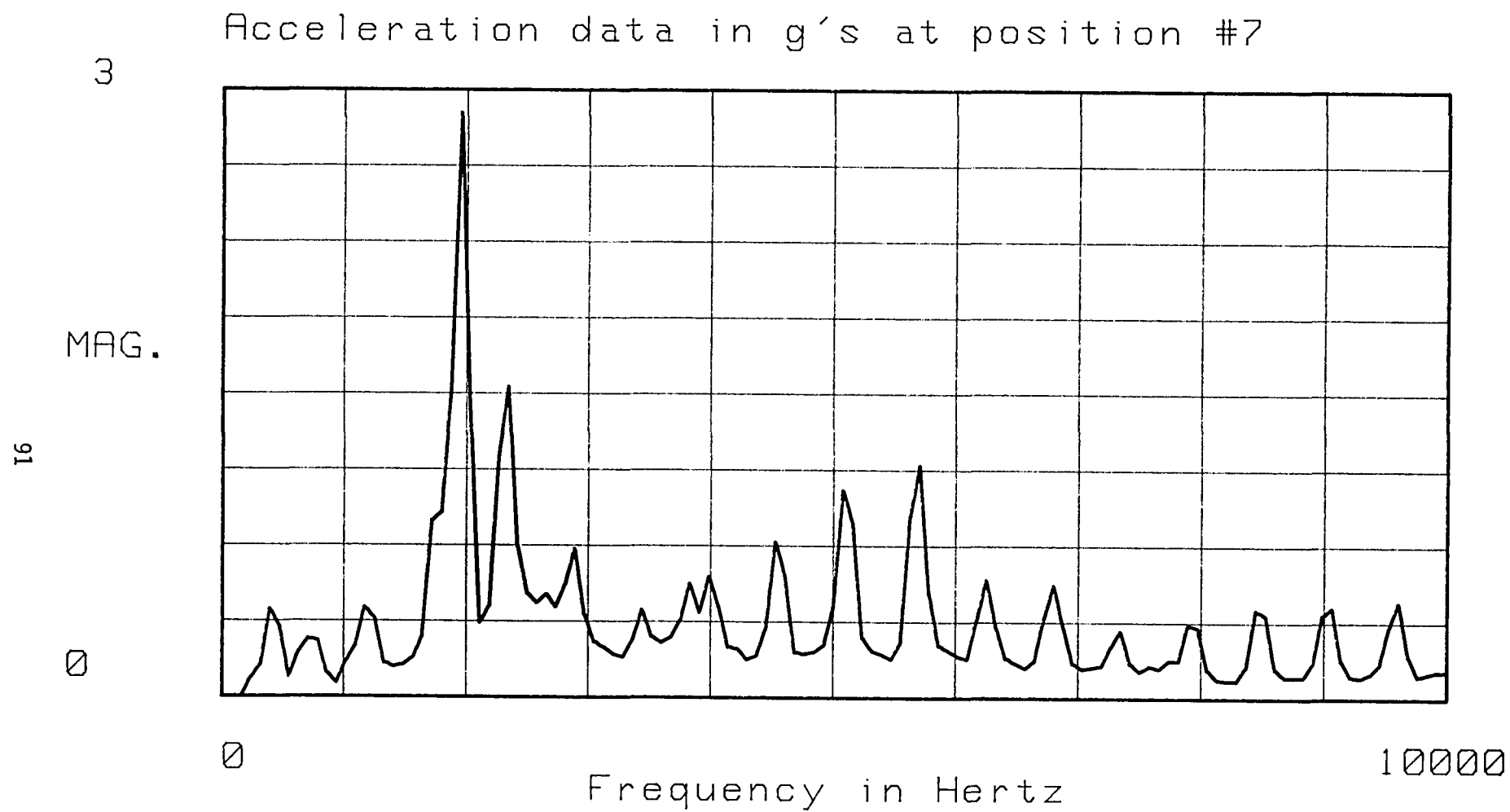85

0

10000

Frequency in Hertz
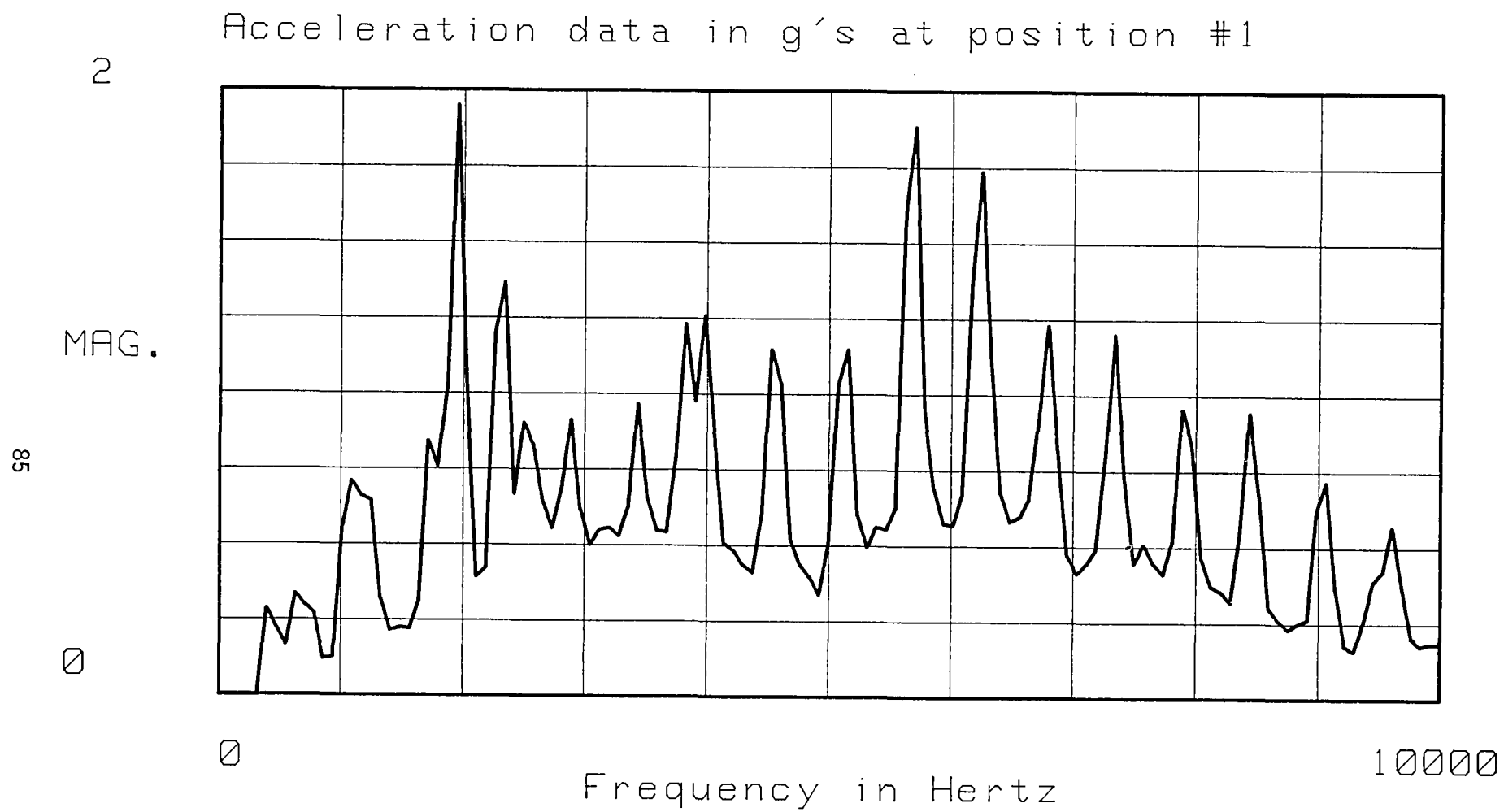
Figure B-19. Acceleration data in g's at position #1.

Figure B-20.   Acceleration data in g's at position #2.

Figure B-21. Acceleration data in g's at position #3.

Acceleration data in g's at position #4

5

MAG.

88

0

0
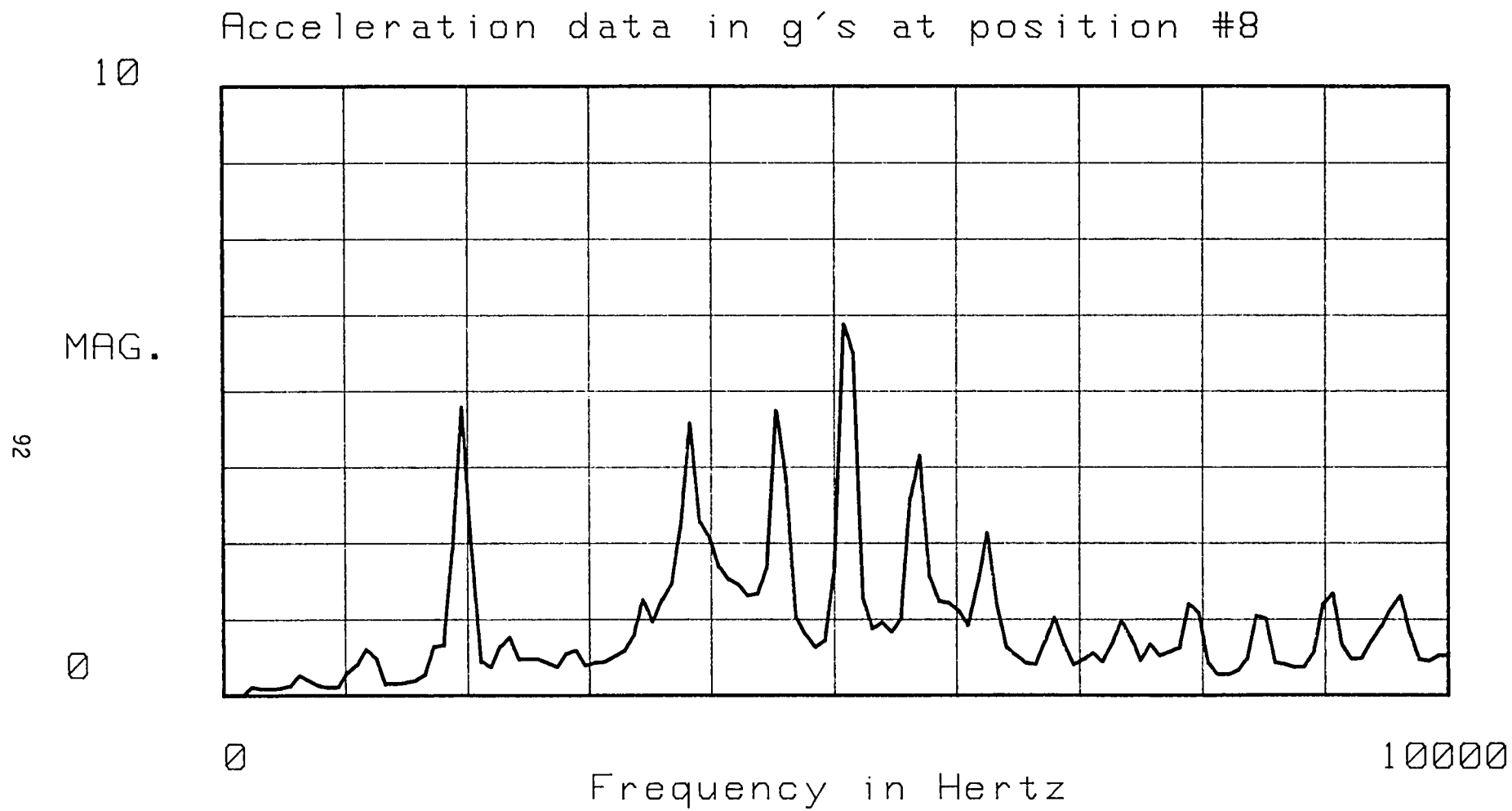
10000

Frequency in Hertz

Figure B-22.   Acceleration data in g's at position #4.

Figure B-23.   Acceleration data in g's at position #5.

Figure B-24. Acceleration data in g's at position #6.

Figure B-25. Acceleration data in g's at position #7.

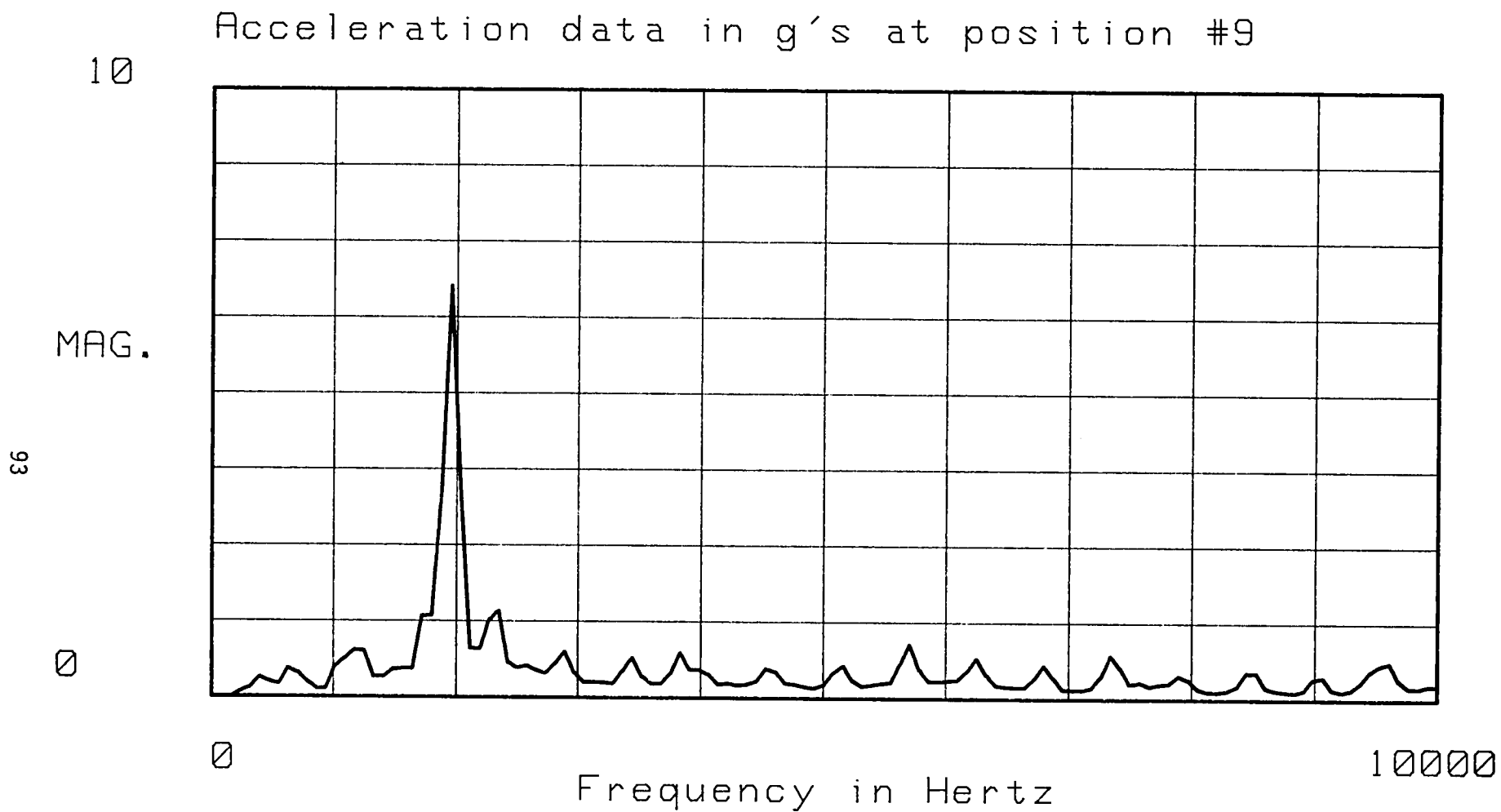Figure B-26. Acceleration data in g's at position #8.

Figure B-27. Acceleration data in g's at position #9.

Acceleration data in g's at position #10

MAG.

1

0

0   10000
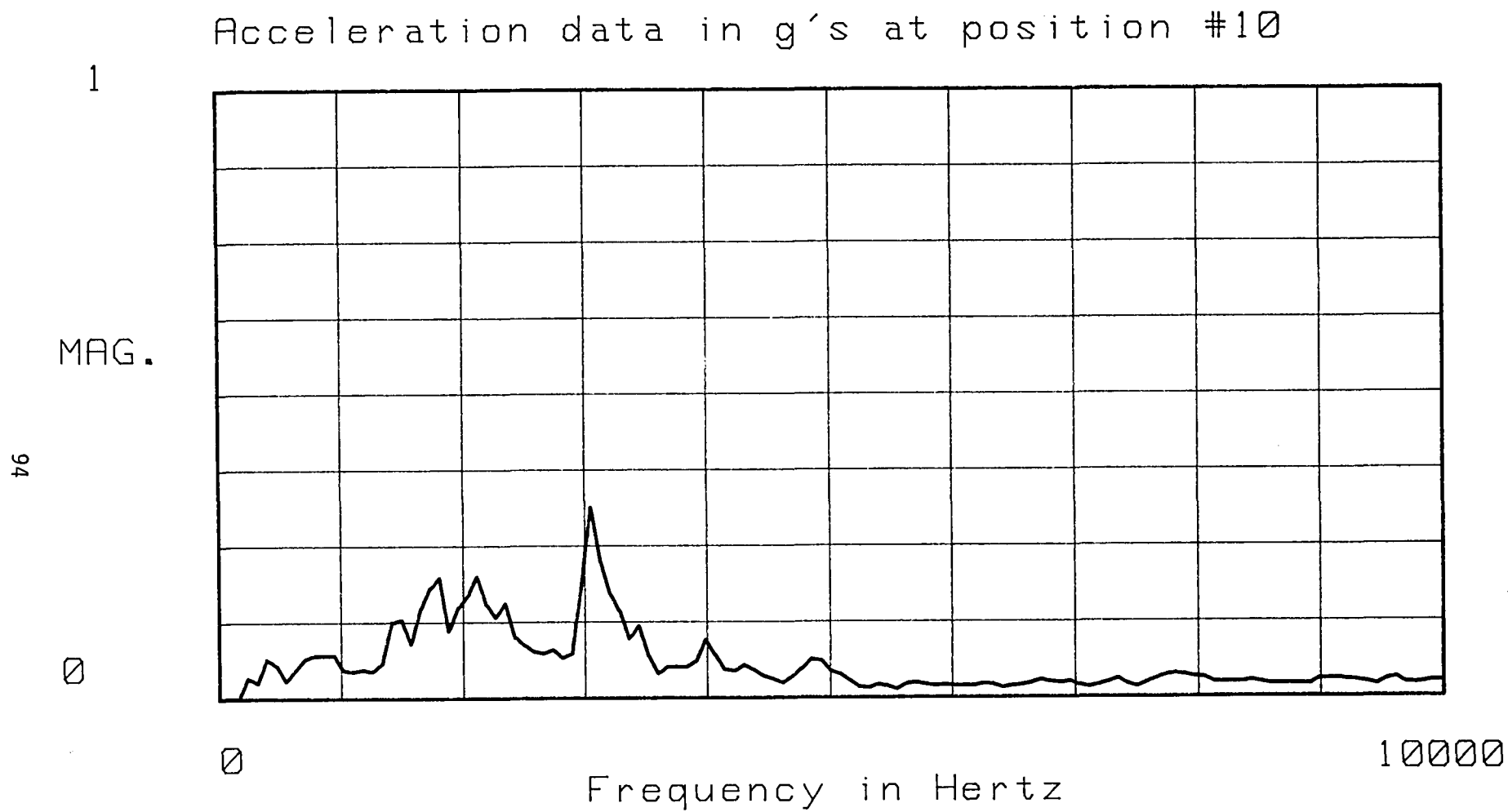
Frequency in Hertz

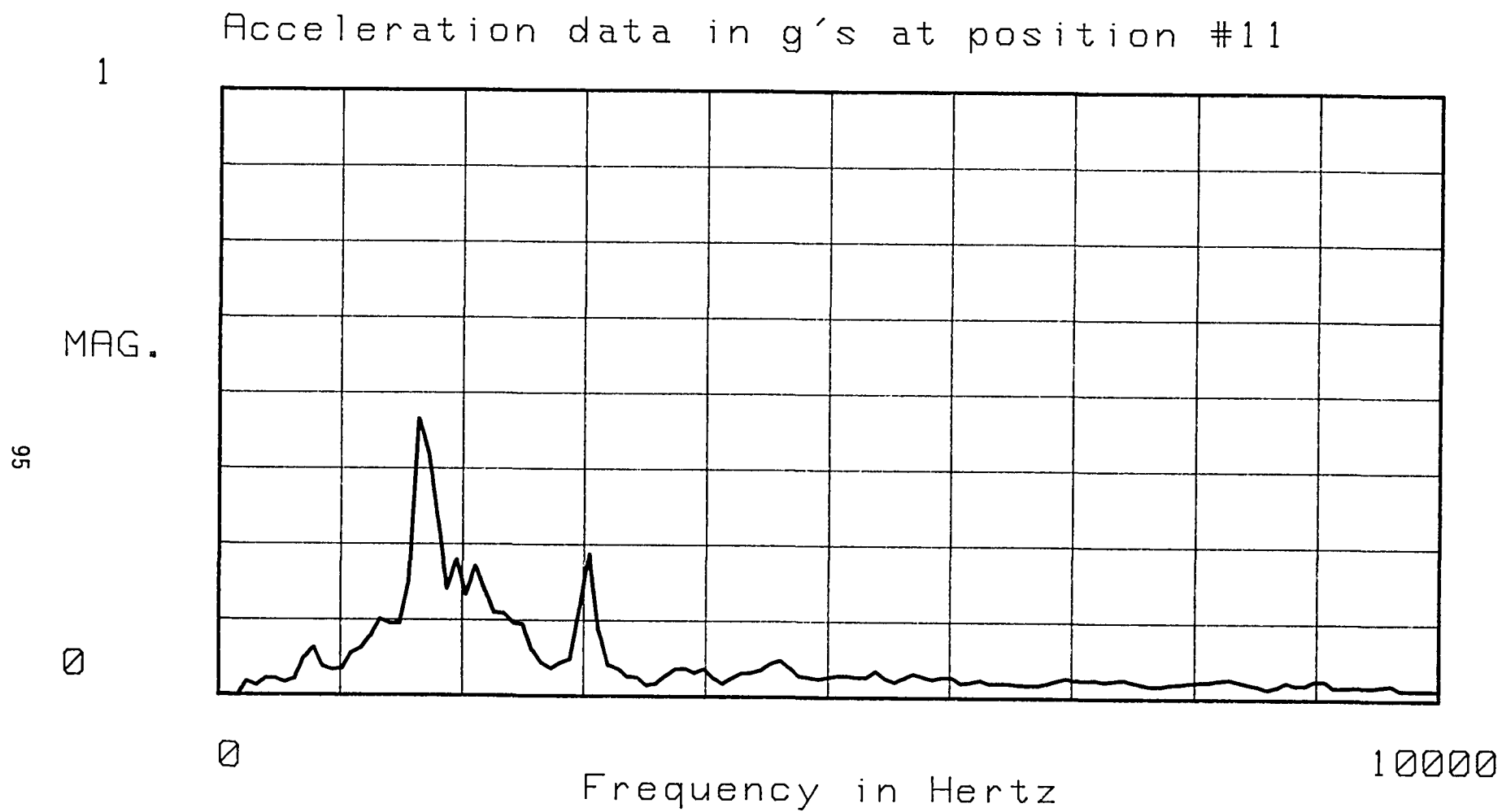Figure B-28.   Acceleration data in g's at position #10.

Figure B-29. Acceleration data in g's at position #11.

Figure B-30.   Acceleration data in g's at position #12.
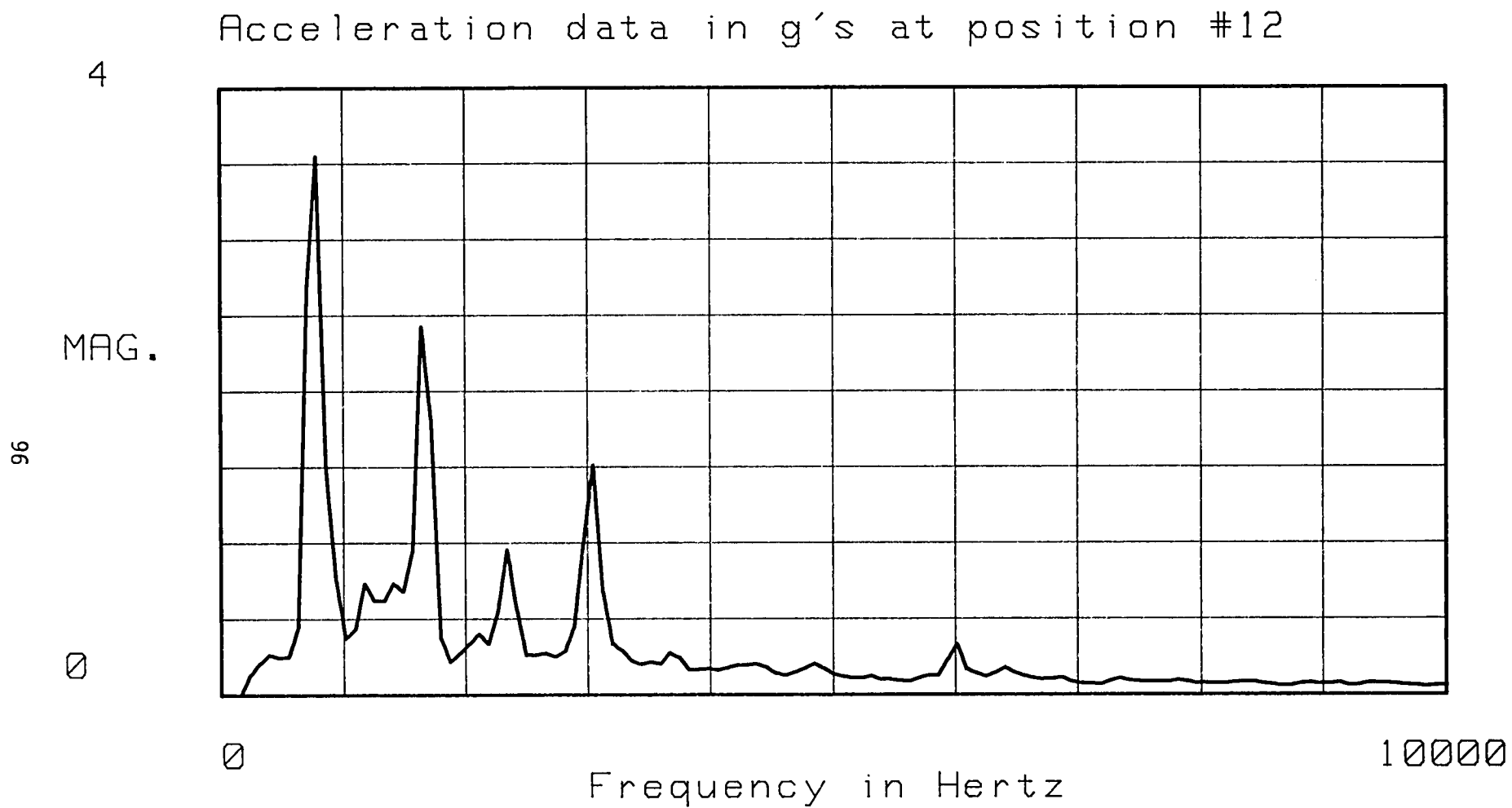
1. Report No. NASA CR-3847	2. Government Accession No.	3. Recipient's Catalog No.
4. Title and Subtitle INVESTIGATION ON EXPERIMENTAL TECHNIQUES TO DETECT, LOCATE, AND QUANTIFY GEAR NOISE IN HELICOPTER TRANSMISSIONS		5. Report Date January 1985
		6. Performing Organization Code
7. Author(s) Patrick M. Flanagan and William J. Atherton		8. Performing Organization Report No. None
		10. Work Unit No.
9. Performing Organization Name and Address Cleveland State University Cleveland, Ohio 44115		11. Contract or Grant No. NAG3-315
		13. Type of Report and Period Covered Contractor Report
12. Sponsoring Agency Name and Address National Aeronautics and Space Administration Washington, D.C. 20546		14. Sponsoring Agency Code 505-40-42 (E-2294)

15. Supplementary Notes

16. Abstract

A robotic system to automate the detection, location, and quantification of gear noise using acoustic intensity measurement techniques has been successfully developed. Major system components fabricated under this grant include an instrumentation robot arm, a robot digital control unit and system software. A commercial, desktop computer, spectrum analyzer and two microphone probe complete the equipment required for the Robotic Acoustic Intensity Measurement System (RAIMS). Large-scale acoustic studies of gear noise in helicopter transmissions cannot be performed accurately and reliably using presently available instrumentation and techniques. Operator safety is a major concern in certain gear noise studies due to the operating environment. The man-hours needed to document a noise field in situ is another short coming of present techniques. RAIMS was designed to reduce the labor and hazard in collecting data and to improve the accuracy and repeatability of characterizing the acoustic field by automating the measurement process. Using RAIMS a system operator can remotely control the instrumentation robot to scan surface areas and volumes generating acoustic intensity information using the "two microphone" technique. Acoustic intensity studies requiring hours of scan time can be performed automatically without operator assistance. During a scan sequence, the acoustic intensity probe is positioned by the robot and acoustic intensity data is collected, processed, and stored. Test results conducted on a speaker system illustrates several important RAIMS features including good spatial resolution for locating a noise source, good repeatability in obtaining acoustic intensity data. This report concludes with a survey of some vibration characteristics of the Bell helicopter OH-58 transmission. This series of tests identified prominent frequencies bands for analysis by RAIMS.

17. Key Words (Suggested by Author(s)) Acoustic intensity; Noise; Helicopter noise; Gearbox noise; Vibration spectra	18. Distribution Statement Unclassified - unlimited STAR Category 71
19. Security Classif. (of this report) Unclassified	20. Security Classif. (of this page) Unclassified	21. No. of pages 100	22. Price* A05

NASA-Langley, 1985

National Aeronautics and
Space Administration

Washington, D.C.
20546

THIRD-CLASS BULK RATE

U.S.MAIL

NASA

POSTMASTER: If Undeliverable (Section 158
Postal Manual) Do Not Return